ONLINE ABSTRACT BOOK

SCR'19

JUNE 13–15, 2019 | ST. GALLEN

SWISS CONGRESS OF RADIOLOGY
SCHWEIZERISCHER RADIOLOGIEKONGRESS
CONGRÈS SUISSE DE RADIOLOGIE

www.radiologiekongress.ch

**Dear Delegates and Visitors of the Swiss Congress of Radiology 2019,
Dear Colleagues!**

The Swiss Society of Radiology (SGR-SSR), the Swiss Society of Nuclear Medicine (SGNM-SSMN) and the Swiss Association of Radiographers (SVMTRA-ASTRM) are delighted about the high quality and the great amount of abstracts which were submitted for presentation at the annual Swiss Congress of Radiology.

The continuous excellent work of all authors is highly appreciated as it makes the congress a very prestigious scientific meeting.
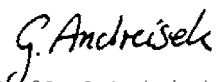
This "Online Abstract Book of the Swiss Congress of Radiology" is the 9th issue which is solely published online. It represents a cost efficient, durable platform independent documentation of scientific abstracts. The integration of the abstract data into either the Society's or Congress' web page as well as permanent accessibility all over the world.

The "Online Abstract Book of the Swiss Congress of Radiology" will permanently be accessible on either the Society's or Congress' web page at www.radiologiekongress.ch. It includes all the abstracts of the scientific talks and posters presented at the annual Swiss Congress of Radiology in St. Gallen.

Proper citation of scientific abstracts is however important, especially in case of online-only web publications. The Swiss Society of Radiology thereof recommends the use of the following structure to cite abstracts from the new "Online Abstract Book of the Swiss Congress of Radiology":

> "Author1 A, Author2 B, …, Author last X. Title of the abstract (abstr.).
> Swiss Congress of Radiology 2019, St. Gallen. Online Abstract Book, www.radiologiekongress.ch"

We look forward to welcoming you to the Swiss Congress of Radiology 2019 in St. Gallen.
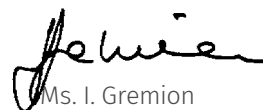
Prof Dr. G. Andreisek
President Scientific Committee SGR-SSR

Prof. Dr. H. Alkadhi
*President of the Swiss Congress
of Radiology SGR-SSR*

Prof. Dr. Dr. F. Forrer
*President of the Swiss Congress
of Radiology SGNM-SSMN*

Ms. I. Gremion
*President of the Swiss Congress
of Radiology SVMTRA-ASTRM*

SWISS CONGRESS OF RADIOLOGY 2019, ST. GALLEN

Congress Presidents

PRESIDENT OF THE SWISS CONGRESS OF RADIOLOGY SGR-SSR
H. Alkadhi, Zurich

PRESIDENT OF THE SWISS CONGRESS OF RADIOLOGY SGNM-SSMN
F. Forrer, St. Gallen

PRESIDENT OF THE SWISS CONGRESS OF RADIOLOGY SVMTRA-ASTRM
I. Gremion, Lausanne

Scientific Committee

PRESIDENT
G. Andreisek, Münsterlingen

REGULAR MEMBERS
M. Becker, Geneva
K. O. Loevblad, Geneva
C. Reiner, Zurich
S. Schmidt, Lausanne
H. von Tengg-Kobligk, Bern
H. Thoeny, Fribourg
C. Zech, Basel

EX-OFFICIO MEMBERS
H. Alkadhi, Zurich (SGR-SSR Congress President)
A. Kobe, Zurich (SGR-SSR Resident representative)
F. Becce, Lausanne (SSSR)
S. D. Qanadli, Lausanne (SSVIR)
J. Geiger, Zurich (SGPR-SSRP)
P.-A. Poletti, Geneva (SSER)
I. Gremion, Epalinges (SVMTRA-ASTRM)
M. Mordasini, Bern (SVMTRA-ASTRM)
F. Forrer, Lausanne (SGNM-SSMN)
M. Wissmeyer, Zurich (SGNM-SSMN)

SGR-SSR Office

Schweizerische Gesellschaft für Radiologie –
Société Suisse de Radiologie (SGR-SSR)
Geschäftsstelle
c/o Ecos Office Center
Bergstrasse 107
8032 Zurich
E-Mail   info@sgr-ssr.ch
Phone   +41 (0) 31 951 00 84
www.sgr-ssr.ch

Congress Services

Education Congress Research GmbH
Wolfgang Duchek/Monique Avril/
Helene Winklmayr/Claudio Brun
Am Gestade 1
1010 Vienna/Austria
E-Mail   info@radiologiekongress.ch
Phone   +43 1 5350599
www.radiologiekongress.ch

SGR-SSR Standing Abstract Reviewer Committee

M. Anooshiravani-Dumont, Geneva
F. Becce, Lausanne
M. Behe, Villigen
J. Brendle, Scherzingen
A. Christe, Bern
G. De Geer, Geneva
S. Dellas, Basel
T. Dietrich, St. Gallen
O. Donati, Zurich
C. Dromain, Lausanne
V. Dunet, Lausanne
M. Fani, Basel
J. Geiger, Zurich
A. Hirschmann, Basel
N. Kawel-Böhm, Chur
K. Kinkel, Chêne-Bougeries
R. Kubik, Baden
F. P. Kuhn, Zurich
C. Kurtz, Luzern
P. Manser, Bern
M. Marcon, Zurich
M. Maurer, Bern
R. Menz, Basel
J.-Y. Meuwly, Lausanne
E. Monnard, Fribourg
L. Mu, Zurich
D. Nanz, Zurich
T. Niemann, Baden
P. Omoumi, Lausanne
T. Pfammatter, Zurich
S. D. Qanadli, Lausanne
C. Reiner, Zurich
S. Schindera, Riehen
S. Schmidt, Lausanne
G. Sommer, Basel
M. Straub, Lausanne
R. Sutter, Zurich
H. Thöny, Fribourg
F. Verdun, Lausanne
S. Wälti, St. Gallen
L. Wissmann, Münsterlingen
R. Wyttenbach, Bellinzona
C. Zech, Basel

SVMTRA-ASTRM Standing Abstract Reviewer Committee

C. Bruguier, Lausanne
E. Fleury, Geneva
I. Gremion, Lausanne
S. Scherz, Bern

SGNM-SSMN Standing Abstract Reviewer Committee

M. Fany, Basel
F. Forrer, St. Gallen
L. Giovanella, Bellinzona
P. Kaufmann, Zurich
S. Kneifel, Chur
E. Nitzsche, Aarau
J. Prior, Lausanne
A. Rominger, Bern
N. Schäfer, Lausanne
R. Schibli, Zurich
K. Strobel, Lucerne
M. A. Walter, Geneva
D. Wild, Basel
M. Wissmeyer, Zurich

SGR-SSR Poster Jury

A. Boss, Zurich
A. Christe, Bern
T. Dietrich, St. Gallen
O. Donati, Zurich
J. Fischer, Samedan
A. Hötker, Zurich
B. K. Kovács, Basel
J.-Y. Meuwly, Lausanne
E. Monnard, Fribourg
A. Platon, Geneva
P.-A. Poletti, Geneva
E. Tenisch, Lausanne
R. Wyttenbach, Bellinzona

SS101

Validation of compressed sensing 4D Flow MRI in clinical practice

A. Juillet de Saint Lager[1], *L. A. Crowe*[1], *A.-L. Hachulla*[1], *M. Kassai*[1], *N. Jin*[2], *C. Forman*[3], *J.-P. Vallee*[1]; [1]*Geneva/CH*, [2]*Columbus/US*, [3]*Erlangen/DE*

Purpose: 4D Flow is an attractive proposition for robust cardiovascular assessment but acquisition time remains restrictively long. We studied internal validation of compressed sensing 4D Flow (CS4DFlow) for use in clinical routine.

Methods and Materials: Respiratory-navigated CS4DFlow was acquired with a prototype sequence in 17 patients scheduled for cardiac MRI on 1.5T/3T clinical MR scanners (MAGNETOM Aera/Skyra, Siemens Healthcare, Germany). Compressed sensing enabled 7-fold acceleration compared to non-accelerated 4D Flow. Depending on patient physiology and anatomy, typical parameters were 44 slices, TR/TE 25/2.2 ms (40/2.2 ms in 6 cases). Systemic and pulmonary vessel flow/volume was calculated at multiple equivalent locations using Siemens '4DFlow' software, and also compared to stroke volume/cardiac output from the left- and right-ventricle cine.

Results: CS4DFlow was successful in all 17 patients with an acquisition time of 6±2 minutes compared to over 15 minutes for standard non-CS (but still 3-fold-GRAPPA-accelerated) 4DFlow.

As these patients had no shunt, several flow measurements are equivalent (ascending aorta, pulmonary artery, and indirect sums of descending aorta plus superior vena cava and left plus right pulmonary arteries. There was excellent correlation between these flow estimates ($R^2 > 0.8$), with the robust indirect measurements performing best having limits of agreement within the clinically relevant 10 ml range[1] and $R^2 = 0.96$. Correlation of CS4DFlow was also good with cine-derived cardiac output ($R^2 > 0.5$)

Conclusion: This internal validation flow study demonstrated that compressed sensing significantly reduces scan time to clinically acceptable duration without loss of accuracy. The acquisition of 4Dflow with additional compressed sensing therefore provides an alternative to 2D and conventional 4DFlow.

(1)CHEST 2011;139(5):1003–1009

SS102

Comparison of standard 3D LGE imaging with novel short inversion time 3D LGE imaging in patients after myocardial infarction

M. Polacin, M. Gastl, I. Kapos, A. Gotschy, J. von Spiczak, H. Alkhadi, R. Manka; Zurich/CH

Purpose: Late gadolinium enhancement (LGE) visualizes myocardial scar and fibrosis. After myocardial infarction (MI), subendocardial infarcts can be missed due to poor contrast between blood pool and subendocardium. We aimed to evaluate the benefit of 3D LGE imaging using an inversion recovery sequence with a fixed, short inversion time (TI = 100 ms) (short3D LGE) over the standard 3D LGE imaging with adjusted TI (3D LGE).

Methods and Materials: 3D LGE and short3D LGE (both sequences with the same spatial resolution of 1.2 x 1.2 mm²; slice-thickness 8 mm; field of view, 350 x 350 mm²) were acquired in 27 patients with MI (8 female, mean age 64.8±12 years) at 1.5T (Achieva, Philips, Best, Netherlands). Two independent, blinded readers evaluated 459 segments (AHA 17-segment model) using a 5-point Likert scale in terms of scar visibility. Contrast-to-noise ratio (CNR) between scar and blood pool was calculated.

Results: 3D LGE showed 98 infarcted segments out of 459 (21.4 %), short3D LGE revealed 107 segments (23.3%). Short3D LGE demonstrated a better scar visibility (4.3 vs 2.8,P < 0.01) and better CNR between scar and blood pool (806.7±256 vs 209.5±149, P < 0.01). Agreement between the readers was moderate for 3D LGE and excellent for short3D LGE (weighted κ = 0.52 vs 0.78).

Conclusion: Short3D LGE provided a remarkable scar visualization and could be used additionally to standard 3D LGE imaging, especially in patients with subendocardial scarring and suboptimal nulling of the myocardium.

SS103

Remote-control cardiac computed tomography examinations – First experience

J. Fornaro, D. Keller, R. Buhmann, D. della Santa, S. Bakker, J. E. Roos; Lucerne/CH

Purpose: Many radiology institutes in Switzerland operate a network of various size and number of connected remote sites. From an operational standpoint, the main challenge is to guarantee adequate staffing tailored to the local workload and to provide high level experience for specific examinations, such as cardiac CT.

The purpose of this study was to evaluate a new remote-control imaging system in performing dedicated cardiac CT at two remote sites of a large public radiology network

Methods and Materials: 30 cardiac CT examinations were performed at the two remote sites by technicians on site without previous experience in cardiac CT and a radiology expert physically not present at the remote but virtually steering the cardiac CT scan by using a remote-control imaging system (Syngo Virtual Cockpit, Siemens Healthineers). The expert had full access to the remote CT console's user interface and assisted the technician during the planning and execution of the cardiac CT. Via video connection the expert was able to monitor the patient's position, ECG signal and motion. Expert and local technician communicated via voice and chat. Success of examination, operator confidence and examination times were noted.

Results: All cardiac CT examinations were successfully performed, with both the expert and the technician reporting a high level of confidence. Examination times were comparable to locally performed examinations.

Conclusion: The use of a remote-control imaging system to perform cardiac CT in remote sites is feasible and safe and has the potential to further increase the efficiency in providing dedicated examinations throughout a large radiology network.

SS104

CT angiography of the aorta: Prospective analysis of a patient-specific post-trigger delay for contrast timing

R. M. M. Hinzpeter, M. Eberhard, K. Reeve, T. Pfammatter, M. Lachat, B. Kolb, H. Alkhadi; Zurich/CH

Purpose: To prospectively evaluate whether a patient-specific, individualized post-trigger delay (PTD) for contrast media timing with bolus tracking improves contrast opacification in computed tomography angiography (CTA) of the aorta.

Methods and Materials: In this IRB-approved, prospective study, CTA of the thoracoabdominal aorta with bolus tracking was performed with a fixed PTD (4 sec) in 108 consecutive patients (*cohort A*) and with a patient-specific, individualized PTD in another 108 consecutive patients (*cohort B*). The algorithm for patient-specific PTD predicts peak arterial enhancement using the actual bolus signal of each patient in real-time and takes into account population-averaged blood circulation characteristics with variations in patient weight and cardiac output. All CT and contrast media protocol parameters were kept identical among cohorts. Objective image quality was evaluated by one reader; two blinded readers assessed subjective image quality.

Results: The patient-specific PTD in cohort B ranged from 6.4-11.3 sec. There was higher attenuation in cohort B than in cohort A across locations (p < 0.001), with differences increasing from the aortic arch to the iliac arteries. An interaction between cohort and measurement location was found (p < 0.001) with more stable attenuation in cohort B. As opposed to cohort A, attenuation in cohort B showed no lower outliers. Image noise was similar (p = 0.41), contrast-to-noise ratio higher (p < 0.05), and subjective image quality higher in cohort B than in cohort A (p < 0.001).

Conclusion: As compared to a fixed, predefined delay time after bolus tracking, a patient-specific, individualized PTD improves image quality and stabilizes contrast attenuation in CTA of the aorta.

SS105

Dual- vs single-energy low dose CT-angiography for endoleak detection in an abdominal aortic aneurysm phantom

S. M. Skawran[1], Z. Szucs-Farkas[2], H. Alkadhi[1], A. Euler[1]; [1]Zurich/CH, [2]Biel/CH

Purpose: To compare image quality and accuracy of endoleak detection between dual-energy virtual monoenergetic imaging (DE-VMI) and low-kV single-energy imaging (SE) for low dose CT-angiography using an aneurysm phantom.

Methods and Materials: An aortic aneurysm phantom containing 36 endoleaks was placed into two water-filled containers to simulate medium- and large-sized patients. Each size was imaged four times in 1.) SE mode at 80 kV and 100 kV, and 2.) DE mode using weight-adapted spectral settings (80/Sn150 kV for the medium- and 100/Sn150 kV for the large size) on a 192-slice dual-source DECT (Somatom Force, Siemens). Radiation dose was kept constant at 3 mGy for the medium and 6 mGy for the large phantom. DE-VMIs at 40 keV and 50 keV were reconstructed. Contrast-to-noise ratio (CNR) of the aorta and two endoleaks with different physical densities were measured and compared among SE images and VMIs using tukey's range test. Accuracy of endoleak detection will be independently performed by six radiologists.

Results: CNR of the aorta was significantly higher for DE-VMIs compared to SE (p < 0.01). CNR of the two endoleaks did not differ significantly between DE-VMI and SE in the large phantom (p > 0.2). However, in the medium phantom, CNR of the less dense endoleak was significantly lower for DE-VMIs (p < 0.01).

Conclusion: DE-VMI improved CNR of the aorta while decreasing the CNR of less dense endoleaks only in the medium phantom compared to low-kV SE images. Accuracy of endoleak detection will determine if DE-VMIs are feasible to replace low-kV SE images for CT-angiography of the abdomen.

SS106

Missed visceral artery pseudoaneurysms: Frequency and causes of misdiagnoses in CT

I. Vittoria de Martini, H. Alkadhi, T. Pfammatter; Zurich/CH

Purpose: Visceral artery pseudoaneurysm (VAPA) carry a high risk of rupture. We made the experience that VAPA were sometimes missed or diagnosed with delay on CT examinations. The aims of this study were to determine the frequency and causes of misdiagnoses of VAPA in CT.

Methods and Materials: We retrospectively identified 77 patients with VAPA in our database who underwent CT. The frequency of missed or delayed diagnosis was assessed, and the reasons for misdiagnosis were noted. We further identified size, affected vessels and etiology of VAPA.

Results: Forty-five of the 77 patients (58 %) had an initial misdiagnosis, meaning that the VAPA was not reported in the first but only in follow-up CT. The majority of VAPA were caused by previous surgical or interventional procedures (n = 48,62 %). The major affected vessel was the hepatic artery in 31 cases followed by the splenic artery in 17 cases. The reasons for misdiagnosis were a missed arterial phase in CT (n = 16,36 %), artifacts masking the aneurysm (n = 9,20 %), misinterpretation of the findings by the attending radiologist (n = 1,2 %), and overlooked pseudoaneurysm (n = 19,42 %). Missed VAPA were smaller (median 8 mm) than those VAPA that were initially diagnosed (median 13 mm, p < 0.01), but occurred with a similar frequency in larger and smaller visceral vessels (p = 0.27).

Conclusion: Misdiagnosis of VAPA occurred relatively often with four main reasons for misdiagnoses. Adding an arterial contrast media phase to the CT protocol, techniques for artifact reduction and increased awareness of the attending radiologist should be considered for reducing the rate of misdiagnosis.

SS107

Comparison of diffusion-weighted MR imaging and 18F Fluorodeoxy-glucose PET/CT in detection of residual tumors and delineation of its spread after (chemo)radiotherapy for head and neck squamous cell carcinoma with the gold standard of histopathology

S. Y. Kim[1], B. Klaeser[2], D. W. Tshering Vogel[1]; [1]Bern/CH, [2]Muri bei Bern/CH

Purpose: To compare the accuracy of diffusion-weighted MR imaging (DW-MRI) and fluorine 18 fluorodeoxyglucose (^{18}F FDG) PET/CT in detection of tumor and its extension, in patients with residual head and neck squamous cell carcinoma (HNSCC) after treatment with (chemo)radiotherapy.

Methods and Materials: This retrospective study, approved by the institutional review board was performed to assess the value of DW-MRI and PET/CT in detection of residual tumor and infiltration of surrounding structures in patients who underwent salvage surgery. 22 patients were included in this study (14 men, 8 women, median age 70 years, range 56-86). The DW-MRI and PET/CT images were anonymized and reviewed retrospectively. The results were compared to the histopathology reports.

Results: Both DW-MRI and PET/CT detected 90 % (20/22) of tumors. MRI showed a sensitivity of 62 % (5/8) and specificity of 85 % (12/14) in detection of perineural infiltration, PET/CT did not detect any cases of perineural infiltration. The sensitivity and specificity of MRI in detection of muscle infiltration was 78 % (7/9) and 76 % (10/13) respectively, while that for PET/CT was 55 % (5/9) and 69 % (9/13) respectively.

Conclusion: Detection rate of residual tumors by MRI and PET/CT was similar. MRI was superior to PET/CT in detection of perineural infiltration and slightly better in detection of muscle infiltration.

SS108

Impact of prophylactic cranial irradiation on 18F-FDG cerebral metabolism in small cell lung cancer patients

S. El Chammah, G. Allenbach, J. Prior, M. Nicod Lalonde, P. Genoud, N. Schäfer, M. Meyer; Lausanne/CH

Purpose: In limited-disease small cell lung cancer (SCLC) patients, prophylactic cranial irradiation (PCI) is associated with increased survival but also with cognitive impairment. The exact mechanisms underlying this cognitive impairment remain poorly understood. Our study aims to evaluate the short-term impact of PCI on ^{18}F-FDG brain metabolism.

Methods and Materials: We retrospectively included 18 SCLC patients. Among these patients, 10 beneficiated from Hippocampal-Sparing PCI.[18]F-FDG PET/CT was performed on average 146±82 days before and 294±327 days after PCI. Brain ^{18}F-FDG PET were automatically segmented using Combined-AAL Atlas from MI-Neurology Software (Syngo.Via, Siemens). For all the regions, we calculated SUVratio using brainstem as reference region (SUVr=SUVmean/Brainstem SUVmean) and we compared SUVr before and after PCI using a Wilcoxon test with a level of significance of $p \leq 0.05$.

Results: We showed a significant decrease in ^{18}F-FDG brain metabolism after PCI in basal ganglia (1.39±0.15 vs 1.33±0.13, p=0.018), central regions (1.32±0.11 vs 1.26±1.00, p=0.012), cingulate cortex (1.32±0.11 vs 1.23±0.13, p=0.004), corpus striata (1.42±0.16 vs 1.35±0.14, p=0.016), frontal cortex (1.31±0.13 vs 1.24±0.12, p=0.012), occipital cortex (1.47±0.15 vs 1.41±0.13, p=0.028), parietal cortex (1.33±0.14 vs 1.28±0.11, p=0.048), precuneus (1.46±0.16 vs 1.39±0.14, p=0.025) and lateral temporal cortex (1.33±0.12 vs 1.27±0.11, p=0.014), but not in cerebellum (1.24±0.08 vs 1.21±0.08, p=0.85) and mesial temporal cortex including hippocampus (1.03±0.08 vs 1.00±0.07, p=0.16).

Conclusion: PCI leads to short-term decrease of ^{18}F-FDG brain metabolism, except in cerebellum and in regions that have been spared during PCI.

SS109

PET/CT radiomics analysis contributes to detection of pulmonary lymphangitic carcinomatosis (PLC) in non-small cell lung cancer (NSCLC)

V. Oreiller, M. Jreige, J. Prior, A. Depeursinge; Lausanne/CH

Purpose: Pulmonary lymphangitic carcinomatosis (PLC) is defined as the spread of cancer through the lymphatic system into the lung interstitium. Radiologic diagnosis on CT is known to be challenging. We aimed to correlate PET/CT Radiomics analysis with the definitive diagnosis of PLC on histopathologic examination in NSCLC.

Methods and Materials: 24 patients addressed for initial staging of NSCLC were retrospectively included (PLC, n=12 and non-PLC, n=12). An initial set of 160 radiomic features were extracted from 18F-FDG PET/CT with the platform QuantImage, including intensity and 3D texture feature groups. A LASSO logistic regression model was built on three distinct feature sets: (i) a subset of 84 features from the PET only, (ii) 76 features from the CT only, and (iii) all 160 features from both modalities. Confidence interval [95 % CI] were assessed with bootstrap analysis.

Results: The following performances were observed: accuracy (i) 0.81 [0.57–1], (ii) 0.83 [0.57–1], (iii) 0.85 [0.60–1]; sensitivity (i) 0.75 [0.33–1], (ii) 0.83 [0.40–1], (iii) 0.81 [0.33–1]; specificity (i) 0.87 [0.5–1], (ii) 0.84 [0.40–1], (iii) 0.89 [0.50–1]; Area Under the ROC Curve (i) 0.86 [0.58–1], (ii) 0.92 [0.67–1], (iii) 0.91 [0.67–1]; number of features (i) 12.2 [2–71], (ii) 9.1 [3–45], (iii) 11.1 [3–49].

Conclusion: These results suggest that even though there is currently no definite CT-based diagnosis capturing all lymphangitis cases, the proposed radiomics model was able to leverage higher-order 3D textural information that is invisible to the naked eye to predict lymphangitis.

SS110

Diagnostic performance of radiolabelled choline PET/CT in detecting hepatocellular carcinoma: An updated meta-analysis

G. Treglia[1], G. Signore[2], M. Nicod Lalonde[3], L. Giovanella[1], J. Prior[3]; [1]Bellinzona/CH, [2]Minturno/IT, [3]Lausanne/CH

Purpose: Different imaging methods are used to detect hepatocellular carcinoma (HCC) with increasing literature data about the role of radiolabelled choline PET/CT in this setting. We aimed to perform an updated meta-analysis about the diagnostic performance of radiolabelled choline PET/CT in detecting HCC.

Methods and Materials: A comprehensive computer literature search of studies published through October 2018 in PubMed and Cochrane library databases regarding the diagnostic performance of radiolabelled choline PET/CT in patients with HCC was carried out. The following search algorithm was used: A) "choline" or "fluorocholine" or "F-choline" or "C-choline" or "FCH" or "CH" or "FECH" or "FMCH" and B) "PET" or "positron emission tomography" and C) "HCC" or "hepatocellular". Pooled detection rate (DR) of radiolabelled choline PET/CT in detecting HCC was calculated, on a per patient- and on a per lesion-based analysis. Subgroup analyses taking into account the radiopharmaceutical used were carried out.

Results: Nine studies published between 2006 and 2017 were included in the pooled analysis. The pooled DR of radiolabelled choline PET/CT on a per patient- and on a per lesion-based analysis was 83 % [95 % confidence interval (95 % CI): 75–89 %] and 79 % (95 % CI: 72–86 %), respectively. A significant heterogeneity among the selected studies was found on a per lesion-based analysis only. No significant publication bias was found. The subgroup analysis demonstrated a slightly higher DR when using ^{18}F-choline compared to ^{11}C-choline.

Conclusion: Radiolabelled choline PET/CT demonstrated a good diagnostic performance in detecting HCC. Large multicenter studies and cost-effectiveness analyses are needed to strengthen the role of this imaging method in this setting.

Detection of extracapsular extension in prostate cancer patients: Multiparametric MRI versus 68Ga-PSMA-11 PET/MRI

U. J. Mühlematter, K. Schawkat, A. S. Becker, A. Hötker, C. S. Reiner, J. Müller, N. Rupp, D. Eberli, I. A. Burger, O. F. Donati; Zurich/CH

Purpose: To compare the diagnostic accuracy and inter-reader reliability of multiparametric MRI (mpMRI) and 68Ga-labeled prostate-specific membrane antigen (68Ga-PSMA-11) PET/MRI for detection of extracapsular extension (ECE) in patients with prostate cancer.

Methods and Materials: Retrospective analysis of 40 consecutive men that underwent mpMRI and 68Ga-PSMA-11 PET/MRI within 6 months for suspected prostate cancer that underwent radical prostatectomy between April 2016 and July 2018. Four readers blinded to clinical and histopathologic findings rated the probability of ECE on mpMRI and PET/MRI in 4 anatomical regions (anterior/posterior on right/left side) using a 5–point Likert-scale. An interval of >3 weeks between readings was maintained to avoid recall bias. Prostatectomy specimen served as reference standard. Accuracy was assessed by calculating the Area under the receiver-operating-characteritics curve (AUC). Sensitivity/specificity was calculated on dichotomized data. Inter-rater reliability was assessed by Krippendorff's alpha.

Results: Mean age was 63 years (range 51–78). 13/40 (33%) patients had ECE. For mpMRI versus PET/MRI, the averaged region-specific results were as follows: AUC 0.67/0.75; sensitivity 0.34/0.58; specificity 0.91/0.87. For mpMRI versus PET/MRI the patient-specific sensitivity was 0.40/0.63 and specificity was 0.73/0.63. There was no significant difference in Krippendorff's alpha of mpMRI (0.67, CI=0.57–0.77) and PET/MRI (0.66, CI=0.56–0.75).

Conclusion: Our results suggest that 68Ga-PSMA-11 PET/MR could improve the sensitivity of mpMRI for the detection of ECE in prostate cancer patients.

68Ga-PSMA-11 PET predicts lymph node metastasis with superior accuracy compared to conventional nomograms

D. A. Ferraro, J. H. Rüschoff, J. Müller, U. Mühlematter, M. Messerli, M. Hüllner, D. Eberli, N. J. Rupp, I. A. Burger; Zurich/CH

Purpose: To compare established pre-treatment risk scores for prostate cancer (PCa) nodal disease prediction, with quantitative PET parameters in man undergoing staging 68Ga-PSMA-11 PET.

Methods and Materials: Retrospective analysis of 60 patients that underwent 68Ga-PSMA-11 PET for staging PCa and had radical prostatectomy. For all 68Ga-PSMA-11 PET scans, positive lesions and quantitative parameters of the primary tumor (SUV_{max}, $PSMA_{Total}$ and $PSMA_{Vol}$) were recorded. Risk scores according to Yale formula (YF) and MSKCC nomogram were calculated based on clinical information. ROC analysis was used to determine the optimal cut-off for all PET parameters and risk scores.

Results: Twelve of 60 (20%) patients had lymph node metastasis (size range 1.2-24 mm). 68Ga-PSMA-11 PET was true positive in 7 patients, and false positive in 1. ROC analysis of the 53 patients without positive nodes yielded the highest accuracy for $PSMA_{Total}$ (AUC 0.902), compared to SUV_{max} (AUC 0.780) and $PSMA_{Vol}$ (AUC 0.894). From the clinical nomograms, YF yielded the highest accuracy (AUC 0.749), followed by MSKCC (AUC 0.720). The resulting sensitivity/specificity including all patients was 100%/65% for $PSMA_{Total}$ and 75%/67% for YF. Using the official threshold of >5% for YF, one case would be missed and lymph nodes suspected in 38 (63%) patients without nodal disease. $PSMA_{Total}$ would have suggested lymph node metastasis in 17 (28%) patients without nodal disease, without any missed case.

Conclusion: In our cohort, a $PSMA_{Total}$ higher than 49 showed superior sensitivity and specificity for nodal metastasis than clinical risk scores. Thus, PSMA-PET could be used to improve patient selection for lymph node dissection or radiation.

Correlation between PSA kinetics and PSMA-PET in prostate cancer restaging: A meta-analysis

G. Treglia, R. Pereira Mestre, M. Ferrari, E. Roggero, L. Giovanella; Bellinzona/CH

Purpose: Serum prostate-specific antigen (PSA) may predict the risk of positive positron emission tomography/computed tomography with radiolabeled prostate-specific membrane antigen (PSMA-PET/CT) in patients with biochemical recurrent prostate cancer (BRPCa). However, to date, there are no clear data regarding the correlation between PSA kinetics and PSMA-PET findings. We performed a systematic review and meta-analysis to provide evidence-based data in this setting.

Methods and Materials: A comprehensive literature search of studies published through October 2018 in PubMed/MEDLINE, EMBASE and Cochrane library databases was performed. A meta-analysis to establish the detection rate (DR) of PSMA-PET using different cut-off values of PSA doubling time (PSAdt) and a pooled analysis to establish whether shorter PSAdt may predict positive PSMA-PET results was performed in patients with BRPCa.

Results: Twelve articles were included in the systematic review and eight articles (including 1,398 patients) were selected for the meta-analysis. The pooled DR including 95% confidence intervals (95%CI) of PSMA-PET in restaging prostate cancer (PCa) patients was 72% (95% CI: 60–82%), increasing to 83% (95% CI: 75–90%) when PSAdt was ≤6 months and decreasing to 60% (95% CI: 37–80%) when PSAdt was >6 months. PSAdt ≤6 months may predict the positive result of PSMA-PET (pooled odds ratio: 3.22; 95% CI: 1.17–8.88). Statistical heterogeneity among the included studies was found.

Conclusion: PSA kinetics, and in particular shorter PSAdt, may be predictor of PSMA-PET positivity in patients with BRPCa. Further larger studies in this setting are warranted.

PSMA expression heterogeneity of the primary tumor on IHC correlates with the detection rate of 68Ga-PSMA-11-PET in patients with biochemical recurrence

D. A. Ferraro, T. Hermanns, N. J. Rupp, M. Messerli, J. H. Rüschoff, E. E. G. Ter Voert, U. J. Muehlematter, D. Eberli, H. Garcia Schüler, I. A. Burger; Zurich/CH; Zurich/CH

Purpose: A small fraction of patients have negative PSMA-PET scans despite high PSA values. This is most likely due to a 10% fraction of prostate cancers (PCa) without significant PSMA-expression. Currently, it is not possible to discriminate these patients before the PET scan. We aimed to investigate if the PSMA-expression of the primary tumor predicts PSMA-PET detection.

Methods and Materials: 52 patients underwent radical prostatectomy between 2007-2017 in our institution and were referred to 68Ga-PSMA-11-PET for biochemical recurrence, with up to two scans if the first one was negative. Lesions suspicious for recurrence were quantified using SUV_{max}. PSMA-IHC staining for the dominant tumor on prostatectomy specimen was quantified using a three-tiered system (1+weak, 2+moderate, 3+strong) for PSMA-positive expression and percentage of PSMA-negative area. Differences between positive and negative scans were assessed using an independent, 2-tailed t-test.

Results: 62 68Ga-PSMA-11-PET scans were available, with a median PSA of 0.9 ng/ml (range 0.05–405.7 ng/ml). Thirty-six (58%) scans were positive (median SUV_{max} of 8.4, range 2.6–128). Comparing positivity of the scan with IHC results we found: the mean membranous PSMA-expression in PCa was 2.6±0.5 for positive and 2.3±0.8 for negative scans (p=0.171); PSMA-negative tumor area showed a significant difference with mean 7.9%±15% for positive and 28%±37% (p=0.014) for negative scans. All 3 cases with a PSA level above 2 ng/ml and a negative scan had PSMA-negative areas of 80%. All seven patients with 80% or more negative tumor area had a negative 68Ga-PSMA-11-PET.

Conclusion: High percentages of PSMA-negative areas on IHC of the primary tumor could predict negative 68Ga-PSMA-11 PET scans.

SS115

Analysis of the specificity of 68Ga-PSMA-11 PET/CT in patients with recurrent prostate cancer

V. Fech, B. Vollnberg, L. Dijkstra, I. L. Alberts, A. Rominger, A. Afshar-Oromieh; Bern/CH

Purpose: ^{68}Ga-PSMA-11-PET/CT has become a widely established modality for prostate cancer (PC) imaging. Its high sensitivity has been shown in numerous studies. Recently, many case reports have been published describing various benign and malignant entities exhibiting PSMA-ligand uptake. The present evaluation was performed in order to further analyze the specificity of ^{68}Ga-PSMA-11 PET/CT in our patient cohort.

Methods and Materials: A retrospective analysis was performed for all patients at our institute who underwent ^{68}Ga-PSMA-11 PET/CT between January 2017 and July 2018 in order to detect recurrent PC (n = 302). Hitherto, 18 patients were found who had received radiation therapy, histology or surgical removal of PSMA-positive lesions, enabling comparison with PSMA-avidity in the previous PET/CT.

Results: So far, 23 PSMA-positive lesions in all 18 patients have undergone external radiation, were biopsied or surgically removed. 22 of them (95.7 %) were true-positive PC lesions (proven by falling PSA following external radiation or by histology). Amongst the mentioned lesions were 15 local relapses, 5 lymph node metastases and 2 bone metastases. One single pararectal tissue was falsely PSMA-positive (proved by biopsy).

Conclusion: Our analysis demonstrates the high specificity of ^{68}Ga-PSMA-11 PET/CT. We propose that PSMA-positive lesions in patients with recurrent PC should be regarded as PC lesions until proven otherwise. Although uptake of PSMA-ligands in various non-prostatic tissues have been described, it must be assumed that their numbers represent only a fraction of the overwhelming numbers of PC lesions detected in clinical practice by PSMA-PET/CT.

SS116

Comparison of 68Ga-PSMA-11 PET/CT and multiparametric MRI for the detection of recurrent prostate cancer in the pelvis

B. Vollnberg, K. H. Härmä, L. Dijkstra, A. Bähler, J. T. Heverhagen, A. Rominger, M. H. Maurer, A. Afshar-Oromieh; Bern/CH

Purpose: Comparison ^{68}Ga-PSMA-11-PET/CT and MRI for detection of recurrent prostate cancer (rPC) in the pelvis.

Methods and Materials: A retrospective analysis was performed for patients who were scanned at our institute with ^{68}Ga-PSMA-11-PET/CT from January 2017 until July 2018 in order to detect recurrent PC. Amongst them, 24 patients had received an additional pelvic multiparametric MRI within a time window of 2 months. Both modalities were compared to each other: in a first step, a consensus reading of PET-data was performed by two nuclear physicians. Lesions were classified as "certainly PC", "possibly PC" and "no PC". The same was conducted by two radiologists for MRI data. In a second step, a radiologist and a nuclear physician compared both modalities for every patient and recorded matches and discrepancies.

Results: Overall, 16/24 (66.7 %) patients presented with a pathologic MRI and 22/24 (91.7 %) with a pathologic ^{68}Ga-PSMA-PET/CT. MRI detected 20 and ^{68}Ga-PSMA-PET/CT detected 35 pelvic lesions classified as "certainly PC". Amongst them were 13 local relapses in 12 patients detected by MRI and 16 local relapses in 15 patients detected by ^{68}Ga-PSMA-PET/CT. In 8 patients, ^{68}Ga-PSMA-PET/CT detected 11 additional PC lesions outside the pelvis. Follow-Ups were selected as gold standard wherever possible.

Conclusion: In our preliminary results, ^{68}Ga-PSMA-11-PET/CT showed to be superior compared to MRI for the detection of recurrent PC in the pelvis. These results included local relapses. In order to detect recurrent PC, a potential future scenario could be conducting first a whole-body ^{68}Ga-PSMA-11-PET/CT. MRI could be used complementary or to further clarify unclear PET-findings.

Compressed sensing, parallel imaging and golden-angle radial sampling for MRI of the prostate

D. J. Winkel, V. Hofmann, T. Heye, M. Benz, C. G. Glessgen, D. T. Boll; Basel/CH

Purpose: To investigate the diagnostic performance of a dual-parameterapproach combining either VIBE-(volumetric interpolated breath-hold examination)or GRASP-(golden-angle, radial sparse-MRI) derived DCE-MRI with established diffusion weighted-imaging (DWI) compared to traditional single-parameter evaluations based on DWI alone.

Methods and Materials: 94 male study subjects (66±7 years) were prospectively evaluated for clinical suspicion for prostate cancer by 3T MRI. We included 101 peripheral zone prostate cancer lesions. Histopathological confirmation on MRI-trans-rectal ultrasound fusion biopsy was matched with normal prostate parenchyma contralaterally. MRI was performed with diffusion weighting as well as DCE using GRASP (temporal resolution, 2.5 s) or VIBE (temporal resolution, 10 s). Perfusion (K^{trans}, K_{ep}) and apparent diffusion coefficient (ADC) parameters were determined by tumor volume analysis. Area under the receiver operating characteristic curve (AUC) values were compared for both sequences.

Results: We evaluated 101 prostate cancer lesions (GRASP = 61, VIBE = 41). In a combined analysis of diffusion and perfusion parameters, ADC plus K^{trans} or K_{ep}acquired with GRASP had higher diagnostic performance compared to diffusion characteristics alone (AUC 0.97 vs 0.93, p < 0.006 and 0.021, respectively), while perfusion maps acquired with VIBE had no additional benefit (AUC 0.94 versus 0.93, p = 0.188 and p = 0.503, combination of ADC with K^{trans} and K_{ep}, respectively).

Conclusion: If employed in a dual-parameter model, incorporating diffusion and perfusion characteristics, the GRASP acquisition technique improves the diagnostic performance of multi-parametric MRI examinations of the prostate. This effect could not be observed with perfusion parameters acquired with VIBE.

Renal diffusion tensor imaging in chronic kidney disease patients

M. Kassai, L. A. Crowe, L. Berchtold, I. Friedli, S. Moll, S. de Seigneux, J.-P. Vallee; Geneva/CH

Purpose: Fibrosis assessment is a key in the diagnosis and management of chronic kidney disease (CKD) patients. Renal diffusion is promising with the corticomedullary apparent diffusion coefficient (ΔADC) inversely correlated to renal fibrosis. Our aim was to study the relation between fractional anisotropy (FA) and renal fibrosis.

Methods and Materials: 17 patients (3 native and 14 allograft kidneys) scheduled for a renal biopsy, underwent MRI Diffusion Tensor Imaging (b values: 0, 50, 250 and 750 s/mm²; directions: 12) on a clinical 3T MAGNETOM Prisma (Siemens Healthcare, Germany). FA and ADC maps were created with Diffusion Toolkit (TrackVis, Massachusetts General Hospital). Cortical and medullary ADC and FA values with corticomedullary differences (ΔADC, ΔFA) were measured and correlated to the percentage fibrosis, from pathologist assessment of biopsies. ROI selection was carried out in ImageJ based on the T1 maps of the corresponding kidney slice, showing the best corticomedullary differentiation.

Results: Successful DTI was obtained and analyzed in all patients. Both cortical FA (R^2 = 0.427, p = 0.004) and ΔFA (R^2 = 0.392, p = 0.007) were linearly related to fibrosis and cortical ADC (R^2 = 0.393, p = 0.007) and ΔADC (R^2 = 0.348, p = 0.013) were inversely linearly correlated to renal fibrosis. These correlation coefficients were not significantly different from each other using a Fisher Z-test.

Cortical ADC and FA, as well as ΔADC and ΔFA, were not correlated with each other and are therefore additive in assessing fibrosis.

Conclusion: FA values were linearly correlated to renal fibrosis in CKD patient and not correlated to ADC values. Therefore, FA has added value to ADC in assessing renal fibrosis.

Diffusion tensor imaging of the abdominal organs: Influence of oriented intravoxel flow compartments

V. D. Phi van, C. S. Reiner, M. Klarhoefer, A. Ciritsis, M. Wurnig, C. Rossi; Zurich/CH

Purpose: This study investigates the influence of this anisotropic intravoxel water flow on Diffusion Tensor Imaging (DTI) of the liver and kidney by using a tensorial generalization of the Intravoxel Incoherent Motion (IVIM) MRI.

Methods and Materials: Diffusion-weighted images were acquired in 5 healthy volunteers using a prototype fat-saturated EPI sequence (TR/TE: 1000 ms/71 ms; b-values: 0 – 1000 s/mm², 12 directions). DTI of liver and kidneys was performed assuming a monoexponential signal decay of the diffusion-weighted signal, and a tensorial generalization of the IVIM model. The diffusion tensors' metrics fractional anisotropy and trace were derived from the two models. Dependence of the tensors' metrics from the anatomical location was evaluated.

Results: Significant differences in trace and fractional anisotropy were found in liver and kidneys comparing the two models. Trace was significantly higher in the monoexponential model than in the tensorial model (renal cortex: mono-exponential $2.53 ± 0.16 \ 10^{-3}$ mm²/s; tensor IVIM $1.91 ± 0.12 \ 10^{-3}$ mm²/s; liver: mono-exponential $1.63 ± 0.45 \ 10^{3}$ mm²/s, tensorial IVIM $1.19 ± 0.78 \times 10^{3}$ mm²/s). Fractional anisotropy was significantly higher in the monoexponential model. The IVIM-derived tensors revealed local differences comparing different area of the liver and renal cortex to medulla.

Conclusion: The anisotropy of the diffusion components affects DTI estimations. The corrected DTI metrics enable the assessment of the solid parenchyma regardless of the organ perfusionor other pseudo-diffusive fluid movements. This may have a clinical relevance in the assessment of parenchymal pathologies (e. g. assessment of liver fibrosis). The pseudo-diffusion components present a detectable anisotropy, which may reflect the organ's microcirculation.

Susceptibility-weighted imaging (SWI) compared to T2* mapping in the presence of hepatic steatosis and fibrosis

V. C. Obmann, N. Mertineit, A. Berzigotti, C. Marx, L. Ebner, M. Ith, J. T. Heverhagen, A. Christe, A. Huber; Bern/CH

Purpose: To show that both susceptibility weighted imaging (SWI) and T2*-mapping are dependent on liver steatosis, which should be taken into account when using these parameters to grade liver fibrosis and cirrhosis.

Methods and Materials: 184 patients without focal liver disease underwent multiparametric MRI at 3T including susceptibility weighted imaging (SWI), T1/T2* mapping, proton density fat fraction (PDFF) quantification and MR elastography. SWI, T2* and T1 measured in the liver (4 locations), as well as their liver-to-muscle-ratio (LMR, measured in the paraspinal muscles) were compared between patients with different steatosis grades (PDFF < 5 %, 5 – 10 %, 10 – 20 % and > 20 %) and between patients with normal, slightly and moderately increased liver stiffness (< 2.8 kPa, 2.8 – 3.5 kPa and > 3.5 kPa, respectively). For statistics, ANOVA with Bonferroni-corrected post-hoc tests, as well as multivariate analysis were used.

Results: Both SWI (98 ± 30, 89 ± 26, 65 ± 33, 42 ± 16) and T2* (22 ± 4, 19 ± 5, 17 ± 4, 15 ± 2) were highly dependent on the degree of liver steatosis (p < 0.001). In Bonferroni-corrected post-hoc analysis, SWI showed significant differentiation in 4/6 comparisons, while T2* was significant in 3/6 comparisons. However, SWI allowed a better differentiation between liver fibrosis grades (p < 0.001) than T2* (p = 0.05). The liver-to-muscle ratios (LMR) were not superior to the respective parameters alone. Best prediction of liver fibrosis could be achieved by including PDFF, age, T1 and SWI in a multiparametric model (combined r^2 = 0.44).

Conclusion: Both SWI and T2*-mapping are highly dependent on liver steatosis grades. Nevertheless, both parameters are useful predictors for liver fibrosis when using a multiparametric approach.

2-Dimensional shear wave elastography for clinically significant liver fibrosis grading: Prospective comparison to magnetic resonance elastography and establishment of a cutoff value

I. Durot, T. Liang, J. Rosenberg, A. Loening; Stanford/US

Purpose: To assess the reliability of liver stiffness measurements obtained from two-dimensional (2D) shear wave elastography (SWE), and compare these measurements to MR elastography (MRE) to obtain a reference cutoff value for differentiating clinically non-significant from significant liver fibrosis.

Methods and Materials: The liver stiffness of 58 patients who had undergone MRE for different indications was assessed with 2DSWE (Philips ElastQ; Epiq7). Several 6-second cine loops with real time stiffness color maps were captured in the right liver lobe during shallow breath hold. Next, 10 circular ROIs ($0.791\,cm^2$) were retrospectively drawn 2 cm deep to the liver capsule. The relationship between MRE and 2DSWE stiffness was tested using a linear regression model. The best cutoff value was obtained by fitting a logistic regression model using a binary classification of the MRE data as the outcome and the observed 2DSWE measurements as the predictor.

Results: IQR/median for all patients were low (0.16 ± 0.07) and no patient was excluded due to an unreliable ultrasound exam. The correlation between expected and observed measurements from 2DSWE and MRE had an R^2 of 0.65. An optimal grading between non-significant and significant liver fibrosis was achieved with the ultrasound cutoff value in the range of 7.5–8.5 kPa, with accurate grading in 54/58 patients (93.1%; 95% CI: 83.3%–98.1%), a sensitivity of 76.5% (95% CI: 50.1%–93.2%), and specificity of 100% (97.5% CI: 91.4%–100%).

Conclusion: 2DSWE reliably measures liver stiffness with moderate correlation with MRE. A 2DSWE cutoff value of 7.5–8.5 kPa for Philips systems can differentiate non-significant from significant liver fibrosis with high accuracy.

Accuracy of GD-EOB-DTPA enhanced MRI for the diagnosis of liver metastases from neuroendocrine tumors

R. H. Hayoz, N. Vietti Violi, J.-F. Knebel, R. Duran, C. Dromain; Lausanne/CH

Purpose: To compare the diagnostic accuracy of dynamic phases, hepatobiliary phase (HBP), after Gd-EOB-DTPA enhanced MRI and diffusion weighted (DW) for the detection of liver metastases from neuroendocrine tumors.

Methods and Materials: After obtaining the approval from the ethical committee of research, 67 patients (mean age: 60 years, range: 18–84 years) were included in this retrospective study. All patients underwent MRI with injection of Gd-EOB-DTPA for suspected liver metastases. Four imaging sets were compared (DWI, HBP, combined DWI + HBP and T2W MRI) by three experienced radiologists with different level of experience. Lesions were evaluated on a 3-point scale. Sensitivity and specificity was calculated for each imaging set. Gold standard was based on histopathological results when available or the interpretation of previous follow-up imaging. Interreader agreement was evaluated by interclass-correlation (ICC). Univariate logistic regression was performed to evaluate lesion criteria such as ADC value, lesion size and enhancing pattern on dynamic sequences.

Results: 618 lesions (545 metastases, 73 benign lesions) were identified. The combined reading of DWI and Gd-EOB-DTPA enhanced MRI led to a significantly higher detection rate of lesion compared to the three other imaging sets (sensibility: 86%, specificity: 94%). Interreader agrement was highest in HBP enhanced (0.96 (0.94–0.97)(CI: 95%), followed by DWI and HBP. High ADC, increasing lesion size and hypervascular enhancing pattern lowers the risk of misinterpretation malignant lesion.

Conclusion: Associating DWI to HBP after Gd-EOB-DTPA enhanced MRI increases diagnostic accuracy in patients with neuroendocrine liver metastases suggesting the potential use of fast MR protocol with pre-injection of Gd-EOB-DTPA.

Reproducibility of fully automated liver volumetric analyses with Artificial Intelligence: Towards laboratory radiology

D. J. Winkel, H.-C. Breit, T. J. Weikert, B. Stieltjes; Basel/CH

Purpose: Laboratory radiology conveys the vision of a norm-based quantitative disease-detection in radiology. Thereto, automated imaging quantification pipelines are mandatory both for large scale norm-collective creation and disease related outlier detection. Here, we test such a pipeline in terms of reproducibility using an AI-based algorithm trained for liver volumetric analyses.

Methods and Materials: Using a RIS/PACS search engine, we obtained 100 CT datasets with six series for each patient: non-contrast (nc), portalvenous (pv) and arterial phase (art) with both 1.5 mm and 5 mm slices thickness. The data was analyzed using multi-scale deep-reinforcement learning for 3D body markers detection and adversarial deep image-to-image learning for 3D anatomical structure segmentation. Variations of liver volumes were compared using Cohen`s coefficient K. Variations of liver volumes were compared using univariate general linear model analyses with the liver volume as the dependent variable and contrast-phase and slice thickness as fixed factors.

Results: The liver volumes for the different scan phases, averaged for 1.5 and 5 mm, were 1902.63 ± 599.54, 1908.13 ± 585.33 and 1927.62 ± 594.65 ml (nc, pv, art). The two cycles of analysis yielded identical liver volumes for the given datasets (K = 1). The liver volume was neither dependent on the contrast phase (p = 0.938) nor on the slice thickness (p = 0.605).

Conclusion: Fully automated AI-based liver volumetry is a reproducible and precise method. The results provide the necessary confidence for future applications of automated abdominal organ volumetric analyses in the sense of laboratory radiology.

Evaluation of an AI-based detection of acute findings in abdominal CTs: Towards an automated work list prioritization of routine CT exams

D. J. Winkel, T. Heye, T. J. Weikert, D. T. Boll, B. Stieltjes; Basel/CH

Purpose: To test the diagnostic performance of a deep learning-based triage system for the detection acute findings in abdominal computer tomography (CT) examinations.

Methods and Materials: Using a RIS/PACS search engine, we obtained 100 abdominal CTs with at least one of the following findings: free-gas, free-fluid or fat-stranding and 100 control cases with absence of the listed findings. The CT data was analyzed using a convolutional neural network-algorithm, previously trained for detection of these findings on an independent sample. The validation of the results was performed on a web-based feedback-system by one radiologist without prior knowledge of image findings through visual confirmation and in comparison with the radiological report. Measures of diagnostic accuracy were then calculated.

Results: 194 cases were included in the analysis, 6 excluded because of technical problems during the extraction of the DICOM datasets from the local PACS. Overall, the algorithm achieved a 93% sensitivity (91/98, 7 FN) and 97% specificity (93/96, 3 FP) in the detection of acute abdominal findings. Intraabdominal free gas was detected with a 92% sensitivity (54/59) and a 93% specificity (39/42), free fluid with a 85% sensitivity (68/80) and a 95% specificity (20/21) and fat stranding with a 81% sensitivity (42/50) and a 98% specificity (48/49). False-positive results were due to streak artifacts, partial volume effects and a misidentification of a diverticulum (each n = 1).

Conclusion: The algorithm's autonomous detection of acute pathological abdominal findings demonstrated a high diagnostic performance, enabling guidance of the radiology workflow towards prioritization of abdominal CT examinations with acute life-threatening conditions.

With regard to the future of radiology, medical students fear Artificial Intelligence, while radiologists fear other disciplines

J. van Hoek, A. Leichtle, A. Huber, D. Hilt, A. Pöllinger; Bern/CH

Purpose: To evaluate the views of radiologists, surgeons and medical students on artificial intelligence (AI) and other potential threats to radiology.

Methods and Materials: An online questionnaire was created using the SurveyMonkey platform aimed at radiologists and surgeons throughout the German speaking part of Switzerland and medical students enrolled at the University of Bern. The questionnaire was divided into a general section and profession-adapted sections. A total of 170 people participated in the survey (59 radiologists, 56 surgeons and 55 students). Statistical analysis was carried out using the Kruskal-Wallis test with Dunn's multiple comparison post-hoc tests.

Results: Across all professions, the majority of participants agreed with potential positive support through AI in radiology (Likert scale 0–10: Mean value 7.34). Students saw a potential threat from AI as more likely than radiologists did (students: 0.42 vs radiologists: −1.85, p=0.0413). When asked whether they were concerned about "turf losses" from radiology to other disciplines, radiologists were much more likely to agree than students (students: −1.31 vs radiologists: 1.7; p<0.001). Of the students that do not want to get into radiology, 25.5% said that AI was one of the reasons.

Conclusion: With regard to AI, radiologists expect their workflow to become more efficient and their work more accurate. Students on the other hand, see AI as a potential threat to radiology. This result is worrisome, as students might not choose radiology as a career path. A better education about this supposed fear seems to be necessary.

Structured reporting: Evolution on a 20 year period in a multicenter radiology group

D. Fournier[1], P. Benedict[2], H. Brat[1], B. Rizk[3], G. Sgourdos[4], J.-M. Steity[5], L. Omarini[6], T. Zand[6]; [1]Sion/CH, [2]Morges/CH, [3]Villars-sur-Glâne/CH, [4]Lausanne/CH, [5]Vevey/CH, [6]Geneva/CH

Purpose: To demonstrate the evolution of radiologic reporting, over a 20-year period, from free-text reports to Structured Reports (SR) in a multicenter private radiology group.
To underline the main advantages for all concerned persons.

Methods and Materials: Improvements from free-text reports to the current structured standardized reporting were: a basis of 96 templates, covering the different types of imaging examinations clear layout with 3 main sections: indication, description, conclusion organ based section for description standardized pre-written normal findings (to be modified when indicated) optimisation of alignment of the paragraphs highlighting abnormal findings in italic key-images illustrating the abnormalities permanent radiologist's consciousness fulfilling the quality requirement: less is more concise and precise style avoiding unnecessary words RIS-PACS integration SSR quality checklist for the radiologist Voice recognition integration

Results:

1. Positive impact on patient care: Report simplicity Comprehensive interpretation Relevant conclusion Diagnostic accuracy Follow-up reproducibility Referring doctors' satisfaction
2. Improvement of communication: Improved readability Easier understanding for the referring doctor the radiologist performing follow-up examinations the patient Direct access to RIS-PACS for images and reports
3. Impact on staff: Less text typing errors Workflow improvement Follow-up facilitated Awareness for guidelines
4. Impact on management: Strengthening of professional self-regulation Risk reduction in complaints Improved cost/clinical effectiveness Quality control evaluation

Conclusion: Choosing to introduce structured reporting in our radiologic group 20 years ago, allowed us, with permanent improvement, to increase readability, simplicity, accuracy, reproducibility and quality of our radiologic reporting, for everyone's satisfaction.

Subspecialization in radiology: Effects on the diagnostic spectrum of radiologists and report turnaround time in a Swiss university hospital

T. P. Meyl[1], M. de Bucourt[2], A. Huppertz[2], J. T. Heverhagen[1], M. H. Maurer[1]; [1]Bern/CH, [2]Berlin/DE

Purpose: To analyze the changes in radiologists' work profiles and the reporting time after the implementation of a professional subspecialization in the radiology department of a Swiss university hospital.

Methods and Materials: In a retrospective analysis, the overall number of different radiologic examinations performed in the department of radiology of a large Swiss university hospital were documented for 2014 and 2016 before and after the implementation of subspecialized reporting (subspecialities: abdominal, musculoskeletal, cardiothoracic, emergency, and pediatric imaging) in May 2015. For six selected radiologists the number and types of reported examinations as well as the related radiology report turnaround times (RTATs) were analyzed in detail and compared between the two one-year periods.

Results: Overall, there was a significant increase of 10.3% in the total number of examinations performed in the whole department in 2016 compared with 2014. For 4 of the 6 radiologists, the range of different types of examinations significantly decreased with the introduction of subspecialized reporting (p<0.05). Furthermore, there was a significant change in the subset of the ten most commonly reported types of examinations reported by each of the 6 radiologists. Mean overall RTATs significantly increased for 5 of the 6 radiologists (p<0.05).

Conclusion: Implementation of subspecialized reporting led to a change in the structure and a decrease in the range of different examination types reported by each radiologist. Mean RTAT increased for most radiologists. Subspecialized reporting allows the individual radiologist to focus on a special field of professional competence but can result in longer overall RTAT.

Deep learning for automatic quantification of rotator cuff muscle degeneration from shoulder CT datasets

E. Taghizadeh[1], O. Truffer[1], S. Eminian[2], S. Gidoin[2], F. Becce[2], A. Terrier[2], A. Farron[2], P. Büchler[1]; [1]Bern/CH, [2]Lausanne/CH

Purpose: We aimed to propose and evaluate a deep-learning method for automatically quantifying the degeneration of rotator cuff muscles on shoulder CT images.

Methods and Materials: The presumed contours of healthy/premorbid rotator cuff muscles from 127 patients scanned with CT during preoperative planning for shoulder arthroplasty were manually drawn by three independent musculoskeletal radiologists on standardized sagittal-oblique CT sections. These premorbid muscle segmentations were also predicted by a deep convolutional neural network (CNN), following a 5-fold cross-validation to iteratively train and test the CNN based on the three manual segmentations. Automatic segmentations from the CNN were evaluated against reference segmentations for each muscle created by aggregating the three manual segmentations using an expectation-maximization algorithm. Automatically predicted premorbid segmentations were then used to quantify the ratio of muscle atrophy, fatty infiltration, and overall muscle degeneration. Automatic results for each of these parameters were compared with values obtained semiautomatically by radiologists.

Results: Average Dice coefficients for automatic segmentations with the CNN ($89\% \pm 9\%$) were comparable with manual segmentations ($89\% \pm 6\%$). No significant differences were found for the subscapularis, supraspinatus, and teres minor ($p \geq 0.120$), while Dice coefficients were significantly higher for automatic segmentations of the infraspinatus ($p = 0.012$). The automatic method was able to provide comparable and reliable estimates of muscle atrophy ($R^2 = 0.87$), fatty infiltration ($R^2 = 0.91$), and overall muscle degeneration ($R^2 = 0.91$).

Conclusion: Deep learning allows rapid automatic quantification of rotator cuff muscle atrophy, fatty infiltration, and overall degeneration from shoulder CT datasets, with diagnostic accuracy comparable to human observers.

Automatic detection of distal radius fractures in X-Ray images using deep learning

C. Blüthgen, I. Vittoria de Martini, A. Meier, A. S. Becker, T. Frauenfelder; Zurich/CH

Purpose: To evaluate the diagnostic performance of a multi-purpose, deep-learning based image analysis software for the detection of radius fractures.

Methods and Materials: 624 radiographs of patients with suspected radius fractures were labeled for the presence of radius fractures, using CT confirmation in uncertain cases. Data was split into training and test sets (85/15%). The DLS was trained on the training set and subsequently used to classify the radiographs in the test set, yielding a score (range 0–1) for each image. ROC analysis was used to estimate the performance. Sensitivity and specificity were calculated (Youden Index). Finally, the test set was evaluated by three radiologists with 2–16 years of experience. To estimate the generalization capacity of the DLS, radiographs from an openly available external dataset (MURA v1.1) were analyzed in the same way.

Results: The diagnostic performance of the software on the test set was excellent with an AUC of 0.94 (95% CI 0.89–0.97). Sensitivity and specificity of the software at the optimal threshold were calculated to be 86% and 81%, respectively. The most experienced radiologist showed a higher sensitivity and comparable specificity (Sensitivity 96%, Specificity 83%, $p = 0.549$), but outperformed the DLS significantly on the external dataset (97% Sensitivity/94% Specificity vs 88%/75%, $p < 0.001$).

Conclusion: The software was able to detect wrist fractures with sensitivity and specificity comparable to a radiology resident but was outperformed significantly on external validation data. Heatmaps created by the DLS were a useful visual feedback to validate the predictions.

Prevalence of pseudoerosions of the hand and wrist: Ultrasound findings in 100 asymptomatic volunteers

A. L. Falkowski[1], J. A. Jacobson[2], V. Kalia[2], A. Atinga[3], G. Gandikota[2], R. G. Thiele[4]; [1]Basel/CH, [2]Ann Arbor/US, [3]Toronto/CA, [4]Rochester/US

Purpose: Cortical erosions can indicate inflammatory arthritis. While cortical depressions have been described in several metacarpal heads simulating erosions, we have noted similar "pseudoerosions" more frequently and also present at the wrist. The purpose was to evaluate the frequency and location of pseudoerosions in asymptomatic volunteers.

Methods and Materials: After IRB approval and obtaining informed consent, 100 subjects without hand or wrist symptoms were prospectively examined bilaterally with ultrasound. Dorsal metacarpal heads, lunate, triquetrum, and distal ulna were examined. Cortical depressions were characterized with regard to location (central, marginal, both), morphology (irregularity, ring-down artifact), and dimensions (length and depth) by two fellowship-trained musculoskeletal radiologists in consensus.

Results: 52 male and 48 female subjects were included (mean age: 47 ± 16 years). Metacarpal (MC) heads showed a central pseudoerosion in various frequencies (MC1: 22%; MC2: 92%; MC3: 86%; MC4: 60%; MC5: 81%). One marginal erosion was present at a MC5 and a marginal plus central at a MC2. Pseudoerosions were present at the lunate (82%), triquetrum (84%), and distal ulna (20%), and were multiple (lunate: 40%; triquetrum: 27%; ulna: 5%). Ring-down artifact (30–50%) was present more than cortical irregularity (13–28%). Mean pseudoerosion length and depth of MC was 3 mm (range: 0.6–9 mm) and 0.7 mm (range: 0.2–8 mm). Dimensions for pseudoerosions varied slightly for the lunate (length: 2.1 mm; depth: 0.8 mm), triquetrum (length: 1.7 mm; depth: 1 mm), and ulna (length: 1.7 mm; depth: 1.1 mm).

Conclusion: Pseudoerosions are a typical finding of metacarpal heads, lunate, triquetrum, and distal ulna in asymptomatic patients and should not be misinterpreted as inflammatory arthritis.

The role of MR imaging in complex regional pain syndrome revisited

C. A. Agten, A. Kobe, I. Barnaure, J. Galley, C. W. Pfirrmann, F. Brunner; Zurich/CH

Purpose: To assess different MRI features in patients with suspected CRPS (complex regional pain syndrome).

Methods and Materials: A retrospective health-record search was conducted. Fifty patients with suspected CRPS were included (37 female (51 ± 13 years) and 13 males (44 ± 15 years)). CRPS diagnosis was made using modified Budapest-criteria. Alternative diagnoses were noted. All patients underwent MRI including gadolinium application and dynamic MR-angiography. Two radiologists assessed MRI: skin (thickness, enhancement, subcutaneous edema); bone (number of bones with edema, bone marrow edema pattern, subcortical enhancement, periosteal enhancement); soft tissue (muscle edema, angiography perfusion pattern, joint effusion). MRI parameters were compared between CRPS patients and non-CRPS patients.

Results: CRPS was diagnosed in 22/50 (44%) patients and non-CRPS in 28/50 (56%) patients. Skin thickness (1.9 ± 0.5 mm vs 1.7 ± 0.3 mm, $p = 0.399$), enhancement and subcutaneous edema showed no differences between CRPS and non-CRPS patients. Bone marrow edema presence and pattern were not different between groups. 45–50% of CRPS patients showed no bone marrow edema. Subcortical enhancement and periosteal enhancement were not different between groups. For reader 1, muscle edema score was higher in the non-CRPS group compared to the CRPS group (0.1 ± 0.2 vs 0.6 ± 1.0, $p = 0.008$), but not different for reader 2 (0.1 ± 0.5 vs 0.2 ± 0.8, $p = 0.819$). Perfusion pattern was more extensive in non-CRPS patients for reader 1 ($p = 0.048$), but not for reader 2 ($p = 0.157$). Joint effusions showed no difference between groups.

Conclusion: CRPS is a clinical diagnosis. MRIs role in CRPS is to exclude differential diagnoses.

Cartilage icing and chondrocalcinosis in the differentiation between gout and pseudogout on radiographs

A. L. Falkowski[1], J. A. Jacobson[2]; [1]Basel/CH, [2]Ann Arbor/US

Purpose: Double-contour sign or crystal "icing" of cartilage is a described ultrasound finding in gout. Additionally, chondrocalcinosis is most often described with pseudogout or CPPD. The purpose of the study was to determine if cartilage-icing and distribution of chondrocalcinosis on radiographs can differentiate between gout and pseudogout.

Methods and Materials: IRB approval was obtained and informed consent was waived for the retrospective study. Electronic medical records from >2.3 million patients were searched for key words "gout", "pseudogout", "CPPD", "joint aspiration", and their combinations. Only aspiration-proven cases of gout or CPPD were included. Knee radiographs from these subjects were reviewed in consensus by two fellowship-trained musculoskeletal radiologists in randomized order, blinded to the patients' diagnosis, for the presence or absence of cartilage icing and chondrocalcinosis for each meniscus and hyaline cartilage (medial, lateral, anterior, and posterior compartments). Descriptive statistics, sensitivity, specificity, positive and negative predictive value were calculated.

Results: 55 patients were evaluated (34 male, 25 female; mean age 66 ± 13 years) with 36 having an aspiration-proven diagnosis of pseudogout and 19 of gout. Cartilage icing was more common in pseudogout (3–36%) than gout (0–21%). Chondrocalcinosis had a positive predictive value of 89–100% to distinguish pseudogout from gout (100% at the lateral compartment) with only one gout patient showing chondrocalcinosis.

Conclusion: While crystal cartilage-icing is not helpful in differentiating gout from pseudogout, the finding of chondrocalcinosis, especially laterally involving the hyaline cartilage and meniscus, showed 100% positive predictive value in differentiating pseudogout from gout.

To biopsy or not to biopsy? – Decision support based on a simple quantitative approach differentiating between subfascial lipoma and atypical lipomatous tumor/well-differentiated liposarcoma on MRI

R. Donners, D. Baumhoer, A. Krieg, D. Harder; Basel/CH

Purpose: To provide MRI based quantitative decision support when to biopsy subfascial lipomatous tumors.

Methods and Materials: MRI of 100 histopathologically proven subfascial lipomas(n=75) and atypical lipomatous tumors/well-differentiated liposarcomas(ALT/WDL) (n=25) were reviewed retrospectively. Exclusion criteria were mass-like non-lipomatous soft tissue components, suprafascial and intraabdominal location. Ratios derived from region of interest based signal intensity (SI) measurements of tumor and adjacent fat on T2 fat saturated(FS) images were calculated(=mean SI_{tumor}/mean $SI_{adjacent-fat}$). Univariate regression analyses were applied and a p-value <0.01 deemed significant. The discriminatory ability was assessed by ROC curve analyses. Interreader agreement was evaluated by calculation of intraclass correlation coefficients (ICC). Tumor size, location, septation and patient demographics were noted.

Results: T2 FS ratios performed well discriminating lipoma from ALT/WDL (p<0.001, area under the ROC curve (AUC)=0.89, cut-off=1.22, specificity=88%, sensitivity=80%). A T2 FS ratio >1.37 indicated ALT/WDL with 95% specificity and 64% sensitivity. Interreader agreement was excellent (ICC=0.924). ALT/WDL were significantly larger than lipoma (p<0.001, AUC=0.87, cut-off=11cm, 92% specificity, 72% sensitivity). Combination of a T2 FS ratio <1.22 and size <13cm as decision support would have spared 61% of lipoma patients from biopsy (combined specificity=98%, sensitivity=60%). Qualitative imaging parameters and patient demographics did not differ significantly (each p>0.022).

Conclusion: Lipomatous subfascial tumors with a T2 FS ratio <1.22 and size <13cm are most likely benign and may not require histologic confirmation. Lipomatous tumors with a T2 FS ratio >1.37 should be biopsied regardless of size.

CT-based texture analysis of cartilaginous bone tumors for differentiation of enchondroma from low-grade chondrosarcoma and low-grade from high-grade chondrosarcoma

B. Fritz, S. Fröhlich, D. Müller, R. Sutter, C. W. Pfirrmann; Zurich/CH

Purpose: To assess the diagnostic accuracy of 2D CT-based texture analysis (TA) for differentiation of enchondroma from low-grade chondrosarcoma and for differentiation of low-grade from high-grade chondrosarcoma.

Methods and Materials: This retrospective study included 65 patients with cartilaginous bone tumors (18 enchondroma, 23 low-grade and 24 high-grade chondrosarcoma). Enchondromas were proven by either histopathology or a follow-up of at least 5-years with unchanged size and shape, chondrosarcomas were proven by histopathology. TA was performed by 2 readers in consensus by segmentation of the tumor on the axial CT-slide showing the largest tumor area using freeware quantitative analysis software. Nine quantitative TA-parameters were evaluated (Mean, Variance, Skewness, Kurtosis, RunLenghtNonuniformity, Grey-LevelNonuniformity, LongRunEmphasis, ShortRunEmphasis, Fraction). Univariate, multivariate and ROC-analysis were performed. p-values of <0.05 were considered statistically significant.

Results: For differentiation of enchondroma from low-grade chondrosarcoma significant differences were found for GreyLevelNonUniformity (p=0.001), ShortRunEmphesis (p=0.043) and Fraction (p=0.012) after univariate analysis. Multivariate analysis revealed GreyLevelNonUniformity and Fraction as independent predictors for differentiation of enchondroma from low-grade chondrosarcoma with an odds ratio of 1.006 and 0.004 and p-values of 0.019 and 0.03, respectively. ROC-analysis showed an area under the curve of 0.882 (95% CI: 0.778–0.986) with sensitivity of 78.3% and specificity of 88.9%. For differentiation of low-grade from high-grade chondrosarcoma no significant TA-parameters existed after univariate analysis (p>0.3).

Conclusion: CT-based TA has the ability to differentiate enchondroma from low-grade chondrosarcoma with good diagnostic accuracy, possibly adding additional benefit to morphologic analysis.

Can portable ultrasound replace conventional non-portable ultrasound for musculoskeletal imaging?

A. L. Falkowski[1], J. A. Jacobson[2], V. Kalia[2]; [1]Basel/CH, [2]Ann Arbor/US

Purpose: The purpose of this study was to evaluate portable hand-held ultrasound in comparison to conventional non-portable ultrasound in the musculoskeletal system.

Methods and Materials: IRB approval was obtained for this prospective study. 100 consecutive patients with informed consent were imaged using both portable (Lumify, Philips) and non-portable (Epiq, Philips) ultrasound equipment using 12MHz linear transducers. Agreement in ultrasound diagnosis was documented, as well as expected clinical changes in outcome if disagreement (definitely no, probably no, uncertain, probably yes, definitely yes). Imaging details of disagreement cases were also recorded. Descriptive statistics were calculated.

Results: 42 male and 58 female subjects were included (mean age: 53 ± 13 years). Anatomical areas scanned were shoulder (30 cases), elbow (11), hand and wrist (15), hip (10), knee (11), foot and ankle (12), and others (11). Scanning with conventional ultrasound revealed pathology in 92%. Agreement in diagnosis made between portable versus non-portable ultrasound was found in 64%, and disagreement in 36%. In 75%, the use of conventional non-portable ultrasound resulted in no change in clinical outcome. In 14%, there was probably no change in outcome, 4% uncertain change, 7% probable change, and 0% definite change in clinical outcome. The diagnoses changing management included: non-detection of a satellite nodule (1), cyst (2), hernia (1), hydroxyapatite deposition disease (1), and underestimated/overlooked tendon tears (2).

Conclusion: Portable ultrasound was able to provide a musculoskeletal diagnosis in 89% of subjects that did not change clinical management compared with conventional non-portable ultrasound.

Comparison of bone imaging between cone-beam CT and ultrashort echo time MR imaging in patients with medication related osteonecrosis of the jaw

F. A. Huber, P. Schumann, J. von Spiczak, R. Guggenberger; Zurich/CH

Purpose: to compare bone imaging between ultrashort echo time (UTE) MR and cone beam computed tomography (CBCT) in patients with medication-related osteonecrosis of the jaw (MRONJ).

Methods and Materials: Retrospective, blinded analysis of CBCT and UTE MR images from patients with histologically confirmed MRONJ of the mandible was performed by two independent radiologists. Osteolysis, periosteal thickening and osteosclerosis as MRONJ hallmarks were rated visually ('0'='physiologic', '1'–'3'='mild'–'severe' changes) for defined mandibular regions. Additionally, standard segmentation of predefined mandible regions were performed on co-registered CBCT/UTE images for ensuing quantitative comparison of grey values (GV) from CBCT and signal intensity (SI) from MR images. Interreader/-method agreement (Cohen's Kappa), diagnostic performance, t-testing and Pearson's correlation of different modalities were used for statistical analysis.

Results: Seven patients were included, undergoing both examinations within 17 ± 9 (mean$\pm$SD) days. The region of anterior mandible was most often affected by MRONJ (p<.001). Overall interreader agreement of qualitative scores was substantial (.67). There were no significant differences between modalities, respectively. Intermethod agreement was substantial for both readers (k=.613 and .699). SI/GV MRONJ-affected areas differed significantly from healthy bones, but not between modalities for both, MRONJ and healthy regions (r=.87; p<.001).

Conclusion: Qualitative assessment of mandibular bone in MRONJ with UTE MR sequences can be equally well performed as with the reference standard CBCT. Quantitative image findings of both modalities significantly and strongly correlate with each other. UTE MR imaging in MRONJ allows thorough interpretation of boney disease extent without ionizing radiation.

Ultrashort time to echo magnetic resonance imaging at 3T for the detection of spondylolysis in cadaveric spines – Comparison with CT

T. Finkenstaedt[1], P. Siriwanarangsun[2], S. Achar[3], M. Carl[3], S. Finkenstaedt[3], N. Abeydeera[3], C. Chung[3], W. C. Bae[3]; [1]Zurich/CH, [2]Bangkok/TH, [3]San Diego/US

Purpose: To compare the diagnostic performance and confidence of conventional, optimized, and ultrashort time to echo (UTE) MR protocols for detection of simulated spondylolysis.

Methods and Materials: Four human lumbar spine specimens with 46 individual pars interarticularis were randomly left intact (n=26) or osteotomized (n=20) using a 1-mm oscillating microsurgical saw. The specimens were imaged using a CT scan along with 3 "Tiers" of MR protocols: Tier 1, conventional; Tier 2, optimized conventional protocol consisting of axial/sagittal-oblique sequences; Tier 3, a sagittal UTE MR sequence. Two blinded readers evaluated each individual pars using a 4-point scale (1=spondylolysis certainly absent, 2=probably absent, 3=probably present, 4=certainly present). For each imaging protocol, diagnostic performance (sensitivity/specificity) and confidence were compared using McNemar test (surgical osteotomy served as reference).

Results: Diagnostic performance was moderate for Tiers 1/2, with a moderate sensitivity (0.70–0.75) and high specificity (1.00). In contrast, CT and Tier 3 UTE MR imaging had both high sensitivity (1.00) and specificity (1.00). The sensitivities of CT or Tier 3 were statistically greater than Tier 1 sensitivity (p=0.041) and almost greater than Tier 2 (p=0.074). Diagnostic confidences of CT or Tier 3 were much greater: Both Tiers 1 and 2 had a large percentage of uncertain (>60%, p<0.001) or wrong interpretations (>10%, p<0.001), unlike CT or Tier 3 (0% uncertain/wrong interpretations).

Conclusion: Detection of spondylolysis using a single sagittal UTE MR sequence is superior in performance and confidence to conventional and optimized MR protocols, whereas matching those from CT evaluation.

Ultrashort time to echo (UTE) MR evaluation of calcium pyrophosphate crystal deposition (CPPD) in human menisci

T. Finkenstaedt[1], R. Biswas[2], N. Abeydeera[2], P. Siriwanarangsun[3], R. Healey[2], S. Statum[2], W. C. Bae[2], C. Chung[4]; [1]Zurich/CH, [2]San Diego/US, [3]Bangkok/TH, [4]Solana Beach/US

Purpose: In human menisci, investigate whether calcium pyrophosphate crystal deposition (CPPD) affects biomechanical and quantitative MR properties, and their zonal distribution.

Methods and Materials: From nine cadaveric knees, anterior and posterior horn menisci were harvested and classified into "Normal" or "CPPD" groups based upon visual inspection. Micro-CT scan verified CPPD. Using MRI, ultrashort echo time (UTE) T2* and spin echo (SE) T2, quantitative values in three zones (red/red-white/white) were determined. Using biomechanical test, indentation forces (g) in the same zones were determined. Effects of CPPD and meniscal zone on indentation force and quantitative MR values were compared.

Results: On UTE MR images, CPPD-affected menisci exhibited punctate dark regions, found mostly (92%) in avascular white and red-white zones. Indentation forces were significantly higher for CPPD samples in the red-white (all p<0.02) and white (all p<0.004) zones but not in the vascular red zone (all p>0.2). Similarly, UTE T2* red zone values were similar between both groups (~6.6ms, p=0.8) while in the red-white and white zones, CPPD samples had significantly lower values (~5.1ms, p=0.005–0.007). In contrast, SE T2 values showed no difference with CPPD (p=0.12–0.16). UTE T2*, but not SE T2, correlated significantly with indentation force (R=−0.29, p=0.009).

Conclusion: Dark CPP deposits were detectable on UTE images featuring high signal intensity from surrounding meniscal tissue. Localization of CPPD in the avascular zones was a novel finding. Compared to normal, CPPD menisci featured higher indentation stiffness and lower UTE T2* values in the affected zones.

Lung cancer screening with ultralow dose chest CT: Potential pitfalls of pulmonary findings in different readers with various experience levels

K. Martini[1], *T. Ottilinger*[2], *B. L. Serrallach*[2], *S. Markart*[2], *N. S. S. Glaser-Gallion*[2], *C. Blüthgen*[1], *S. Leschka*[2], *R. W. Bauer*[2], *S. Wildermuth*[2], *M. A. Messerli*[1]; [1]*Zurich/CH*, [2]*St. Gallen/CH*

Purpose: To quantify the accuracy of ultralow-dose CT for lung cancer screening in radiologists with various experience-levels.

Methods and Materials: Six radiologists with different degrees of clinical experience in radiology (range 1–15 years), rated 100 ultralow-dose chest-CTs as either negative screening finding (no nodules), indeterminate finding (nodules 5-10mm), positive finding (nodules >10 mm). Each radiologist interpreted the scans randomly ordered and reading time for each scan was recorded. Reading time was correlated with reader experience using Pearson correlation. Interobserver agreement was assessed with a k-statistic. Nodule size agreement was calculated using the interclass-correlation-coefficient. Reasons for differences in nodule classification were analysed on a case-by-case basis.

Results: Mean overall reading time per scan was of 2 min 2 s (range: 7 s–7 min 45 s) and correlated with reader-experience (r=−0.824). In 46 patients, all radiologists agreed on the differentiation of negative (no further action required) and intermediate/positive finding (further work-up needed). In 45 cases disagreement between readers led to different nodule classification. In 34 of these cases disagreement led to different management: in 26 cases some readers rated the nodule as benign (N1–N3), while other rated the finding as intermediate – in other 7 cases some readers rated the nodule as benign, whereas others scored the case as positive. Overall, disagreement in nodule classification was mostly due to failure in identification of target lesion (n=40), lesion measurement (n=44) or missed calcium/fat-content (n=26).

Conclusion: Our study showed substantial interobserver variability for the detection and classification of pulmonary nodules in low-dose CT, which should be considered in surveillance recommendations and prognostic determination.

Pulmonary nodules in melanoma patients: Metastases?

S. Stadelmann[1], *C. Blüthgen*[1], *G. Milanese*[2], *T. D. L. Nguyen-Kim*[1], *T. Frauenfelder*[1], *M. Eberhard*[1]; [1]*Zurich/CH*, [2]*Parma/IT*

Purpose: To examine differences between benign pulmonary nodules (PN) and pulmonary metastases in melanoma patients with AJCC stage III or IV undergoing baseline staging CT.

Methods and Materials: In this IRB-approved study we retrospectively evaluated 236 patients (mean age: 57 years; range: 19–86 years) with a diagnosis of melanoma undergoing chest CT between 01/2010 and 12/2016 at the University Hospital Zurich. In patients with a follow-up period of at least 1.5 years, PN were evaluated for size, location, vessel or pleural attachment, morphology and multiplicity. PN with a significant size change within the follow-up period according to the definition of the Fleischner Society were judged as metastases. Differences of morphology and size were evaluated using the Fisher-Exact, Chi-Square- or the Mann-Whitney-U-test where appropriate. p<0.05 was considered statistically significant.

Results: 61% of patients (n=144) showed PN at baseline screening CT. 50 patients (mean age: 58 years; range: 39–82 years) were eligible for our study. In total, we evaluated 439 PN (1 to 78 PN per patient; 339 metastases), most of them located in the lower lobes and the middle lobe (n=298; 68%). 318 PN (72%) had an average diameter between 5 and 10 mm. Metastases were significantly larger at baseline CT (median: 6 mm, range: 1–24 mm) compared to benign PN (median: 4 mm, range: 1–30 mm) with p<0.001. Subsolid nodules (n=41) were more likely to be benign (p<0.001).

Conclusion: Our study showed that approximately three-quarter of PN found at baseline staging CT in advanced stage melanoma patients were metastases. Small and/or subsolid PN were more likely to be benign.

Evaluation of an AI-powered algorithm for the automated detection and 3D segmentation of primary tumours in NSCLC

T. J. Weikert[1], *M. Pradella*[1], *J. Sperl*[2], *F. Durlak*[2], *J. Cyriac*[1], *B. Stieltjes*[1], *G. Sommer*[1], *A. Sauter*[1]; [1]*Basel/CH*, [2]*Forchheim/DE*

Purpose: Manual tumour segmentation is time-consuming and cost-intensive, but mandatory for radiation treatment planning, therapy response monitoring or Radiomics. The purpose of this study was to assess the performance of an AI-based radiology assistant to automate this task.

Methods and Materials: We preselected 75 FDG-PET/CTs for non-small-cell lung cancer (NSCLC) staging from our RIS/PACS archive (all confirmed by histology, solid and peripheral T1/T2 stages). First, all main masses were fully segmented and annotated manually by a radiologist on the CT component. Lesion volumes were calculated. In parallel, the same series were fed into interlinked AI-algorithms applying deep convolutional neural networks for automated detection and segmentation. The intraclass correlation coefficient (ICC) for the detected volumes as measure of interrater reliability between manual and automatic analysis was calculated based on a single-rater, absolute agreement, 2-way random-effects model.

Results: The algorithm correctly detected 75 of 75 main lesions and attributed them to the respective lung lobe. Mean tumour volumes were: $6,810.52 \pm 8,353.53$ mm^3 for manual segmentation versus $7,105.45 \pm 8,989.48$ mm^3 for automated analysis. ICC was 0.956 (95% CI 0.931–0.972; p<0.001). Mean processing time of the algorithm was 64 ± 23 seconds compared to a mean of 342 ± 382 seconds for manual tumour segmentation.

Conclusion: The algorithm facilitates a fast and reliable detection and 3D segmentation of solid peripheral pulmonary T1 and T2 tumours. Further evaluation regarding the performance on advanced and more challenging tumours (T3/T4, central, subsolid) is warranted.

Automated detection of pulmonary embolism in CT pulmonary angiograms: Testing the diagnostic performance of a prototype algorithm

T. J. Weikert, *D. J. Winkel*, *J. Bremerich*, *B. Stieltjes*, *A. Sauter*, *G. Sommer*; *Basel/CH*

Purpose: To validate the performance of a deep convolutional neural network optimised for the detection of pulmonary embolism (PE) on CT pulmonary angiograms (CTPAs).

Methods and Materials: We downloaded all CTPAs performed in 2017 along with the corresponding reports (n=1,499) from our RIS/PACS archive using an in-house-developed search engine. The reports were manually reviewed by a radiologist. CTPAs with other clinical questions than PE or poor diagnostic quality were excluded. The remaining exams were then classified into positive (n=232) and negative (n=1,204) for PE. All emboli in positive exams were labeled by a radiologist using bounding boxes. The data served as ground truth for the external testing of a prototype algorithm (Aidoc, Tel Aviv, Israel) that had previously been trained on 28.000 independent CTPAs from other centers. The algorithm was a fully convolutional neural network with a backbone based on the Resnet architecture.

Results: The algorithm achieved a sensitivity of 93% and a specificity of 95%. This corresponds to a positive predictive value of 77%.

Conclusion: The algorithm we validated is capable of detecting pulmonary embolism in CTPAs with a high sensitivity and specificity. In a clinical setting, this can complement conventional workflows with a worklist prioritisation and has the potential to improve the quality of healthcare by accelerating the diagnostic process and communication. We plan to further test the algorithm and finally implement it in the clinical routine to perform prospective evaluations.

SS143

Automatic classification of breast background parenchymal enhancement

N. Berger, M. Marcon, A. Ciritsis, A. Boss, S. Stieb, C. Rossi; Zurich/CH

Purpose: High background parenchymal enhancement (BPE) in contrast-enhanced MRI is rated in the categories minimal, mild, moderate and marked. This tissue classification can be challenging. In this study we developed a deep convolutional neural network (dCNN) for the automatic classification of BPE according to the American College of Radiology Breast Imaging Reporting and Data System (ACR BI-RADS) Atlas.
Methods and Materials: Dynamic T1-weighted fat-suppressed 3D fast spoiled gradient-echo sequences were acquired before and after intravenous administration of gadolinium. Image subtraction was performed in 10147 original slices. A dCNN with 11 convolutional layers and 3 fully connected layers was trained and validated on an augmented dataset. A hierarchical approach was implemented for classification of each slice of the MRI volume. The first model was trained for the differentiation of slices including the breast from slices imaging the sole chest or both side breast implants. The second model was trained for BPE classification.
Results: For the first model, 200 epochs were necessary to achieve a validation accuracy of 84.9% and a training accuracy of 83.7%. The training of the model for BPE classification required 150 epochs. A validation accuracy of 84.8% was measured, while the training accuracy measured 78.3%.
Conclusion: BPE in breast-MRI based on the ACR BI-RADS system can be adequately classified by a dCNN. In future, it might be used as standardized and observer-independent BPE rating.

SS144

Diagnostic utility of breast DCE-MRI in patients with biopsy diagnosis of atypical ductal hyperplasia

V. Bertani[1], M. La Grassa[1], L. Balestreri[1], N. Berger[2], M. Urbani[1], T. Frauenfelder[2], A. Boss[2], M. Marcon[2]; [1]Aviano/IT, [2]Zurich/CH

Purpose: To evaluate the diagnostic utility of DCE-MRI in predicting upgrade to malignancy (UM) after a percutaneous biopsy (PB)diagnosis of ADH.
Methods and Materials: In this IRB approved study (January 2016 – December 2017) 68 women (median age, 51years; range 31–73years) with a PB diagnosis of ADH and subsequently undergoing DCE-MRI at 1.5 T were retrospectively included. PB was performed under stereotactic guidance using 8–11 gauge vacuum-assisted-biopsy (VAB)systems in case of mammography-only findings (40 lesions) or under ultrasound-guidance using 14 gauge core-needle-biopsy (CNB) (28 cases). All cases underwent surgical excision and final histologic diagnosis was recorded. Two radiologists in consensus evaluated: a) maximum diameter (MD) of the lesion in images prior to biopsy b) presence of a MRI-correlation to the lesion. MD and biopsy modality were compared in cases with/without MRI-correlation as well as with/without UM. Comparison between cases with/without MRIcorrelation and UM was also performed. Mann-Withney U test was used to compare median values and X2 to compare proportions.
Results: Median MD was 18mm (IQR 11–30mm, range 6–63mm) and 12mm (IQR 8–20mm, 6–40mm) for cases undergoing VAB and CNB, respectively (p =.054). A MRI-correlation was present in 17/40 (42.5%) and in 19/28 (67.8%) which underwent VAB and CNB, respectively (p =.081). 17/68 (25%) had UM: 13/17 (76.5%) low-and intermediate grade DCIS and 4/17 (23.5%) invasive carcinoma. 8/40 (20%) cases after VAB and 9/28 (32.1%) cases after CNB had UM (p = 0.272). All but two cases with UM had a MRI-correlation (88.2%) and both cases without were classified as low-grade DCIS (MD at surgical excision 3mm).
Conclusion: DCE-MRI can be used to predict UM after a PB diagnosis of ADH and should be used in lesion assessment to avoid unnecessary surgical procedures.

SS145

Outcome of microcalcifications classified as BI-RADS 3, 4a and 4b in patients with and without a history of breast cancer

M. Marcon[1], M. La Grassa[2], L. Balestreri[2], N. Berger[1], M. Urbani[2], K. Lång[3], T. Frauenfelder[1], A. Boss[1], V. Bertani[2]; [1]Zurich/CH, [2]Aviano/IT, [3]Villigen/CH

Purpose: To compare the outcome of microcalcifications classified as BI-RADS3, 4a and 4b at mammography in patients with a history of breast cancer to that of women undergoing mammography screening.
Methods and Materials: 176 patients (mean age 61 years) with microcalcifications classified as BI-RADS3, 4a and 4b, without sonographic correlation, whom had undergone vacuum-assisted biopsy (VAB) between Oct 2016 – Oct 2017 were retrospectively included. The agreement imaging/pathologic result from VAB was verified and for BI-RADS4b lesions and B2 pathologic result excisional biopsy was performed. For each BI-RADS category, pathologic results from VAB in case of B2diagnosis and from surgical specimens in all the other cases were compared between patients with a history of breast cancer(groupA, n =45) and women undergoing screening(groupB, n =131). Positive predictive values (PPVs) were compared using Fisher's exact test.
Results: A total of 73 lesions were classified as BI-RADS3 (41.5%), 57 BI-RADS4a (32.4%) and 46 BI-RADS4b (26.1%). The overall PPV for BI-RADS 3,4a and 4b were 5.5% (4/73), 10.5% (6/57) and 58.7% (27/46). The PPV for BI-RADS3 lesions in group A and B were 13.0% (3/23) and 2.0% (1/50), respectively (p = 0.089). The PPV for BI-RADS4a lesions in group A and B were 15.4% (2/13) and 9.1% (4/44), respectively (p = 0.611). The PPV for BI-RADS4b lesions in group A and B were 77.8% (7/9) and 54.0% (20/37), respectively (p = 0.270).
Conclusion: The likelihood of malignancy in cases of microcalcifications classified as BI-RADS 3, 4a and 4b at mammography tends to be higher in women with a history of breast cancer than in women undergoing screening, the difference was however not statistically significant.

SS146

Intraindividual comparison of breast radiation dose in conventional mammography and tomosynthesis

M. S. Vieira, N. Zuber, A. Mayor, G. Müller, M. K. Werner; Zurich/CH

Purpose: Compared to conventional mammography (2D), tomosynthesis generates a three-dimensional (3D) representation of the breast promising improved diagnostic performance. The aim of this study was to investigate whether female patients are exposed to a higher radiation dose when examined by an imaging protocol including tomosynthesis compared to conventional mammography technique only.
Methods and Materials: In this retrospective study, 93 consecutive female patients who were under active surveillance underwent mammography using two different imaging protocols on the same mammography unit (GE Senographe Pristina™) at two time-points. In the first examination the protocol consisted of 2D mediolateral oblique (MLO) and 2D craniocaudal (CC) views (conventional protocol). In the second examination within one year the imaging protocol consisted of 3D tomosynthesis in MLO combined with 2D mammography CC views (tomosynthesis protocol). Compressed breast thickness and density were taken into account and patients with intermittent surgery were excluded. Statistical significance was analyzed by using the robust Wilcoxon test.
Results: 176 breasts were examined in MLO views with both techniques and 114 breasts were examined in 2D CC views only. The average radiation dose of 3D tomosynthesis in MLO had a minimally smaller dose than 2D mammography in MLO *(3D MLO: 1.40mGy, 2D MLO: 1.44mGy, p = 0.002)*. The average dose of 2D mammography in CC views of both protocols showed no statistically significant difference *(p = 0.851)*.
Conclusion: For the tested mammography unit, the results demonstrate that 3D tomosynthesis and conventional mammography in MLO view is dose-neutral. Therefore, 3D tomosynthesis can be implemented in routine mammography imaging protocols without increasing radiation dose.

Evaluation of high-contrast spatial resolution and low-contrast detectability for the first clinical spiral breast CT: Evidence from a phantom study

S. S. Shim, N. Saltybaeva, N. Berger, M. Marcon, A. Boss, H. Alkadhi; Zurich/CH

Purpose: Recently introduced dedicated breast CT (BCT) systems have the potential to improve early detection of breast cancer compared to conventional techniques such as mammography and tomosynthesis. The aim of the study was to perform quantitative analysis of image quality of the first clinical spiral-BCT and to optimize scanner output parameters for efficient dose utilization.

Methods and Materials: A custom-made breast phantom with integrated microcalcifications (µCa) and tumor masses of different sizes was used for measurements on the BCT equipped with a CdTe photon-counting detector. The phantom consists of several slabs with diameters from 10–16 cm, representing different sizes of female breasts. Measurements were performed with a tube voltage of 60 kVp; tube currents were varied from 5 to 125 mA. Feldkamp-type filtered back-projection (FBP) algorithm with a smooth kernel and a voxel size of 50 µm³ and 300 µm³ was used for image reconstruction. The spatial resolution measured as an FWHM *of the* µCa-signal and contrast-to-noise ratio (CNR) for tumor masses were defined as a function of tube current for different slabs sizes.

Results: For both spatial resolution and CNR a strong inverse correlation with applied tube current and slab sizes was found (p < 0.01). In 10 cm-diameter slab microcalcifications of 0.20 mm in diameter and 1.80 mm mass could be detected at a minimum tube current of 25 mA, while 16 cm-diameter microcalcifications require a minimum of 50 mA. Accordingly, 60 kVp/25 mA and 60 kVp/50 mA settings are proposed for breasts with smaller (10cm) and bigger (16cm) diameters, respectively.

Conclusion: We propose optimized dose settings for the spiral-BCT system as a function of breast size.

Dedicated breast-CT with a photon-counting detector: Initial results of clinical in-vivo imaging

N. Berger[1], M. Marcon[1], N. Saltybaeva[1], W. Kalender[2], H. Alkadhi[1], T. Frauenfelder[1], A. Boss[1]; [1]Zurich/CH, [2]Erlangen/DE

Purpose: The purpose was to present the first clinical in-vivo application of a new dedicated spiral breast-CT (B-CT) equipped with a photon-counting detector.

Methods and Materials: The institutional review board approved this retrospective study. Twelve women referred for breast cancer screening were included and underwent bilateral spiral B-CT acquired in prone position. Additional sonography was performed in case of dense breast tissue or any B-CT findings. In 3 women previous mammography was available for comparison. Soft-tissue (ST) and high-resolution (HR) images were reconstructed. Two independent radiologists performed separately the read-out. Objective image quality evaluation was performed in consensus and included spatial resolution; contrast resolution; signal-to-noise ratio (SNR) and contrast-to-noise ratio (CNR).

Results: The major pectoral muscle was included in 15 (62.5 %) breast CT scans; glandular component was partially missing in 2 (8.3 %). A thin "ring artifact" was present in all scans but had no influence on image interpretations; no other artifacts were present. Subjective image quality assessment showed excellent agreement between the two readers (κ = 1). Three masses were depicted in B-CT and were confirmed as simple cysts in sonography. 5 simple cysts and 2 solid benign lesions were additionally found. A total of 12 calcifications were depicted with a median size of 1.1 mm (IQR 0.7–1.7 mm) on HR and 1.4 mm (IQR 1.1–1.8 mm) on ST images. Median SNR_{gl}, SNR_{fat} and CNR were significantly higher in ST than in HR reconstructions (each, p < 0.001).

Conclusion: The new dedicated B-CT equipped with a photon-counting detector provides high quality images with potential for screening of breast cancer.

Pelvic MRI for endometriosis: A diagnostic challenge for the inexperienced radiologist

C. Bruyère[1], I. Maniou[2], A. M. Kalovidouri[1], C. Habre[1], M. M. N. Pluchino[1], X. Montet[1], D. Botsikas[1]; [1]Geneva/CH, [2]Lausanne/CH

Purpose: To investigate the degree of radiologists' experience needed for interpretation of pelvic MRI studies for the clinical indication of endometriosis.

Methods and Materials: In this prospective study all pelvic MRI examinations performed for pelvic endometriosis from December 2016 to August 2017 were evaluated by readers with different experience levels ; junior resident (1–6 weeks of experience in female imaging), senior resident (6–24 weeks), fellow (6 months to 2 years) and expert (10 years) in female imaging for the presence of endometriomas and deep pelvic endometriosis (DPE). Their evaluations were compared with surgery combined with pathology. Diagnostic performances of readers with different levels of experience were studied by the means of ROC curves and areas under the curve (AUC) were compared with the ones of the expert reader.

Results: Overall, 174 patients were evaluated. The standard of reference was available for 59 among them, consisting the final population of the study. The AUC for endometriomas, DPE for the posterior and anterior pelvic compartment, for rectosigmoid DPE and for overall evaluation were 0.983, 0.921, 0.615, 0.862, 0.914 for the expert reader, 0.966 (p = 0.177), 0.805 (p < 0.001), 0.605 (p = 0.9187), 0.872 (p = 0.317) and 0.849 (p < 0.001) for the fellow level, 0.877 (p = 0.002), 0.757 (p < 0.001), 0.585 (p = 0.761), 0.744 (p = 0.239) and 0.787 (p < 0.001) for the senior resident level and 0.861 (p = 0.177), 0.649 (p < 0.001), 0.648 (p = 0.774), 0.862 (p = 1) and 0.721 (p < 0.001) for the junior resident level.

Conclusion: According to our results, interpretation of pelvic MRI for DPE should be performed by specialists as, even the performance of radiologists with up to two years of experience in female imaging was statistically inferior to that of experts.

SS201

Balloon-assisted coil embolisation and large stent delivery for cerebral aneurysms with a new generation of dual lumen balloons

A. Guenego[1], J.-B. Zerlauth[2], F. Puccinelli[2], P. J. Mosimann[3]; [1]Toulouse/FR, [2]Lausanne/CH, [3]Essen/DE

Purpose: Dual coaxial lumen balloon micro-catheters that can serve as a remodeling device and through which small stents can be delivered. We report a series of a new dual lumen balloon catheter with parallel lumens enabling enhanced inflation and deflation properties and through which larger stents may be deployed, including flow diverters (FD).
Methods and Materials: All aneurysms that were treated with a Copernic2L (COP2L) dual lumen balloon catheter at a single institution between February 2014 and December 2016 were assessed. Patient, aneurysm, procedural characteristics, clinical and angiographic follow-up.
Results: A total of 18 aneurysms in sixteen patients (14 women) were treated with the COP2L. Mean aneurysm height x width and neck size were 1.1 (min 0.5; max 2,1) and 3.3 mm (min 1; max 6.3) respectively. The COP2L was used for balloon-remodeled coiling exclusively in two aneurysms; coiling and FD stenting in eight; coiling and braided stent delivery in three; coiling, braided and FD stenting in one and for FD stenting without coiling in four (stenting alone). There were three technical complications (3/16, 18.7 %), including a perforation and two thromboembolic asymptomatic events that were rapidly controlled with the COP2L. There was no immediate or delayed morbidity or mortality.
Conclusion: According to our initial experience, the COP2L is a new type of dual lumen balloon catheter that appears to be safe and effective for balloon or stent-assisted coiling of cerebral aneurysms. and may be used to optimise stent-wall apposition.

SS202

Hypo-perfusion intensity ratio predicts patient eligibility for thrombectomy

A. Guenego, G. Albers, M. Wintermark, J. Heit; Stanford/US

Purpose: Hypoperfusion intensity ratio (HIR) correlates with collateral status in acute ischemic stroke (AIS) patients with anterior circulation large vessel occlusion (LVO). We assessed whether HIR might be a marker of patient eligibility for mechanical thrombectomy (MT).
Methods and Materials: We performed a retrospective study of consecutive AIS patients with a proximal middle cerebral artery occlusion who underwent MT triage with perfusion imaging. Clinical data, ischemic core (mL), HIR (defined as TMax>10 seconds/TMax>6 seconds (TMax>6 s)), mismatch volume, and MT details were assessed. Primary outcome was favorable HIR collateral score (HIR<0.4) between patients who underwent MT (MT+) and those who did not (MT−) according to AHA guidelines both in the <6 h and 6–24 h windows.
Results: We included 197 patients (145 MT+ and 52 MT−). MT+ patients had a significantly lower median HIR compared to MT− patients (0.4 [IQR 0.2–0.5] versus 0.6 [IQR 0.5–0.8], p<0.001) and a higher mismatch volume (96 mL versus 27 ml, p<0.001).
Among MT− patients, 43 had a core >70 ml, and 9 had a NIHSS<6.
MT− patients with NIHSS <6 had a lower HIR than MT− patients with core >70 ml (0.2 [IQR 0.2–0.3] versus 0.7 [IQR 0.6–0.8], p<0.001) but their HIR was not significantly different that MT+ patients.
Conclusion: Patients who meet AHA guidelines for thrombectomy are more likely to have favorable collaterals (low HIR). HIR may be a marker for eligibility and useful for MT triage.

SS203

Can abdominal CT findings predict the need for laparotomy in a setting of an „interventional artery first" treatment of acute embolic mesenteric ischemia (AEMI)?

E. Appenzeller, L. Widmer, G. D. Puippe, H. Alkadhi, T. Pfammatter; Zurich/CH

Purpose: CTA is an effective test to timely diagnose AEMI. Recently, endovascular mesenteric revascularization has gained acceptance. Because of the high mortality of bowel and colon infarction, revascularization is often immediately followed by diagnostic laparoscopy and if needed, bowel resection. We tried to find out to what extent secondary CT changes of arterial occlusions may predict the need for GI-surgery.
Methods and Materials: 16 patients (2008–2018, 75 % females, mean age=74 yrs [range 45–95]), who had undergone emergent interventional revascularization of acute embolic occlusions of the superior mesenteric artery at a single center were retrospectively analyzed. Contrast enhanced multislice CT had initially been obtained in all patients to diagnose AEMI. Written reports of those pre-interventional scans were compared to clinical data (laparotomy, bowel resection, in-hospital mortality).
Results: The delay between CTA, interventional revascularization and potential laparoscopy was 206 min [= median, range 60–497] and 5.8 hrs [= median, range 2.5–24]. An "artery first"-approach had been chosen in 15/16 pt. The in-hospital mortality was 38 % (6/16). Complete or near complete mesenteric revascularization was achieved in all pat. Out of the 8 surgically explored patients 6 underwent bowel resection and one was considered beyond resectability (62 % mortality). Of these 7 pt with proven bowel ischemia, 4 pt had positive CT findings. Of the 6 pt with positive CT findings, 4 pt underwent surgery (50 % mortality).
Conclusion: Preinterventional CT is of limited value as a decision-making tool regarding subsequent surgery in a setting of "interventional artery first" treatment strategy in patients with AEMI.

SS204

Outcome of Nellix-EVAS: Single center mid-term results

A. Najafi; Winterthur/CH

Purpose: Endovascular aortic sealing (EVAS) using the Nellix system is a new approach to reduce the frequency of type II endoleaks after endovascular aortic repair. Our study analyzed the mid-term results after EVAS using the Nellix system.
Methods and Materials: Our retrospective single center study assessed the CT-angiographic follow-up of patients who between 2014 and 2016 underwent EVAS at 3, 6, 12, 24 and 36 months post treatment, looking at complications and consecutive secondary interventions. Patient age and sex, aneurysm size and shape, proximal neck length, diameter, and angulation were recorded.
Results: 10 patients underwent elective EVAS treatment during our study period. Technical success rate was 100 % and there were no short-term vascular complications.
A total of 6 out of 9 patients (67 %) experienced complications such as proximal graft kinking, limb divergence or caudal migration, 2 patients after 12 months, 4 patients after 36 months. 5 patients (55 %) also showed type Ia endoleak. There was no statistically significant difference between patients that suffered from complications from those who did not. All patients received secondary treatment: proximal extension of both limbs, 5 of these with embolization of the aneurysm sac. 1 patient underwent conversion to open surgery with graft removal and surgical aortic repair while the other patient opted for a "watchful waiting" approach.
Conclusion: While no complication occurred short-term, the Nellix system showed a high percentage of caudal graft migration and type Ia endoleak on mid-term follow-up, likely due to insufficient anchoring of the device. Secondary salvage interventions can be performed for stabilization.

Angiographic detection and management of utero-ovarian anastomosis in uterine artery embolization treatment

G. T. Sheikh, A. Najafi, C. A. Binkert; Winterthur/CH

Purpose: To assess the detectability and frequency of the different types of utero-ovarian anastomosis, the correlation between type of anastomosis and ovarian failure, as well as the impact of coiling as a strategy to prevent ovarian failure

Methods and Materials: We retrospectively studied a population of 92 women treated with uterine artery embolization at our institution between 2007 and 2017. Utero-ovarian anastomoses where categorized on angiographic sequences by two radiologists based on the classification published by Razavi et al. in 2004. Ovarian failure was defined as an increase of serum FSH above 27 mIU/ml three months after embolization.

Results: Out of a total of 184 anastomoses 27 % were classified as type Ia, 45 % as type Ib, 1 % as type II and 24 % as type III. 3 % of anastomoses could not be determined. Interobserver agreement on the type of anastomoses was 91 %. Ovarian failure occurred in 6 out of 92 women (7 %). All patients with ovarian failure had at least one type Ib (n = 4) or type III (n = 1) with the exception of one patient in which one anastomosis could not be determined. No patient had bilateral type Ia anastomses. All women presenting with ovarian failure were 45 years of age or older. No patient with protective coiling developed ovarian failure.

Conclusion: Utero-ovarian anastomoses can be reliably detected with excellent interobserver agreement. Patients with type Ib and type III anastomoses carry the highest risk of ovarian failure after uterine artery embolization. Protective coiling seems to be an adequate strategy to avoid ovarian failure in those types of anastomoses.

Retrograde embolization with Foam sclerotherapy with Lauromacrogol (Sclerovein), for symptomatic varicocele

J. Carrard[1], E. Monnard[2], H. C. Thoeny[3]; [1]La Tour-de-Peilz/CH, [2]Fribourg/CH, [3]Bern/CH

Purpose: The aim of our study is to assess the technical and clinical success of the retrograde embolization with foam sclerotherapy.

Methods and Materials: We retrospectively assessed 22 patients treated with retrograde embolization from January 2015 to August 2018 in our department. Embolizations were performed due to infertility (n = 7) or pain in the left scrotum (n = 15). In all patients, after catheter positioning in the distal spermatic vein, a mixture of 5 % Lauromacrogole (Sclerovein), air and contrast media was injected. Technical success, the duration of the procedure, 1-month follow-up (FU) and mid-term (3 – 6 month) FU by ultrasound and clinical check-up were recorded and analyzed.

Results: The technical success rate was 100 % and no complication was recorded. The mean duration of the procedure was 30 minutes. At the 1-month FU, all the patients were asymptomatic and only one patient showed a persistent grade I varicocele. The mid-term FU showed no recurrence of symptoms neither of varicocele. In the seven patients with the diagnosis of infertility, two of them showed an improved spermiogramm and three pregnancies were recorded. The great majority of the patients (21/22) were highly satisfied of the embolization and the clinical outcomes.

Conclusion: Retrograde embolization with foam sclerotherapy is a fast and easy procedure for the treatment of symptomatic varicocele with a high technical and clinical success rate.

Mid-term results of MR-guided High Intensity Focused Ultrasound treatment for relapsing superficial desmoids

A. Najafi; Winterthur/CH

Purpose: Desmoids are locally infiltrative, non-malignant soft tissue tumors. Surgery, radiation therapy and chemotherapy have been the mainstay of therapy, but relapse is common and side effects can result in significant morbidity. MR-HIFU is increasingly recognized as an alternative treatment modality. We assessed the success rate of MR-HIFU for the treatment of extra-abdominal desmoids at our institute.

Methods and Materials: Five patients with relapsing desmoid tumors (three males, two females; age range 40 – 79 years) were treated. All patients were treated without general anesthesia as outpatients using the Sonalleve system (Philips). Changes in total tumor volumes were measured with a tumor tracking software (IntelliSpace, Philips). Adverse events were documented.

Results: MR-HIFU was successful in all patients without severe side effects. Follow-ups range from 13 to 60 months. Initial median tumor volume was 23 ml (range 3 – 70 ml), volumes decreased significantly in all patients after treatment (range 73 % – 100 %). Three patients required more than one treatment session. After MR-HIFU, there was no relapse or tumor progression. Skin injury in two patients was correlated with short distance to skin (average 1.0 cm [0.5 – 1.5 cm]) and proximity to bone (i.e. ribs). Skin burns healed within weeks.

Conclusion: MR-HIFU shows good midterm result for extra-abdominal desmoids with complete response for small lesions and stabilization of larger lesions. MR-HIFU for desmoids can be performed under regional anesthesia/sedation as outpatients. There is an increased risk of skin burns when lesions are in proximity to bone or less than 10 mm away from skin.

Percutaneous biliary puncture simulator

L. Szabo[1], D. Benz[1], T. Reyes Del Castillo[2], J. E. Roos[1], R. López-Benitez[1]; [1]Lucerne/CH, [2]Mexico City/MX

Purpose: Because of ethical reasons and increased risk of complications the procedures of interventional radiology should not be practiced in the first instance on patients. The lack of experience contributes to increased time of radiation exposure and increased stress for the patient and the practitioner.

A prototype percutaneous biliary puncture simulator was created in order to provide a semi-realistic model of the anatomy and mechanics without the need to use fluoroscopy or ultrasound.

Methods and Materials: An anatomical model of the bile duct was made with a system of nylon/cotton strings (1.8 mm) tied to a three-dimensional wooden frame. The pleura was simulated with an air cushion. Ribs, thoracic muscles and subcutaneous tissue were constructed from a 2 cm thick polystyrene foam panel and curved plastic tubes covered with sponge. For the puncture, 20G-Chiba needles and a metal guide with double distal arch (Duo-System, Somatex, Berlin) were used; in addition, a camera was installed above the model and the live image was transmitted to simulate hand-eye coordination during the procedure.

Results: The percutaneous biliary puncture simulator was evaluated by measuring comprehensibility and applicability in 50 participants WITHOUT experience in biliary puncture. After a brief introduction and some attempts, all the participants managed to anchor themselves to a cord (successful puncture). No probes punctured the simulated pleural space.

Conclusion: We believe it is important for physicians in training to have ethical training options without risk to patients.

SS209

Stereotactic Image-Guided Microwave Ablation for malignant liver tumors - Can computer-assistance broaden treatment eligibility?

M. H. Maurer, A. Lachenmayer, V. Banz-Wüthrich, S. Weber, D. Candinas, J. T. Heverhagen, P. Tinguely; Bern/CH

Purpose: Treatment success of microwave ablation for liver lesions depends on tumor reachability and accurate ablation probe positioning. We investigated factors influencing targeting accuracy, procedural efficiency and technical success of percutaneous Stereotactic Image-guided MicroWave Ablation (SIMWA) for malignant liver lesions.

Methods and Materials: Data from all patients treated with SIMWA from January 2015 to December 2017 were analyzed retrospectively. A computed tomography (CT)-based navigation system was used for needle trajectory planning, stereotactic needle positioning, validation of needle positions and validation of ablation zones and technical success. Factors potentially influencing target positioning errors (TPE) of positioned ablation needles were analyzed using univariable and multivariable linear generalized estimating equations (GEE).

Results: Overall 301 lesions (174 HCC, 87 CRLM, 17 NET, 23 other) were treated in 153 patients and 191 interventions. In 25 (8%) lesions multiple parallel needles were placed to create larger ablation zones. Correction of needle position was necessary in 4 (1%) lesions. Median TPE per ablation needle was 2.9 mm (0.2–14.1 mm) (n = 384). Factors significantly influencing TPE in multivariabe analysis were underlying cirrhosis, trajectory length and intercostal entry point. Subcapsular or superior dorsal lesion location (segments VII or VIII) did not influence TPE. Median time per intervention was 67 min (20–253 min), and primary technical success rate was 96% (290/301 lesions).

Conclusion: Due to precise trajectory planning and stereotactic needle positioning, SIMWA allows highly accurate and successful targeting of intrahepatic lesions, even for otherwise difficult-to-target tumors. This might allow broadening of treatment eligibility for patients with malignant liver tumors not reachable with conventional image-guidance.

SS210

Stereotactic image-guided microwave ablation of hepatocellular carcinoma

M. H. Maurer, V. Banz-Wüthrich, G. Beldi, D. Candinas, C. Kim-Fuchs, P. Tinguely, J. T. Heverhagen, A. Lachenmayer; Bern/CH

Purpose: To assess the therapeutic success of percutaneous stereotactic image-guided microwave ablation in patients with hepatocellular carcinoma (HCC).

Methods and Materials: We retrospectively analyzed a cohort of patients treated with percutaneous stereotactic image-guided microwave ablation for HCC at our institution between 01/2015 and 12/2017. All interventions were performed based on CT imaging with needle trajectory planning by landmark-based registration and an aiming device for precise needle placement.

Results: In total 163 interventions were performed in 92 patients (mean age 66 (50–84) years, 81 (83.5%) men). Patients presented on average with one tumor (1–6). Forty-three patients (44.3%) had one or more previous HCC treatments, 14 (14.4%) were transplanted afterwards. Mean tumor size was 16 (5–43) mm, mean ablation time per lesion was 5 (1–24) minutes. Within 30 days, no major or liver-specific complications occurred, six (4.6%) patients had minor (grade 1 and 2) complications after a total of 131 interventions. Of the 77 patients with a minimum 6-month follow-up after intervention, mean overall survival was 13.9 months after ablation and 23.7 months after initial diagnosis. Local recurrence occurred in 20/131 (15.2%) lesions, but could successfully be re-ablated in 14 cases (12.2%). Tumor size ≥3 cm was significantly correlated to local tumor recurrence (p = 0.005).

Conclusion: Percutaneous stereotactic image-guided microwave ablation is safe and efficient for the treatment of HCC. It might offer a curative treatment approach especially for inoperable and conventionally unablatable lesions by an accurate and precise needle positioning in a minimally invasive setting.

SS211

Survival prediction following Y90-radioembolization in patients with uveal melanoma liver metastases: Quantitative volumetric and metabolic assessment of early tumor response

F. Tabotta, S. Gnesin, A. F. M. Ponti, A. Denys, A. Hocquelet, A. Digklia, J. Prior, J.-F. Knebel, N. Schäfer, R. Duran; Lausanne/CH

Purpose: To determine early tumor response and survival predictors using quantitative volumetric and metabolic parameters in patients with uveal melanoma liver metastases treated with Y90-radioembolization.

Methods and Materials: Ten patients with 25 lesions (mean, 63-year-old) were retrospectively included (2012-2015). Patients underwent MRI/CT, 18F-FDG PET/CT before and 3–6 months after Y90-radioembolization and Y90 PET/CT immediately post-radioembolization. Image analyses evaluated lesion intensities/attenuations, size (Response Evaluation Criteria in Solid Tumors (RECIST)), tumor volume (volumetric RECIST), volumetric tumor enhancement (quantitative European Association for the Study of the Liver [qEASL]), and quantitative metabolic parameters (Total Lesion Glycolysis (TLG), Standardized Uptake Value (SUV), volumetric lesions radiation dosimetry). Paired-*t*-test was used to compare measurements before and after therapy. Measurements were correlated to the absorbed dose using Pearson's chi-squared test and Spearman's rank-order correlation. Kaplan-Meier method with the log-rank test was used to calculate overall survival.

Results: Lesions' size (RECIST), volumetric enhancement (qEASL) and metabolic activity (TLG, SUVbw max/mean/peak) decreased significantly post-radioembolization (*p* < 0.05). Mean absorbed dose was 139 Gy (range, 15–594 Gy). All lesions responded even with low absorbed dose; however response did not correlate with the absorbed dose. Baseline and post-treatment TLG and SUV parameters were predictive of survival (*p* < 0.05). qEASL demonstrated a clear trend for survival prediction (*p* = 0.058).

Conclusion: Quantitative metabolic parameters may be used as a surrogate biomarker for survival prediction in patients with uveal melanoma after the first Y90-radioembolization. Low administered doses were sufficient to achieve response.

SS212

Ultrashort time to echo (UTE) MR morphology of disco vertebral junction: Correlation with disc grade and T2 values

T. Finkenstaedt[1], K. Chen[2], P. Siriwanarangsun[3], M. Carl[2], N. Abeydeera[2], S. Statum[2], G. Bydder[2], C. Chung[4], W. C. Bae[2]; [1]Zurich/CH, [2]San Diego/US, [3]Bangkok/TH, [4]Solana Beach/US

Purpose: In this cadaveric study, we sought to determine if the discovertebral junction (DVJ) morphology as assessed by ultrashort time to echo (UTE) MRI correlates with disc Pfirrmann grades and T2 values.
Methods and Materials: Lumbar spines from 37 cadavers (30 males, 60±10.1yrs, mean±SD) were imaged at 3T using UTE (TR=300 ms, TEs=0.01 and 5.5 ms, FOV=16 cm, matrix=512x512) and spin echo (SE) T2 map (TR=2000 ms, 8 TEs=10 to 70 ms) sequences. UTE images were used to define morphology of the DVJ as being normal (i.e., with distinct linear high signal intensity) or abnormal with focal signal loss and/or irregularity. SE data were used to perform Pfirrmann grading of the disc, and T2 mapping. T2 values of nucleus pulposus were determined using an atlas-based automated region of interest. Using statistics, we compared proportion of disc grades and nucleus T2 values when the disc was adjacent to normal DVJs, 1 abnormal DVJ, or 2 opposing abnormal DVJs.
Results: Out of 278 DVJs, 198 were normal, 45 had focal signal loss, and 35 were irregular. There was a greater proportion of higher disc grades (chi-square p=0.00004), as well as lower T2 values (ANOVA p=0.18), in discs adjacent to 2 opposing abnormal DVJs, compared to discs adjacent to normal DVJs.
Conclusion: These results suggest that the prevalence of abnormal DVJs in human lumbar spines are quite high (~25%), and given the association between DVJ and disc degeneration, altered DVJs could be important for the etiology of disc degeneration.

SS213

Does skeletal muscle mass predict outcome in patients with pelvic fractures?

A. Gallot-Lavallée, T. Zingg, J. Yerly, S. Eminian, M. Bourgeat, E. Uldry, P. Omoumi, F. Becce; Lausanne/CH

Purpose: We aimed to assess whether skeletal muscle mass at admission in the emergency department is associated with and predicts mortality in patients with pelvic fractures.
Methods and Materials: Prospectively collected data (1/2008–12/2016) of 230 patients (mean age 44 years, range 16–92; 153/77 males/females) with pelvic fractures (54 Tile A, 81 Tile B, 95 Tile C injury types) extracted from the institutional trauma registry were retrospectively analyzed. Two radiologists independently measured the skeletal muscle area (SMA) on axial CT images at L3 vertebral level. To adjust SMA for patient height, the skeletal muscle index (SMI) was calculated. We tested the association of SMA, SMI, patient age, injury severity scale (ISS) score, shock index (SI), base excess (BE), serum lactate and Tile fracture type at admission with mortality. Multiple linear regression was used to analyze whether any of these parameters predicted patient outcome.
Results: Patient age (r=0.310, p<0.001), SMA (r=−0.146, p=0.026), SMI (r=−0.129, p<0.043), ISS (r=0.438, p<0.001), SI (r=0.218, p=0.002), BE (r=−0.234, p=0.001) and serum lactate (r=0.252, p<0.001) were all significantly associated with mortality. Among these parameters, only age (p=0.002) and ISS (p<0.001) predicted patient outcome. By Tile fracture type, SMA and SMI were both significantly associated with, but not predictive of, mortality in type B injuries only. Inter- (ICC=0.994) and intraobserver (ICC=0.987) reliability for SMA were both excellent.
Conclusion: Although associated with mortality, SMA and SMI do not predict outcome in patients with pelvic fractures. Nevertheless, these parameters should be taken into account when estimating injury severity and prognosis of such patients.

SS214

Interobserver reliability of the tile pelvic fracture classification system among radiologists and surgeons with varying levels of training

T. Zingg, E. Uldry, P. Omoumi, D. Clerc, A. Monier, B. Pache, M. Y. Moshebah, F. Butti, F. Becce; Lausanne/CH

Purpose: To assess the interobserver reliability (IR) of the Tile classification system among radiologists and surgeons with varying levels of training for the interpretation of computed tomography (CT) images of pelvic fractures.
Methods and Materials: Prospectively collected data (1/2008–12/2016) of patients with pelvic fractures (n=238) from the institutional trauma registry were retrospectively analyzed. Median age was 42 years (IQR 27–59), 66% were males. There were 54 Tile A, 82 Tile B and 102 Tile C type injuries. The six observers, three radiologists and three surgeons with varying levels of training (Attending/Resident/Intern), reviewed all CT images and classified each fracture into one of the 26 second-order subcategories. Weighted Kappa coefficients were used to assess the IRs for the three main Tile categories and the nine first-order subcategories.
Results: No association of mortality (15%) with the Tile fracture type was found (p=0.06). The overall IRs of the Tile system for the first-order subcategories and the main categories were fair and moderate, with Kappa values of 0.31 and 0.44, respectively. IR was fair to moderate (0.35–0.47) among radiologists, but only fair (0.22–0.34) among surgeons. By level of training, IR was moderate between attendings (0.41–0.59) and between residents (0.41–0.51), whereas it was only fair between interns (0.32–0.39). IR was moderate to substantial between the radiology attending and resident (0.56–0.70).
Conclusion: The overall IR of the Tile classification system is only fair to moderate and depends on the level of training and specialty of the observers. IR increases with level of training and is better among radiologists than among surgeons.

SS215

MRI-based 3D models of the pelvis can replace CT-based 3D models for range of motion analysis in femoroacetabular impingement

F. Schmaranzer, C. Degonda, T. Lerch, J. L. Cullmann, J. T. Heverhagen, K. Siebenrock, M. Tannast, G. Zheng; Bern/CH

Purpose: For complex cases of femoroacetabular impingement (FAI), CT-based 3D impingement simulation is the current gold standard for impingement detection. 3D MRI-based impingement simulation would offer a radiation-free alternative. We asked, (1) how many surface points of 3D models derived from 3D CT versus 3D MRI differ <1mm? (2) Whether impingement-free range of motion values correlate between 3D models derived from CT/MRI?
Methods and Materials: IRB-approved comparative, retrospective study of 20 symptomatic hips with FAI. 3D CT scans (isovoxel: 1mm³) of the entire pelvis and the distal femoral condyles were obtained. Preoperative MR arthrograms of the hip were obtained including 0.8 mm³ isovoxel T1 3D VIBE- and 1mm³ isovoxel 3D T1 VIBE DIXON sequences of the entire pelvis and the distal femoral condyles. Threshold-based manual segmentation was performed using commercial software (AMIRA). Both 3D models were compared with inhouse developed software to calculate (1) percentage of the surface points with <1mm difference between the CT-/MR-based 3D models and to assess (2) correlation in impingement-free range of motion (in: flexion; extension; internal rotation 90° of flexion; external rotation in 90° of flexion; abduction; adduction) and location of impingement on CT/MRI.
Results: (1) 83%/79% of the surface points of the proximal femur respectively of the acetabulum differed <1mm between the CT-based and MRI-based 3D models. (2) Correlation for the range of motion values was excellent (spearman rho=0.993, p<0.05) between CT/MRI.
Conclusion: MR-based 3D models of the hip joint can replace CT-based 3D models for impingement simulation in young FAI patients.

3D T1 mapping of hip cartilage: Comparison of a new inversion-recovery based method with conventional dual-flip angle acquisition

F. Schmaranzer, T. Lerch, J. L. Cullmann, K. Siebenrock, M. Tannast, J. T. Heverhagen, M. Ith, B. Jung; Bern/CH

Purpose: Although commonly used for quantitative imaging of hip cartilage, 3D dual flip angle (DFA) techniques are highly sensitive to flip angle variation (B1 inhomogenities), even more at 3T. To compare precontrast T1 values of hip cartilage using a new inversion-recovery (IR) based method with conventional DFA acquisition in asymptomatic volunteers.

Methods and Materials: IRB-approved study of 18 asymptomatic hips (9 volunteers; mean age 27±2 years, 60% female). Subjects underwent non-contrast, quantitative T1 imaging of hip cartilage at 3T: (1) 3D DFA GRE-based technique ($0.9\,mm^3$ isotropic T1 VIBE; acquisition time 8:30 min) including a prescan for B1 correction. (2) 3D dual IR approach that has been recently introduced in brain imaging ($0.9\,mm^3$ isotropic T1 MP2RAGE; acquisition time 7:30 min) in which T1 values are calculated based on two different inversion pulses. Radial images were reformatted for both T1 techniques. Regions of interest were placed manually, based on anatomic landmarks within the cartilage at each hour position of the clockface.

Results: Mean T1 values and standard deviation of overall (1488±174 ms vs 1036±41ms), anterior (1533±219 ms vs 1026±45 ms) and posterior (1444±157 ms vs 1047±43 ms) hip cartilage was higher for the DFA compared to the IR based method (all p<0.001).

Conclusion: Despite the B1 prescan inter-individual differences (=standard deviation) T1 values of cartilage were greater with the DFA method compared to the IR method due to the greater flip-angle variations at 3T. Thus, 3D MP2RAGE may provide a more robust alternative for T1 mapping of hip cartilage.

Metal artifact reduction MRI of patients with painful hip arthroplasty implants: Conventional sampled SEMAC versus vastly undersampled compressed sensing SEMAC

B. Fritz[1], R. Sterling[2], M. Nittka[3], R. Sutter[1], J. Fritz[2]; [1]Zurich/CH, [2]Baltimore/US, [3]Erlangen/DE

Purpose: To compare conventional sampled slice-encoding for metal artifact correction (SEMAC) and vastly undersampled compressed sensing-(CS)-SEMAC sequences for metal artifact reduction MRI in patients with total hip arthroplasty (THA).

Methods and Materials: Following IRB approval and informed consent, 30 patients with pain and dysfunction following THA underwent prospectively 1.5T MRI, including coronal intermediated-weighted (IW)- and short-tau inversion recovery (STIR) SEMAC (22:39 min) and CS-SEMAC (9:55 min) pulse sequences with otherwise identical parameters. Following anonymization and randomization, two fellowship-trained musculoskeletal radiologists independently evaluated the datasets. Outcome variables included image quality parameters, bone implant interface visibility, overall reader satisfaction, detection rate of abnormalities of the hip joint. Statistical analysis included kappa statistics and paired rank sum tests. p-values ≤0.01 were considered significant.

Results: Inter-observer agreements were at least adequate for all categories (kappa >0.58). There was no significant difference for the technical parameters, including motion (p=0.69), blur (p=0.37), noise (p=0.06), metal artifact reduction (p=0.46), tissue contrast(p=0.81), and fat-suppression (p>0.99). The visibility of bone implant interface of the acetabular and femoral component was rated on average as „good" indicting minimal impairment with preservation of all structural details without significant differences between SEMAC and CS-SEMAC (p=0.51). Overall reader satisfaction was „good" for both SEMAC and CS-SEMAC (p=0.85). For SEMAC versus CS-SEMAC, readers found an average of 18 versus 18 osteolyses, 15 versus 17 cases of synovitis, 23 versus 21 peritorchanteric fluid accumulations and 23 versus 19 abductor tendon tears (all p>0.34), respectively.

Conclusion: In patients with painful THA, conventional sampled and vastly undersampled SEMAC pulse sequences produce similar image quality and afford similar detection rates of abnormalities.

MRI with state-of-the-art metal artifact reduction one year after total hip arthroplasty: Periprosthetic findings in asymptomatic and symptomatic patients

L. Filli[1], P. Jungmann[2], P. O. Zingg[1], H. Rüdiger[1], J. Galley[1], R. Sutter[1], C. W. Pfirrmann[1]; [1]Zurich/CH, [2]Freiburg/DE

Purpose: To evaluate periprosthetic MRI findings 1 year after primary uncemented total hip arthroplasty (THA).

Methods and Materials: This multi-center cohort study was performed in a consecutive series of 31 asymptomatic (WOMAC score ≤1; mean age and standard deviation, 65.7±12.7 years) and 27 symptomatic patients (62.3±11.9 years). MRI was performed at 1.5T using Compressed Sensing Slice Encoding for Metal Artifact Correction (CS-SEMAC) and high-bandwidth sequences. The femoral stem and the acetabular cup were assessed for bone marrow edema, osteolysis and periosteal reaction. The amount of joint fluid was measured. Differences between asymptomatic and symptomatic patients were evaluated with Student t-test and Fisher's exact test.

Results: Bone marrow edema was common in Gruen zones 1 (asymptomatic: 13/31 (41.9%); symptomatic: 16/27 (59.3%)) and 7 (asymptomatic: 20/31 (64.5%); symptomatic: 16/27 (59.3%)) (p≥0.18). Osteolysis was frequent in Gruen zones 1 (asymptomatic: 12/31 (38.7%); symptomatic: 8/27 (29.6%)) and 8 (asymptomatic: 12/31 (38.7%); symptomatic: 7/27 (25.9%)). Osteolysis in Gruen zone 7 was significantly more common in the symptomatic group (9/27 (33.3%)) compared to the asymptomatic group (3/31 (9.7%)) (p=0.006). Periosteal reaction was present in Gruen zone 9 in 5/31 (16.1%) of asymptomatic and in 1/27 (3.7%) of symptomatic patients (p=0.20). In the acetabulum, bone marrow edema was encountered in DeLee&Charnley zones I and II in 2/27 (7.4%) of symptomatic patients but not in asymptomatic patients.

Conclusion: Bone marrow edema, osteolysis and periosteal reaction around the proximal femoral component are frequent nonspecific MRI findings both in asymptomatic and symptomatic patients 1 year after THA.

Quadriceps tendon tears: MRI characterization of location and patterns

A. L. Falkowski[1], J. A. Jacobson[2], V. Kalia[2]; [1]Basel/CH, [2]Ann Arbor/US

Purpose: The purpose was to evaluate quadriceps tendon tears with regards to which tendon components are torn, tear sites, and presence of bony involvement.

Methods and Materials: IRB approval was obtained and informed consent was waived for this retrospective study. Electronic medical records from >2.3 million patients were searched for key words, like quadriceps tendon rupture or tear and knee MRI. Cases were randomized and evaluated retrospectively and independently by two fellowship-trained musculoskeletal radiologists. Presence or lack of bone avulsion was documented on knee radiographs. MRI was used to characterize each individual quadriceps tendon as tendinosis, tear (location, partial versus complete including size and retraction distance), and bony avulsion. Descriptive statistics were calculated. Interreader reliability was calculated using Cohen's Kappa and Wilcoxon-signed-rank test.

Results: 52 patients with 53 quadriceps tears (28 right, 25 left knees) were evaluated (45 male, 7 female; mean age: 51±13 years). The vastus intermedius (VI) tendon more often incurred a partial rather than a full width tear (39.6% vs 37.7%), while the rectus femoris (RF), vastus medialis (VM), and vastus lateralis (VL) incurred full width tears more commonly (63.2–66%). Subjects with bone avulsion on radiographs had higher-grade tears of the RF, VM, and VL tears (*p*=0.020–0.043) but not the VI. Most tendons tore at or proximal to the patella (89.3%). Torn tendon retraction ranged from 2.3–2.7 cm. Inter-reader reliability was substantial to almost perfect (k=0.624–0.953).

Conclusion: Quadriceps tendon tears most commonly involve the RF or VL/VM layers usually in proximity to the patella. A bone avulsion on radiographs indicates a more extensive tear.

SS220

Early, mid- and long-term MRI follow up of collagen meniscal implant in patients with good clinical outcome

B. K. Kovács[1], D. Harder[1], F. Amsler[2], L. Cedro[1], L. Bethge[3], R. Berbig[4], M. T. Hirschmann[5], A. Hirschmann[1]; [1]Basel/CH, [2]Biel-Benken/CH, [3]Uster/CH, [4]Zurich/CH, [5]Bruderholz/CH

Purpose: Early, mid- and long-term MRI evaluation of collagen meniscal implants (CMI) and the osteochondral unit in asymptomatic patients.

Methods and Materials: 79 patients after arthroscopic CMI were included. Of these, 57 patients (mean age 44±11 years) were clinically asymptomatic at every follow-up (FU) time-point. In total, 79 MRIs one, two and three to eight years postoperatively were assessed by two radiologists for the following criteria: characteristics of CMI as morphology, signal intensity (SI), homogeneity, size; chondral defects; subchondral bone marrow edema (BME). Meniscal volume was measured. Inter-reader reliability and Pearson correlation were calculated (P < 0.05).

Results: One year postoperatively, the majority of CMI was hypertrophic (60 % [24/40]), hyperintense (100 %) and inhomogeneous (100 %). In long-term FU, the size of CMI decreased (35 % [6/17] hypertrophic; 41 % [7/17] small; 18 % [3/17] normal, 6 % [1/17] resorbed) and the majority was still hyperintense (87 % [17/16]). Only 13 % (2/16) of CMI showed normal SI. Full-thickness femoral chondral defects were increasingly present (early FU 33 % [13/40]; 65 % [11/10] late FU). One-year postoperatively femoral BME was present in 58 % (23/40) and tibial BME in 82 % (33/40); BME decreased in the long-term FU to 43 % (7/17) and 35 % (6/17), respectively. CMI-volume did not change over time. Inter-reader reliability was almost perfect for BME (0.84 – 0.88), good for femoral cartilage (0.62) and moderate to fair for morphology assessment of the CMI (0.41 – 0.48).

Conclusion: Abnormal and inhomogeneous SI of the early postoperative CMI on MRI are findings typically seen in asymptomatic patients and should not be overcalled when reporting MRI. These features tend to decrease over time.

SS221

The "calcaneal crescent" in patients with and without plantar fasciitis – An Ankle MRI study

T. Finkenstaedt[1], P. Siriwanarangsun[2], S. Statum[3], R. Biswas[3], K. Anderson[3], W. C. Bae[3], C. Chung[4]; [1]Zurich/CH, [2]Bangkok/TH, [3]San Diego/US, [4]Solana Beach/US

Purpose: The bundled, crescent-shaped trabeculae ("calcaneal crescent") within the calcaneal tuberosity may represent a structural adaption to the prevailing forces. We sought to investigate morphologic differences of the calcaneal crescent in patients with and without plantar fasciitis.

Methods and Materials: MR images of 37 patients (age 51±13yrs, body-mass-index (BMI) 26.8±6.3, females n = 27) referred for work-up of foot/ankle pain were retrospectively evaluated by two blinded readers in this IRB–approved study. Patients were assigned to two groups: (A) fifteen subjects without clinical signs or MRI-findings of Achilles-calcaneal-plantar (ACP)-system pathology and (B) twenty-two patients with findings of plantar fasciitis. The thickness and cross-sectional-area (CSA) of the Achilles tendon, calcaneal crescent and plantar fascia were measured on PD-weighted MR images. The entire crescent volume was manually measured using OsiriX on consecutive sagittal PD-Cube images. Additionally, contrast-to-noise-ratio (CNR) as a surrogate marker for trabecular density and the mean thickness of the crescent were determined on PD-weighted MR images. Using ANOVA, the group-wise difference in the morphologic measurements were evaluated, BMI as co-variate. Partial correlation was used to assess measurement relationship for plantar fasciitis group. ICC statistics were performed.

Results: Patients with plantar fasciitis had a greater CSA/volume of the crescent and lower CNR (i. e., denser trabeculae) compared to those without ACP-system pathology (CSA: 100 mm[2] vs 74 mm[2], p = 0.019; volume: 3.1 cm[3] vs 2.0 cm[3], p = 0.006; CNR: −28.4 vs −38.1, p = 0.009). Inter-reader agreement was excellent (ICC = 0.85 – 0.99).

Conclusion: In patients with plantar fasciitis, the calcaneal crescent is enlarged compared to those without pathology of the ACP-system. An enlarged and trabeculae-rich crescent may potentially indicate abnormally increased forces exerted onto the ACP-system.

SS222

Inflammation and hypervascularization in a large animal model of knee osteoarthritis: Imaging with patho-histological correlation.

A. M. Korchi[1], A. Samak-Cengarle[2], Y. Okuno[3], J. P. Pelletier[2], J. Martel-Pelletier[2], J. Doyon[2], N. J. Bureau[2], G. Soulez[2]; [1]Geneva/CH, [2]Montreal/CA, [3]Tokyo/JP

Purpose: To evaluate if synovial inflammation and hypervascularization are present in a dog model of knee osteoarthritis (OA) and can be detected on conventional MRI (MRI), dynamic-contrast-enhanced-MRI (DCE-MRI), contrast-enhanced-MRI (CE-MRI) and quantitative digital-subtraction-angiography-imaging (Q-DSA).

Methods and Materials: 6 dogs underwent MRI and angiography of both knees before and 12-weeks after right knee ACL injury. Synovial vascularity was evaluated on CE- and DCE-MRI, and Q-DSA by 2 independent observers. Synovial inflammation and vascularity were histologically scored independently. Cartilage lesions and osteophytes were analyzed macroscopically, and cartilage volumetry by MRI. Vascularity and OA markers imaging were compared before and after OA generation, and between the OA-model and control knee, using linear mixed models taking into account within-dog correlation.

Results: In all knees, baseline imaging showed no abnormalities. Control knees did not develop significant OA changes, synovial inflammation or hypervascularization. In OA knees, mean synovial enhancement score on CE-MRI increased by 13.1±0.59 (p < 0.0001), mean synovial inflammation variable increased from 47.33±18.61 to 407.97±18.61 on DCE-MRI (p < 0.0001), and area under curve on Q-DSA increased by 1058.58±199.08 (p = 0.0043). Synovial inflammation, hypervascularization, and osteophyte formations were present in all OA knees. Histology scores showed strong correlation with CE-MRI findings (Spearman Correlation Coefficient (SCC) = 0.742; p = 0.0002) and Q-DSA findings (SCC = 0.763; p < 0.0001), and weak correlation with DCE-MRI (SCC = −0.345; p = 0.329). Moderate correlation was found between CE-MRI and DSA findings (SCC = 0.536; p = 0.0004).

Conclusion: In this early stage OA dog model, synovial inflammation and hypervascularization were found on imaging and confirmed by histology.

SS223

The association of brush sign and poor collaterals on baseline MRI predicts fast infarct growth

A. Guenego, G. Albers, M. Wintermark, J. Heit; Stanford/US

Purpose: The hypo-perfusion intensity ratio (HIR) evaluate collaterals and the "brush sign" on T2* sequence might reflect oxygen hyper-extraction in acute ischemic stroke (AIS) with large vessel occlusion (LVO) before mechanical thrombectomy (MT). We assessed the performance of the 2 parameters to predict infarct growth among MT candidates.

Methods and Materials: Between January 2015 and March 2018, consecutive patients with an AIS caused by a MCA-M1 occlusion addressed for a MT who underwent an initial diffusion-weighted, T2* and perfusion imaging were included. Clinical data, ischemic core (mL), HIR (defined as TMax>10 volume/TMax>6) were assessed. Infarct growth (mL/hour) was calculated, presence of the brush sign on T2* was assessed.
Primary outcome was infarct growth (mL/h) depending on brush sign, HIR, and both signs combined.

Results: We included 93 patients. Brush sign was present in 69 patients (74%). HIR was trichotomized according to its distribution. The association of a high HIR (>0.54) and a brush sign better predicted a high infarct growth rate (26.2 mL/hour, 12.5 times higher than patients with a low HIR and no brush sign) compared to brush sign (12.7 mL/hour) or HIR>0.54 (23.4 mL/min) alone. The association of a low HIR (<0.34) and absence of the brush sign better predicted a slow infarct growth rate (2.1 mL/hour) compared to absence of the brush sign (5.0 mL/hour) or low HIR (3.1 mL/min) alone.

Conclusion: The association of a brush sign and poor collaterals depicted by a high HIR at baseline imaging is a strong predictor of infarct growth, and could be useful for decision making before MT.

SS224

Influence of spatial resolution on error of stroke infarct core volume measurement in DWI-MRI

J. M. Ospel[1], V. Schulze-Zachau[1], K. Blackham[1], S. Kozerke[2], C. Federau[2]; [1]Basel/CH, [2]Zurich/CH

Purpose: To compare the extent of error in stroke infarct core volume measurement using standard and high-resolution DWI-MRI and to evaluate how often this error might lead to changes in interventional therapy decision making.

Methods and Materials: 483 stroke DWI-MRI exams with a resolution of 2.0 x 2.0 x 4.0 mm were segmented and the infarct volumes calculated. Since partial volume effects occur in surface voxels only, surface volume is an established measure of error. Surface volume was calculated for the standard resolution, and after virtually doubling and quadrupling spatial resolution. In addition, the number of cases for each resolution, in which 70 ml – the established endovascular therapy threshold – was contained within the margin of error, was extracted.

Results: Mean infarct core volume was 23.5 ml. Mean surface volume was 12.2 ml for 2.0 x 2.0 x 4.0 mm resolution, 8.7 ml for 1.0 x 1.0 x 2.0 mm resolution and 5.2 ml for 0.5 x 0.5 x 1.0 mm resolution. With standard resolution, in 52 cases, 70 ml were within the margin of error, with double and fourfold resolution this was the case in 39 and 22 cases respectively.

Conclusion: With DWI imaging in standard resolution, a maximum error of 12 ml could have occurred due to partial volume effects, and this potentially would have affected endovascular therapy decision in 52/483 patients. Doubling the resolution reduced this inaccuracy by approximately 30% and a fourfold resolution by 50%. High resolution DWI sequences should be considered in order to accurately measure infarct cores and come to a solid endovascular therapy decision.

SS225

Should we obtain a gadolinium-enhanced extracranial MRA before mechanical thrombectomy?

A. Guenego[1], R. Blanc[2], M. Piotin[2], R. Fahed[2]; [1]Toulouse/FR, [2]Paris/FR

Purpose: To assess whether pre-intervention gadolinium-enhanced extracranial magnetic resonance angiogram (MRA) in addition to non-contrast intracranial MRA improves the duration, efficacy or safety of mechanical thrombectomy (MT).

Methods and Materials: Consecutive patients treated by MT at a large comprehensive stroke center between January 2012 and December 2017 and who underwent a pre-intervention MRI were included. Patients and procedural characteristics were collected. Univariate and multivariate analysis were performed to compare MT delays, efficacy, complications and clinical outcomes between patients with and without pre-intervention gadolinium-enhanced extracranial MRA.

Results: A total of 912 patients were treated within the study period, including 288 (31.6%) patients with and 624 (68.4%) patients without extracranial MRA. There was no significant difference between groups in the time (min) from groin puncture to clot contact (RR=1.07 [0.98–1.18], p=0.14) or recanalisation (RR=1.08 [0.97–1.20], p=0.15), time from onset to recanalisation, rates of successful recanalisation (defined as a mTICI 2b or 3, RR=1.07 [0.71–1.61], p=0.74), per-procedure complications (RR=1.24 [0.79–1.97], p=0.36) and good clinical outcome (defined by a mRS ≤2 at 3 months follow-up, RR=0.95 [0.66–1.38], p=0.79) after multivariate analyses.

Conclusion: Performing a pre-intervention gadolinium-enhanced extracranial MRA in addition to non-contrast intracranial MRA at stroke onset might not be associated with an improvement of MT speed or efficacy for acute ischemic stroke patients. Benefits could exist in procedure planning and etiology assessment. Further studies are necessary to confirm these findings.

SS226

Haemorrhagic transformation after stroke: Interrater and intrarater agreement

A. Guenego[1], M. Piotin[2], R. Blanc[2], R. Fahed[2]; [1]Toulouse/FR, [2]Paris/FR

Purpose: Haemorrhagic transformation (HT) is a complication of stroke that can occur spontaneously or after treatment. We aimed to assess the interrater and intrarater reliability of HT diagnosis.

Methods and Materials: Studies assessing the reliability of the European Cooperative Acute Stroke Study (ECASS) classification of HT or of the presence (yes/no) of HT were systematically reviewed. Eighteen raters independently examined 30 post-thrombectomy computed tomography scans selected from the aspiration vs stentriever (ASTER) trial. They were asked whether there was HT (yes/no), what the ECASS classification of the particular scan (0/HI1/HI2/PH1/PH2) was, and whether they would prescribe an antiplatelet agent if it was otherwise indicated. Agreement was measured with Fleiss' and Cohen's kappa statistics.

Results: The systematic review yielded 4 studies involving few (≤3) raters with heterogeneous results. In our 18-rater study, agreement for the presence of HT was moderate (κ=0.55, 95% CI [0.41–0.68]). Agreement for ECASS classification was only fair for all 5 categories, but agreement improved to substantial (k=0.72, 95% CI [0.69–0.75]) after dichotomising ECASS into 0/HI1/HI2/PH1 versus PH2. The interrater agreement for the decision to reintroduce antiplatelet therapy was moderate for all raters, but substantial among vascular neurologists (κ=0.70 [0.57–0.84]).

Conclusion: The ECASS classification may involve too many categories and the diagnosis of HT may not be easily replicable, except in the presence of a large parenchymal haematoma.

Dual energy CT in acute stroke: Could non-contrast CT series be replaced by virtual non-contrast CT images?

G. Herpe, A. Platon, K.-O. Loevblad, P. Machi, P.-A. A. Poletti; Geneva/CH

Purpose: To evaluate whether virtual non-contrast CT (VNCCT), reconstructed from intra-venous contrast-enhanced dual-energy cerebral CT (iv-DECT) could replace true non-contrast CT (NCCT) in patients admitted with suspicion of acute cerebral ischemia.

Methods and Materials: The retrospective study (IRB 2018-00476) included all consecutive patients in whom a NCCT followed by an iv-DECT were performed for suspicion of acute ischemia in our emergency department, over one month period. Signs of acute ischemia in the anterior and posterior circulation (ASPECT score), presence of hemorrhage and alternative findings were evaluated, randomly, on NCCT and VNCCT, in consensus, by two readers, blinded to the final diagnosis. An intra-class correlation between VNCCT and NCCT was performed for the ASPECT score. Both techniques were evaluated for their capacity to detect ischemic lesions (ASPECT score <10), when compared to the final discharge diagnosis (reference standard).

Results: 148 patients (80 men, 68 women, mean age 64 years) were included; 46 (30%) had an acute ischemia, 6 (4%) an intracerebral hemorrhage, 11 (7%) an alternative diagnosis, 85 (59%) no pathological findings. The intra-class correlation coefficients of the two methods were 0.973 (0.963–0.981) for the anterior circulation and 0.777 (0.691–0.839) for the posterior circulation, respectively. Sensitivity of VNCCT in detecting acute ischemia was higher (41% (19/46)) than of NCCT (33% (15/46)), specificity was similar for both techniques (94% (97/103) and 98%(101/103)) respectively.

Conclusion: Our results showed that VNCCT achieves the same diagnostic performance as NCCT and could safely replace NCCT in the assessment of patients with suspicion of acute cerebral ischemia.

Evaluation of 3D-FatNav based motion correction in the clinical setting of patients with brain tumors

C. G. Glessgen[1], D. Gallichan[2], N. Hainc[1], M. Moor[1], C. Federau[1]; [1]Basel/CH, [2]Cardiff/UK

Purpose: A 3D fat-navigator (3DFatNavs) based motion correction is an elegant approach to correct for motion as it requires no additional hardware and can be acquired during existing 'dead-time' within common 3D protocols. The purpose of this study was to clinically evaluate 3DFatNavs in the work-up of brain tumors.

Methods and Materials: An MRI-based fat-excitation motion navigator incorporated into a standard MPRAGE sequence was acquired in 40 consecutive patients with (or suspected) brain tumor, pre and post-Gadolinium injection. Each case was categorized into key anatomical landmarks, the temporal lobes, the infra-tentorial region, the basal ganglia, the bifurcations of the middle cerebral artery and the A2-segment of the anterior cerebral artery. First, the severity of motion in the non-corrected MPRAGE was assessed for each landmark, using a 5-point score from 0 (no artifacts) to 4 (non-diagnostic). Second, the improvement in image quality in each pair and for each landmark was assessed blindly using a 4-point score from 0 (identical) to 3 (strong correction).

Results: The mean image improvement score throughout the datasets was 0.54, significantly differing from 0. Uncorrected cases with light and no artifacts displayed scores of 0.50 and 0.13 respectively, while cases with moderate, severe artifacts, and non-diagnostic image quality, revealed a mean score of 1.17, 2.25 and 1.38 respectively.

Conclusion: Fat-navigator based motion correction significantly improved MPRAGE image quality in restless patients during MRI acquisition. There was no loss of image quality in patients with little or no motion, and improvements were consistent in patients who moved more.

Meningeal carcinomatosis metastasis in prostate cancer: Does it really exist?

T. Molteni[1], H. C. Thoeny[2], A. S. Allal[1], S. Thalmann[1]; [1]Fribourg/CH, [2]Bern/CH

Purpose: To determine typical findings of meningeal carcinomatosis (MC) in prostate cancer (PCa) patients.

Methods and Materials: Between 2003-2014, 1157 patients with PCa were treated in HFR radio-oncology department (882 without and 276 with metastasis). Typical imaging and clinical findings are reported.

Results: The most frequent metastasis site was bone (n=250). A total of 10 patients with PCa and MC was found. All patients had metastasis elsewhere.

Three patients were diagnosed by MRI only, six by CT-scan followed by MRI and one by CT-scan only.

The typical findings of MC, seen in 100% of brain contrast-enhanced MRI, was meningeal enhancement and thickening. In four cases findings were nonspecific (meningioma-like n=2, hemorrhage n=1, mass n=1). Meningeal thickening was found in all head CT-scan (n=7).

Three patients had nonspecific neurologic symptoms (headache, nausea and vomiting n=1, convulsions n=2). Three had stroke-like symptoms (facial hypoesthesia n=1, limb paralysis n=2). One had mass effect symptoms (bilateral exophthalmia) and one was asymptomatic. All patients were metastatic at the time of diagnosis.

Conclusion: MC is a rare condition in PCa, which is a more frequent tumor manifestation in multimetastatic patients.

The typical MRI findings are meningeal thickening and enhancement.

Neurologic symptoms are nonspecific therefore it is important to be aware of this diagnosis.

Investigating brain metastastatic compartments using deep learning-aided automatic segmentation for personalized medicine

T. D. L. Nguyen-Kim[1], S. Trebeschi[2], Z. Bodalal[2], B. Jasperse[2], C. U. Blank[2], J. B. Haanen[2], R. Beets-Tan[2]; [1]Zurich/CH, [2]Amsterdam/NL

Purpose: In the era of modern therapeutic options as immunotherapy-(ITX),it is important to identify imaging characteristics to improve tumor response assessment. We aimed to evaluate the potential of volumetric analysis of deep learning-aided automatic segmentation to predict patient outcome.

Methods and Materials: Retrospectively inclusion of 110 melanoma patients treated with ITX from 2015–2018(median age 63y, 59 male) and 237 patients with Chemotherapy(CTX) from 2010–2017(median age 59y, 135 male).All patients underwent clinically-indicated brain MRIs. DeepMedic was used to automatically delineate BMs and three compartments were identified:viable,non-enhancing disease,and tumor-related edema. Progression was defined as an increase of 20% in volume nadir. Tumor compartment volumes were correlated with patient outcome. Differences in clinical characteristics were statistically analyzed to evaluate OS and influence of clinical and imaging factors on PFS.

Results: ITX-group had a significantly longer PFS (median 389 days vs 275 days,p=0.004). In patients with at least one follow-up, OS was significantly higher in ITX-group (median 655 days vs 362 days, p=0.0002). In ITX-group, positive predictive factors for patient outcome were a high volume of edema (p=0.008) and cerebellar BMs (p=0.002). In contrast, for the CTX-group, a greater edema to tumor volume (p=0.031) was a negative predictive factor as well as an increased number of BMs (>3) (p=0.031).

Conclusion: Information about imaging characteristics, number and location of BMs provided by deep learning may be used as indirect predictive parameters for drug activity in personalized treatment response assessment in melanoma patients. Compartment volumetric analysis was able to differentiate between patients receiving CTX and ITX.

Machine learning algorithms for more completeness in trauma head computer tomography reports

N. Schmidt, I. Nesic, M. Moor, J. Cyriac, D. W. Zumofen, B. Stieltjes, K. Blackham; Basel/CH

Purpose: Regular reevaluation of trauma head CT report quality is of great importance but cannot be performed manually. Here we test a Machine learning (ML) approach for automated completeness detection in reports.

Methods and Materials: Literature and neurosurgical suggestions were combined to establish vital items required in a report: intracranial bleeding (ICB), fracture, signs of hydrocephalus, midline position, and vessel status were selected. All CT reports from the last 8 years were retrieved and labeled. ML model creation was done with Python 3.6 with the scikit library. We applied Support Vector Machines (SVM) for item detection. Positive Predictive value (PPV), Sensitivity and F1-score were calculated in comparison to hand labelled reports.

Results: 1906 reports were retrievable from our RIS. 146 reports had to be excluded due to missing labelling. 100 of the mentioned reports were also analyzed manually for direct comparison. The results of the SVM indicated the presence of a single critical finding ranging from 63.9% (vessel status) to 92.9% (ICB). In the manual analysis, this range was between 67% (midline) and 99% (ICB). The difference between the manual and the automated detection rate was only statistically significant ($p < .5$) for ICB and vessels.

Conclusion: SVM is suitable for the estimation of level of completeness reports in an automated fashion. It can be implemented as a quality control system and can be trained and applied to any report type. Structured reporting may help to improve the substantial level of incompleteness described here.

Rathke cleft cyst apoplexy is a newly characterized distinct entity?: Clinicoradiological comparison of pituitary apoplexy between Rathkes cleft cyst and pituitary adenoma.

H. N. Jung, S. T. Kim, S.-I. Suh, I. Ryoo; Seoul/KR

Purpose: Rathke cleft cyst (RCC) apoplexy began to be noticed as a distinct entity that was newly characterized. We compared clinicoradiological findings of pituitary apoplexy between RCC and pituitary adenoma (PA).

Methods and Materials: We retrospectively evaluated clinical data and MR images of 30 patients with RCC and 25 patients with PA who underwent surgery and confirmed pathologically between November 1999 and December 2016. We compared clinicoradiological features between the two groups.

Results: RCC group had a higher prevalence of younger age, lower tumor volume and lower pituitary stalk deviation than the PA group ($p = 0.01$, 0.02, and < 0.0001, respectively). Patients with intracystic nodule were more likely to have RCC [relative risk (RR), 2.359; 95% confidence interval (CI) of RR, 1.51–3.66] and patients with RCC were more likely to have residual or recurrent tumors on initial postoperative MRI (odds ratio, 3.50; 95% CI, 1.049–11.79). On the other hand, patients with decreased visual acuity, cranial nerve palsy, nodular enhancement, or the pituitary stalk deviation had greater probability of PA (RR, 95% CI of RR; 1.906, 1.08–3.32 in decreased visual acuity; 2.39, 1.48–3.86 in cranial nerve palsy; 2.30, 1.39–3.82 in nodular enhancement of the tumor, 2.14, 1.07–4.29 in the pituitary stalk deviation, respectively).

Conclusion: RCC apoplexy have different clinicoradiological features compared to PA apoplexy. Patients with RCC are younger and present with milder ocular symptoms in comparison to those with PA. Presence of intracystic nodule could suggest RCC apoplexy.

Diffusion Weighted Imaging to differentiate human papillomavirus positive from human papilloma virus negative head and neck squamous cell carcinoma: How do b-values influence results?

V. Lenoir, B. Delattre, Y. M'rad, M. Becker; Geneva/CH

Purpose: This retrospective study investigates whether choice of b-values for ADC map calculation influences the ability to differentiate between human papillomavirus positive (HPV+) from negative (HPV-) head and neck squamous cell carcinoma (HNSCC).

Methods and Materials: 37 patients with primary HNSCC (26 HPV– and 11 HPV+) underwent 3T-MRI with DWI including 6 b-values (b0, 50, 100, 500, 750, 1000). Reconstruction of different ADC maps (using monoexponential model) and D maps (using bi-exponential IVIM model) were performed with different combinations of b-values. The largest tumor area was delineated once and copied on the all maps. Histogram parameters were evaluated for each ADC map and compared between tumor groups.

Results: About the ADC maps calculated with different combinations of b-values, there was a significant difference between each of the mean ADC values, with the exception of D maps and ADC maps with only high b-values (combinations excluding b0). Between the two groups, a significantly lower mean ADC for HPV+ HNSCCs was seen for maps including at least b0 and b1000. Only ADC maps using 2 to 4 b-values, including b0 and b1000, showed significantly different skewness between groups, higher in HPV+ tumors. Except for ADC maps using only high b-values, all ADC maps kurtosis were significantly higher in HPV+ than in HPV– HNSCCs, whereas D maps did not show any difference.

Conclusion: To discriminate HPV+ from HPV– HNSCCs, our results show that ADC calculated with 2 b-values, b0 and b1000, are sufficient and that ADC calculated only with high b-values are not able to differentiate both tumor types.

Pulmonary hypertension in children: Beware of the liver!

M. Laurent, V. Mc Lin, R. Joye, L. Wenk, B. Wildhaber, M. Beghetti, M. Anooshiravani-Dumont, A.-L. Hachulla; Geneva/CH

Purpose: Liver-related pulmonary vascular diseases (either hepatopulmonary syndrome HPS or portopulmonary hypertension PoPH) are increasingly diagnosed. We discuss 6 patients with PoPH in 4 of whom liver disease was unknown prior to the cardio-pulmonary work up.

Methods and Materials: Six patients presented with pulmonary hypertension (PH) (mPAP: 30–54 mmHg) at a mean age of 13 years (range: 11–16). The associated liver pathologies either discovered at the time of PH workup or known before: 1 cirrhosis (biliary atresia), 1 end-stage NASH, 1 surgical mesocaval shunt for cavernous transformation of the portal vein and 3 congenital porto-systemic shunts (CPSS). The symptoms of PH were: dyspnea (5), syncope (2), and hoarsness (1). The workup in all included echocardiography, right heart catheterization, liver imaging by US and CT as well as chest CT (5 had dual energy studies) and liver biopsy. Two children with CPSS underwent pre-op abdominal angiography.

Results: All patients met criteria for PH. Dual energy CT allowed complete imaging of PH by displaying vascular (pulmonary artery and right ventricular dilatation) and parenchymal morphology and functional assessment (heterogeneities on perfusion maps). Liver imaging showed extra hepatic CPSS in 3 cases and signs of portal hypertension and abnormal liver morphology. All were treated with oral vasodilators for their PH. Two patients underwent surgical shunt closure and 2 underwent successful liver transplantation.

Conclusion: PoPH is a life-threatening condition and must be recognized by radiologists who should carefully image the abdomen in case of PH and the thorax in chronic liver disease and porto-systemic shunts.

Assessment of ventricular function using 4D-flow MRI in patients following surgical repair of d-transposition of the great arteries

F. Callaghan, B. Burkhardt, E. Valsangiacomo, C. J. Kellenberger, I. Geiger; Zurich/CH

Purpose: To assess systemic and non-systemic ventricular flow using 4D-flow MRI in patients with repaired d-transposition of the great arteries (d-TGA) and normal subjects.

Methods and Materials: Pathline tracking of ventricular volumes was performed using of 4D-flow MRI data from a 1.5T GE Discovery MR450 scanner. Ten patients following arterial switch (mean age14.7±8.2yrs) and eight patients following atrial switch (Senning) procedures (34±9.7yrs) were included. Pathlines were classified by their passage through the ventricle and kinetic energy data were calculated. Data from nine subjects with normal ventricular function were used for comparison (12±4.1yrs). T-tests were used to test population mean.

Results: The fraction of systemic ventricular flow following a direct flow route (i.e. entering and exiting the ventricle within one cardiac cycle) was significantly lower in the atrial switch patients compared with normal subjects (16.7±1.7% vs 29.4±7.2%, $p=0.03$), but not in arterial switch subjects.

The ratio of kinetic energy entering to exiting the ventricles was slightly greater than one in the systemic ventricle for the normal and arterial switch subjects (1.25±0.27 and 1.04±0.37) and significantly less for the atrial switch subjects (0.50±0.21, $p=0.002$ for both comparisons). In the non-systemic ventricle all groups showed a kinetic energy entrance to exit ratio of approximately 0.5 with no significant differences.

Conclusion: 4D-flow MRI shows that the energetics of morphological right ventricles functioning in the systemic circulation of atrial switch d-TGA subjects mimic that of the normal non-systemic ventricle, with lower energy preservation compared with the systemic left ventricle. Ventricles of arterial d-TGA subjects behave similarly to normal ventricles.

Algorithmic management of pediatric blunt abdominal trauma

S. Toso, A. Ahmed, C. Habre, M. Laurent, G. La Scala, P.-A. A. Poletti, S. Hanquinet; Geneva/CH

Purpose: Pediatric abdominal blunt trauma management varies among centers, countries and continents. The use of the published BATIC (blunt abdominal trauma in children) score, with a cut-off to scan at 7, can provide efficient patient care with less irradiation.

Methods and Materials: Retrospective review of epidemiology and diagnosis of all pediatric patients undergoing abdominal CT for blunt abdominal trauma from January 2005 to December 2016. Clinical, biologic and imaging work-up were analysed. The number of CT scans and findings before and after the implementation of the BATIC score were compared.

Results: 342 children underwent abdominal CT with a median age of 12 years (IQR 7–15). Mechanisms included: motor vehicle accidents (38%), falls (28%), bicycle (13.2%), ski (6.1%), horse riding (5%), other (8.8%). The patients were seen in either the pediatric (55%) or adult emergency departments (45%). Ultrasound was performed in 68.1% of patients. Fewer ultrasounds were performed in patient admitted in the adult vs pediatric emergency department (58.4% vs 10.1%, p<0.05). The number of normal CT scans with a BATIC <7, significantly decreased from 58% to 7%, p<0.05. CT was positive in 93% of cases with BATIC >7, p<0.01. The most frequently injured organs were the liver and spleen.

Conclusion: In our experience, the BATIC score has significantly decreased the number of CT scans for abdominal trauma. The score is a simple, systematic and transparent method of triage that can increase efficiency and decrease unnecessary irradiation in the work-up of pediatric blunt abdominal trauma.

Prenatal imaging of anorectal malformations

L. Rohrer, Y. Vial, R. A. Meuli, L. Alamo Mastre; Lausanne/CH

Purpose: Describe the imaging findings of anorectal malformations (ARMs) at prenatal echography (US) and magnetic resonance imaging (MRI); compare the accuracy of both methods in the diagnosis and classification of ARMs and evaluate the relevance of the information obtained at complementary MRI.

Methods and Materials: All patients with ARMs treated in our institution in the last 10 years were identified and those with available prenatal exams and final diagnosis selected for the study. Prenatal studies were reviewed, suggestive imaging findings listed and proposed classification compared with the initial reports and the final diagnosis.

Results: 15 ARMs – 2 low type and 13 intermediate/high type, including 6 cloacae – filled the inclusion criteria. Associated anomalies were present in 93% of cases. Prenatal exams included 14 US and 8 MRI with 7 patients having both exams. Main findings were small or absent anus, distended rectum and abnormal echogenicity/signal intensity of rectal fluid. Vaginal distension and genital duplication were seen in cloacae. Suggestive signs were prenatally detected in 53% and after review in 80% of patients. Prospective and retrospective detection rate were 36% and 57% respectively at US and 62% and 100%, respectively at MRI exams. Suggestive signs were detected in 50% low type and in 54% intermediate/high types and cloacae.

Conclusion: Prenatal diagnosis of ARM requires a systematic examination of the fetal pelvis and perineum, not always performed at screening US. Complementary MRI provides relevant information that improves diagnosis, especially in low type ARMs and cloacae.

SS238

Preliminary experience with three-dimensional morphometric assessment of the face with "black bone" magnetic resonance imaging

M. J. Kupka[1], J. Aguet[1], M. W. Wagner[1], A. S. Becker[1], F. Callaghan[1], S. Abramowicz[2], C. J. Kellenberger[1]; [1]Zurich/CH, [2]Atlanta/US

Purpose: To evaluate feasibility of "black bone" magnetic resonance imaging (MRI) for assessing orofacial deformity in children with juvenile idiopathic arthritis (JIA).

Methods and Materials: Black bone three dimensional (3D) gradient echo images (flip angle 5°, submillimetre isotropic resolution) from 10 children (median age 13 years, range 2–16 years), who underwent MRI of the temporomandibular joints, were evaluated with the 3D rendering and multiplanar reconstruction tools of SECTRA PACS and Advantage Workstation. Intra- and interrater reliability was investigated for measuring the height of the mandibular ramus and condyle, basal length of the mandible, gonion angle and mandibular inclination angle by Bland Altman analysis and intraclass correlation coefficient (ICC).

Results: Black bone images required inversion of the signal intensity and removal of air before they could be processed with standard volume rendering tools. Reliability for linear measures was best on thin minimum intensity projection images (agreement bias <1mm , range ±4mm, ICC 0.97–0.99). Variability of angle measures was higher (agreement bias <4°, range ±8°, ICC 0.99).

Conclusion: Morphometric measures of the face can be obtained from black bone MRI with a comparable reliability to that reported for cone beam CT. With improvements of 3D rendering techniques and software, black bone MRI may become a radiation free alternative to CT in children with JIA.

SS239

Suspected septic osteo-arthritis in children: Do we need intravenous Gadolinium injection?

C. Habre, S. Ferey, S. Toso, M. Laurent, P. Lascombes, S. Hanquinet; Geneva/CH

Purpose: To assess the need of contrast-enhanced MRI to identify bone/joint infection and collections for the surgical management of septic osteo-arthritis in children.

Methods and Materials: Retrospective MRI study (1,5T) of children with suspected septic osteo-arthritis presenting to the emergency department. Spinal infection were excluded. A standard institutional protocol with Gadolinium (Gd) injection was used: 3D short TI inversion recovery, T1- and T2-weighted spin-echo, diffusion and Gd fat-saturation T1. Section plans were chosen according to the anatomical location. Surgical criteria were established by our orthopedic surgeons and included: anatomical location, bone oedema, joint effusion, bone/subperiosteal/soft tissue collection. Two radiologists indepedently evaluated all non-enhanced sequences followed by enhanced-sequences for the presence or absence of surgical criteria. MRI results before and after gadolinium were discussed with the surgeon to determine whether patient management would have altered.

Results: Twenty-six children underwent MRI for acute septic osteo-arthritis (mean 5.9 years, range 12 months–14 years). Sites of infection were ankle (8), foot (6), knee (5), hip (5), wrist (1) and elbow (1). In all cases, non-enhanced MRI proved sufficient in identifying location of bone/joint infection and all types of collections. Surgical management did not change with contrast injection. In 3/5 hip MRIs, Gadolinium showed altered enhancement of femoral head which changed follow-up but not initial treatment.

Conclusion: Non-enhanced MRI is sufficient for surgical management in septic osteo-arthritis with shorter acquisition time and avoidance of Gadolinium. Contrast injection may change prognosis but has no impact on initial treatment.

SS240

Impact of patient off-centering on organ radiation doses for pediatric CT of the head and trunk

A. Euler, _N. Saltybaeva_, H. Alkadhi; Zurich/CH

Purpose: To assess the impact of patient positioning on organ radiation doses for CT of the head and trunk in a phantom simulating a 5-year old child.

Methods and Materials: An anthropomorphic phantom (Model 705-C, CIRS, USA) simulating the dimensions of a 5-year old child was used. Semiconductor dosimeters were placed in various organs of the head and trunk. One dosimeter was placed at the thyroid to measure scattered radiation adjacent to the scan fields. The phantom was imaged separately for the head and trunk using vendor-specific pediatric CT protocols. Scans were repeated at different table positions from –6cm to +6cm in y-direction from optimal patient positioning. Organ radiation doses were measured and compared among table positions.

Results: Depending on the table off-centering, differences in organ doses in relation to the optimal patient positioning ranged from –10 to 27% for the supratentorial brain, –14 to 24.7% for the infratentorial brain, –16.4 to 12.6% for the eyes, –17.5 to 3% for the lungs, –16.9 to 11% for the stomach and –13.7 to 7.7% for the liver, respectively. In addition, the effect of table position on organ radiation dose was dependent on the relative position of each organ to the optimal patient positioning. The increase in scattered radiation dose due to table off-centering was substantially higher for trunk (up to 18.9%) compared to head CT (up to 9.7%).

Conclusion: Patient positioning demonstrated a substantial impact on radiation doses for various organs in pediatric CT of the head and trunk.

SS241

Catheter-related arterial thrombosis in neonates

G. Manasseh, A. Lamri, L. Alamo Mastre, E. V. Tenisch; Lausanne/CH

Purpose: Catheter-related arterial thrombosis in neonates (CATN) is increasingly recognized and associated with serious complications. Catheters are introduced in the aorta through umbilical artery, internal and common iliac arteries where the CATN are typically found. Those can easily be missed, when not actively searched for. The purpose of this study is to present the actual incidence and imaging findings of CATN and associated complications.

Methods and Materials: We reviewed all abdominal ultrasounds performed in our neonatal unit between May 1st and November 30th, 2018 (7 months) in patients under 30 days of age, for any indication.

Results: We found 247 abdominal ultrasounds performed in 137 patients. 7 patients had an aortic thrombosis (mean age=7 days). All patients had indwelling umbilical aortic catheter (IC) before the exam. Thromboses involved the celiac trunk and superior mesenteric artery in 15% of patients, and renal arteries in 43%. In the other cases, the thrombosis remained under the level of the renal arteries but eventually extended in the common and internal iliac arteries, on the side of the IC. 2 patients had radiologic organ complication with 1 splenic and 2 renal infarcts. 4 patients were treated with intravenous anticoagulant, and the 3 others showed spontaneous resolution.

Conclusion: We present 7 cases of CAT encountered in our neonatal unit, with their complications and evolution. These cases emphasize the need for a careful evaluation of the abdominal aorta and its branches in newborn with umbilical artery catheter.

SS242

Catheter-related portal thrombosis in neonates

A. Lamri, G. Manasseh, E. V. Tenisch, L. Alamo Mastre; Lausanne/CH

Purpose: Umbilical venous catheter (UVC) placement in the neonate is commonly used as a central venous access. The most often observed complication is the portal venous thrombosis. The purpose of the study is to present the real incidence of the complications related to UVC during a short time in the Unit of Neonatology. We describe the imaging findings of these complications and their evolution

Methods and Materials: During a 7 months period (01.05.2018 – 30.11.2018), 247 abdominal ultrasound (US) studies were performed in patients between 0 and 30 days of life. The US exams were performed on a Philips Infinity 70 G. All studies (initial and follow-up US) were reviewed by two pediatric radiologists.

Results: The most frequent complication was a total or subtotal portal venous thrombosis (n = 14 patients). All of them had previously UVC placement. In 11 cases, a misplacement of the UVC was seen, either intrahepatic or prehepatic.

At follow up, complete resolution of the thrombus was observed in 5 cases, partial regression in 6 cases, whereas in 2 cases the thrombus remained unchanged. 1 patient had no follow up.

Hepatic complications after UVC were detected in 3 patients: 1 developed an atrophy of the left liver lobe and 3 of them hyperechogenic foci in the parenchyma, most probably calcification.

Conclusion: Even if UVC is a common procedure, portal thromboses can be observed, especially in case of misplacement. These thromboses cause hepatic abnormalities in rare cases. In conclusion, a mispositioned UVC shouldn't be left in place.

Swiss national CT dose registry

D. Sigrist[1], T. V. M. Lima[1], A. Hostettler[1], C. Aberle[2], S. T. Schindera[1];
[1]Aarau/CH, [2]Basel/CH

Purpose: There are 309 CT scanners in Switzerland resulting in a combined total of over a million CT exams per year. Systematic and comprehensive analysis of dose data requires high manual effort. However, such an analysis of patient exposure is inevitable for quality assurance and improvements in radiological processes. A national dose registry can be used for semi-automatic benchmarking and optimizing the exposure of various CT protocols.

Methods and Materials: Building a national dose registry requires the collaboration and participation of many institutes equipped with dose management systems (DMS). Data submission is designed as a semi-automatic process, thus minimising the recurring effort of participating institutes and fostering a larger and more up-to-date data corpus.

The feasibility study elaborates strategical topics such as financing and operations, but also entails the definition of processes and the development of a proof-of-concept web platform.

Results: The end-to-end process for dose data integration and analysis with the national registry has been demonstrated. Technical aspects of the web platform, data structure and transfer preferences have been set in collaboration with major DMS vendors. Data validation and cleansing steps are implemented and can be adapted.

Conclusion: The Swiss National CT Dose Registry aims to semi-automatically collect, aggregate and analyse CT radiation dose data from Swiss radiology institutes based on a broad and up-to-date data corpus. Gained insights can then be utilised for quality assurance and process optimisation in radiology institutes, allow more frequently updated diagnostic reference levels, aid in protocol optimisation and may indirectly lead to patient dose reduction.

Impact of dose-reduction systems and proposed reference levels for thrombectomy in acute ischemic stroke: An international, multicentric, retrospective study

A. Guenego[1], P. J. Mosimann[2], R. Fahed[3], J. Gralla[4], M. Piotin[3], R. Blanc[3], C. Cognard[1]; [1]Toulouse/FR, [2]Essen/DE, [3]Paris/FR, [4]Bern/CH

Purpose: International dose reference levels are lacking for thrombectomy in acute ischemic stroke patients with large vessel occlusions. We studied whether radiation dose reduction systems (RDS) effectively reduce exposure and propose reference levels.

Methods and Materials: We retrospectively included consecutive patients treated with thrombectomy on a biplane angiography system (BP) in five international, high-volume centers between January 2014 and May 2017. Institutional Review Board approvals were obtained. Technical, procedural and clinical characteristics were assessed. Efficacy, safety, radiation dose and contrast load were compared between angiography systems with and without RDS. Multivariate analyses were adjusted according to Bonferroni. Proposed International Reference cutoff levels were set at the 75th percentile.

Results: Out of the 1096 thrombectomised patients, 520 (47 %) were treated on a BP equipped with RDS. After multivariate analysis, RDS significantly reduced DAP [91 vs 140 Gy·cm², relative effect 0.74 (CI: 0.66; 0.83), 35 % decrease, p < 0.001] and Kerma [0.46 vs 0.97 Gy, relative effect 0.63 (CI: 0.56; 0.71), 53 % decrease, p < 0.001] with 75th percentile reference levels of 148 Gy·cm² and 0.73 Gy, respectively. There was no difference in contrast load, rates of successful recanalisation, complications or clinical outcome.

Conclusion: Radiation dose reduction systems can reduce DAP and Kerma by a third and a half respectively, without affecting thrombectomy efficacy or safety. The respective thresholds of 148 Gy·cm² and 0.73 Gy may serve as baseline quality-control reference levels. As technology and operator experience evolve, we expect these values to decrease in the future.

Comparison of patient dose during CT-guided lumbar spine interventions

Y. Käser; Uetikon am See/CH

Purpose: National diagnostic reference levels are published by the FOPH for common CT examinations and are a valuable tool in optimization. CT-guided lumbar spine pain interventions are not included in this list but are commonly conducted in radiological practices. This study aimed at determining references for those interventions.

Methods and Materials: Dose data from lumbar spine pain interventions was collected from a total of 265 patients in 16 Institutes. For each institute the average dose length product (DLP) was determined for the complete interventions. Additionally the average DLP for the planning and fluoroscopy part were calculated. The 75th and 25th percentile of those averages were determined as references for benchmarking.

Results: While patient doses varied strongly between individual patients for each institute, also large differences could be observed between the evaluated institutes. Minimal average total DLP was 59.2 mGy·cm (18.6 mGy·cm and 19.1 mGy·cm for planning and fluoroscopy respectively). Maximum average total DLP was 592.9 mGy·cm (378.1 mGy·cm and 472.8 mGy·cm). The 75th percentile was calculated to be 240.5 mGy·cm for total DLP (126.5 mGy·cm and 82.0 mGy·cm). The 25th percentile was 97.0 mGy·cm for total DLP (54.9 mGy·cm and 35.0 mGy·cm).

Conclusion: Patient doses during CT-guided lumbar spine pain interventions vary greatly for individual patients as well as for different institutes. The determined references can be used to compare an institutes practice with common practice in other institutes and thus if necessary optimise the used protocols.

Dose optimization of abdominal CT protocols: Implementation of a task-based approach to assess image quality in relation to the national diagnostic reference level in Switzerland

D. Racine[1], A. Viry[1], C. Aberle[2], F. R. Verdun[1], S. T. Schindera[3]; [1]Lausanne/CH, [2]Basel/CH, [3]Aarau/CH

Purpose: To study patient dose optimization of abdominal CT that considers the dose and the image quality aspects for various CT scanners.

Methods and Materials: An abdominal anthropomorphic phantom (QRM) with a module containing spherical 8mm diameter targets of 20 HU contrast was scanned at 5 CTDIvol (4, 8, 12, 16 and 20mGy) to assess the image quality of a diverticulitis protocol on three different CT scanners (BrightSpeed, CT750 HD and Revolution CT; GE HealthCare). The same phantom with a second module containing calcium targets was scanned at 5 dose levels (2, 4, 6, 10, 15 mGy) on the same CTs to assess a renal stone protocol. Two model observers (a Channelized Hotelling Observer and a non prewhitening with an eye filter) were used to assess the detectability of low contrast spheres and high-contrast calcium targets. The area under the curve was used as figure of merit (FOM).

Results: For the search of diverticulitis, the AUC is similar between the two newest CT scanners, except at the lowest dose. Furthermore, the Brightspeed CT had an AUC 10 % inferior than the two other CTs whatever the CTDIvol used. In the clinical dose range used when dealing with renal stones protocol, the dose variation has no major impact on the detection (AUC equal to 1.0).

Conclusion: A comparable image quality cannot be reached on different scanners facilities at the same dose level for specific clinical questions. Therefore, the image quality requirements, related to the clinical question to be answered, should be the starting point for patient dose optimization.

Automatic patient positioning in CT using a 3D camera

N. Saltybaeva, H. Alkadhi; Zurich/CH

Purpose: Tube current modulation (TCM) is a major technique for radiation dose optimization in CT. However patient precise centering is crucial for optimal utilization of the TCM. The aim of this study is to evaluate 3D-camera based algorithm for automatic individualized patient positioning based on body surface detection and to compare the results with manual positioning performed by technologists.

Methods and Materials: This study included data of 120 patients underwent routine chest and abdomen CTs. For 52 patients table height was manually selected by technologists; while other 68 were automatically positioned based on patient-specific body surface detection. For each of the patient table position was recorded. The ground truth table height (T_{GT}) was defined from the DICOM data as the table height that aligns the axial center of the patient's body and the scanner isocenter. Off-centering was defined as the difference between T_{GT} and table position actually used in CT. The *t*-test was performed to determine the significance of the differences in vertical offset when automatic vs manual positioning was used.

Results: We found significant improvement in patient centering (offset of 5±3 mm) when using the automatic positioning compared to the manual one (offset of 19±10 mm) (p < 0.005). The absolute maximal offset was 39 mm and 43 mm for chest and abdomen CT, respectively, when patients were positioned manually, while with automatic positioning the offset did not exceed 15 mm.

Conclusion: Automatic patient positioning using 3D camera provides better patient centering as compared to manual positioning, thus, resulting in better radiation dose utilization in CT with TCM.

Creation of curated datasets from unstructured radiology reports using natural language processing- exemplified on CT reports regarding pulmonary embolism

T. J. Weikert, I. Nesic, M. Moor, J. Bremerich, A. Sauter, G. Sommer, B. Stieltjes; Basel/CH

Purpose: Retrospective classification of exams in positive vs negative findings is a frequent first step in the development of curated datasets. Given that radiology reports offer this information mostly in a non-structured fashion, we wanted to test the performance of a self-developed NLP-based procedure.

Methods and Materials: We downloaded all reports of CT pulmonary angiograms (CTPAs) conducted at our institution in 2016/2017 (n = 2,917; language: German). We then extracted the impression sections. The status (pulmonary embolism: yes/no) was manually assessed by a radiologist. CTPAs with other clinical questions than pulmonary embolism or poor diagnostic quality were excluded. The labelled impression sections from 2017 (n = 1,436) served as ground truth to train a deep neural network for NLP (linear support vector machine classifier). The performance of this network was tested using the exams from 2016 (n = 1,367).

Results: Our NLP approach reached a sensitivity of 88.9 % and specificity of 96.5 %. The positive predictive value was 81.6 %, the negative predictive value was 98.1 %. In total, the status of 1,303 of 1,365 exams was correctly predicted (accuracy: 95.5 %). The cases with wrong classifications had a higher mean word count (40.1) than those with correct predictions (33.5).

Conclusion: Our NLP based approach allows for an automated and highly accurate retrospective classification of CTPA data solely using the unstructured impression section from radiology reports. A higher word count, likely related to a higher number of secondary diagnoses, may be a potential cause of misclassification.

Implementation of a Monte Carlo simulation tool for Grating Interferometry Breast Computed Tomography (GI-BCT)

S. Tessarini[1], M. Fix[2], W. Volken[2], D. Frei[2], M. Stampanoni[1]; [1]Villigen/CH, [2]Bern/CH

Purpose: The aim of this work is the development of a Monte Carlo simulation tool for grating-interferometry modules as they are currently implemented in clinical breast computed tomography (GI-BCT) prototypes.

Methods and Materials: GI-BCT aims at significantly improving breast imaging quality by acquiring full three-dimensional information of the uncompressed breast, boosted by superior soft-tissue visibility and discrimination thanks to X-ray phase and dark-field contrast as produced by a gratings-interferometer.

We expanded EGSnrc – a well-known Monte Carlo particle transport code – with additional features required for the simulation of grating-based imaging devices such as: physics libraries for refraction at interfaces and diffraction at gratings as well as geometry packages, particle sources and scoring routines.

Results: We present here a stable EGSnrc extension library which enables the MC simulation framework to take into account complex scattering contributions, beam spectra propagation and phase and absorption images. These are all relevant aspects that have to be taken into account when designing a clinical device based on GI.

Conclusion: The implementation of the necessary features for GI-BCT in EGSnrc was successful and first validations have been obtained. The code will further be refined to reduce computational time for the simulation of clinical-scale systems.

Influence of metal artifacts correction techniques on CT radiomics stability in head and neck cancer patients

K. Karava, H. Gabrys, M. Bogowicz, D. Vuong, M. Guckenberger, S. Tanadini-Lang; Zurich/CH

Purpose: CT metal artifacts greatly influence the image quality. This study aims: a) to evaluate the stability of radiomic features between filtered back projection (FBP) and iterative metal artifact reduction (iMAR) algorithm, and, b) to investigate a manual removal of artifact affected slices, in combination with a reconstruction algorithm, as an effective metal artifact reduction approach.

Methods and Materials: The patient cohort, comprising of 40 head and neck cancer patients, was collected retrospectively to obtain two groups of 20 patients with and without metal dental fillings, i.e. artifact group and control group, respectively. CT images of all patients were reconstructed with both FBP and iMAR. An experienced radiation oncologist manually segmented the gross tumor volume (GTV). Additional structure was created (adaptGTV) by manual removal of initial contour (GTV) from artifacts affected slices. Radiomic features were calculated and evaluated in both GTV and adaptGTV. Stability of features was evaluated with intraclass correlation coefficient (ICC) and an ICC > 0.9 was considered stable.

Results: Eight patients were excluded from the artifact group as over 50 % of their GTV was affected by imaging artifacts. Comparison of FBP and iMAR in the control group revealed that over 95 % of features were stable. In the artifact group, 74 % fulfil this criterion. The fraction of stable features varies around 60 % when the manual adapted method was involved independently from the image reconstruction algorithm.

Conclusion: A majority of radiomic features was transferable between FBP and iMAR when no artifacts were involved. Manual artifact removal considerably influenced feature stability.

Discrimination between crystal suspensions in plain radiography utilizing spectral photon-counting technique

F. A. Huber[1], T. Thuering[2], S. Gkoumas[3], F. Becce[4], R. Guggenberger[1];
[1]Zurich/CH, [2]Villigen/CH, [3]Baden-Dättwil/CH, [4]Lausanne/CH

Purpose: To differentiate between suspensions of gout-typic monosodium urate crystals (MSU) and calcium hydroxyapatite (HA) in plain radiography.

Methods and Materials: Suspensions of MSU and HA (both 200 mg/ml) were custom-made and boxed in industry-standard polystyrene containers. Supported on a polymethylmethacrylate (PMMA) plate, all samples were scanned with a microfocus X-ray tube (50 kV/300 uA) using a high-end detector prototype for spectral photon-counting (PC). Four energy thresholds were set at 15, 25, 30 and 35 keV, all images were then reconstructed using two energy bins of 15–25 and 30–50 keV. Prior to material decomposition, calibration was done with pure PMMA and polyvinylchloride of known thicknesses from 1 to 48 mm, respectively. Open-source software was used for material decomposition, eventually resulting in ROI-derived effective atomic numbers (Z_{eff}) for each sample. Additionally, all samples were validated in concordance with the institute-own clinical workflow of gout imaging with CT, using a dual-energy scanner of the latest generation (Siemens Force) and proprietary post-processing software for gout detection (syngo.via CT DE Gout).

Results: MSU was significantly less attenuating and showed significantly lower Z_{eff} (range: 6.4–6.8 vs 9.8–9.9, p<.001) than HA. Furthermore, material decomposition was also possible for HA and PMMA, which were attenuating similarly, but had significantly different Z_{eff}. Dual energy CT validation scans and PC radiography showed comparable Z_{eff} values for all samples.

Conclusion: MSU and HA can be separated in PC radiography based on Z_{eff}. Further research has to be done investigating the clinical applicability of this proof of concept study.

Laboratory X-ray phase contrast imaging for improved pathology

J. Vila-Comamala[1], C. Arboleda Clavijo[2], L. Romano[2], W. Kuo[2], K. Lång[1],
K. Jefimovs[1], G. Singer[3], M. Stampanoni[2], Z. Wang[1]; [1]Villigen/CH,
[2]Zurich/CH, [3]Baden/CH

Purpose: Histopathological inspection of tissue specimens is a key diagnostic tool in clinical medicine. Based on a previously synchrotron-implemented technique, we developed a laboratory X-ray phase contrast imaging (XPCI) system for improved pathology that provides full 3D tomographic datasets of the samples under examination.

Methods and Materials: The higher sensitivity of X-ray phase contrast is specifically well-suited for biological soft tissues, for which ordinary X-ray absorption radiography does not typically yield enough signal to noise ratio contrast. We have designed and built a new laboratory X-ray grating interferometer system using an X-ray microsource, in-house fabricated X-ray gratings and an X-ray detector. The instrument can easily inspect biopsy samples with minimal preparation in formalin solutions or embedded in paraffin blocks and no staining is required. After the 3D tomographic acquisition, the sample can be virtually sliced.

Results: We present the first 3D tomograms of human biopsies of knee tendon, prostate and breast tissue obtained with our new instrument. In particular, we examined paraffin-embedded breast biopsies containing Fibroadenomas and Phyllodes. In addition, we identified the structure of an invasive cancer, its calcifications and the nearby ductal carcinoma in situ (DCIS) inside a human breast biopsy in formalin solution without any staining. Typically, our instrument can image samples as big as 2 x 2 x 2 cm³ with an approximate resolution of 20 micrometer.

Conclusion: We have developed a laboratory XPCI system that can deliver full 3D imaging capabilities of biological soft tissues. The tool might become a powerful instrument to support pathologic investigations at hospitals.

Recovery coefficients for different signal to background ratios

M. Hentschel, M. Fürstner, G. A. Prenosil, A. Rominger, T. Weitzel; Bern/CH

Purpose: Constancy tests for PET/CT scanners are performed with phantoms containing spherical inserts and fixed signal to background ratios (SBR) only. The recovery curve (RC) is depending on the partial volume effect (PVE) which in turn depends on the SBR. In order to investigate this influence systematic acquisitions were performed with varying acquisition times and different reconstruction methods.

Methods and Materials: Acquisitions of a Jaszczak phantom were performed with a Biograph mCT 128 TrueV (+TOF). SBRs ranged from 0.3/1 to 83/1 and acquisition times from 21 to 2651 s. Data were reconstructed by several different reconstruction methods (FBP, OSEM, PSF) with isotropic voxel sizes of 1.5, 2 and 4 mm³ and different Gaussian post filters. The analysis of the data was performed with an in-house multi-paradigmen software using an embedded expert system.

Results: In total, 560 data sets were analyzed. The RC show a strong dependence from the SBR, reconstruction type, post-filter parameters and acquisition time. Small spheres, short acquisition times, small voxel sizes and the PSF reconstruction method lead to increased (up to a factor 2) and scattered RC-values. Increased values occur as well for large spheres and large SBR. The FBP reconstruction method, on the other hand, results in rather stable RC-values.

Conclusion: The results demonstrate the importance of the background for quantitative PET imaging. Therefore, the characterization of a tomograph should encompass SBR over a wider range. Since, the RC-curves acquired with parameter typical used in clinical routine show a strong dependence from SBR, reconstruction method, post-filter parameter and acquisition time.

Metal artifact reduction in quantitative 99mTc-DPD-SPECT/CT for the detection of prosthetic loosening in patients with hip- and knee joint replacement - an interims analysis of 22 prostheses

M. L. Braun[1], M. Cachovan[2], G. Pagenstert[1], D. Wild[1], M. Kretzschmar[1];
[1]Basel/CH, [2]Forcheim/DE

Purpose: To evaluate the impact of metal artefact reduction (iMAR, Siemens) on the diagnostic performance of standardized quantitative 99mTc-DPD-SPECT/CT in patients with painful knee and hip joint prostheses suspicious for loosening.

Methods and Materials: Thirteen patients with a total of 22 prostheses (13 hip and 9 knee prostheses) underwent 99mTc-Dicarboxypropandiphosphate (DPD)-SPECT/CT 3 h after injection of 99mTc-DPD (mean dose 697 MBq). Quantitative reconstruction was performed with Siemens xSPECT-Quant and xSPECT-Bone, with and without iMAR-reconstruction of CT data. SUVmax means were correlated to intraoperative findings or clinical outcome after 1 year. Cut-off values and accuracy of the different reconstructions were calculated using receiver operator characteristics (ROC) and compared to the accuracy of visual readings by a senior physician and a trainee blinded for the quantitative data and clinical outcome.

Results: SUVmax were significantly higher in loose prostheses compared to stable prostheses, with all methods of quantification used (p = 0.018 – 0.001). Without iMAR, accuracy of xSPECT Bone quantification was 91 % was (cut-off SUVmax 13.4, sensitivity 88 %, specificity 93 %). With iMAR, accuracy of xSPECT Bone was 95 % (Cut-off SUVmax 13.8, sensitivity 100 %, specificity 93 %), Diagnostic accuracies of blind-readers were 79 % for an experienced reader, and 71 % for a trainee.

Conclusion: Quantitative uptake values of periprosthetic bone metabolism using 99mDPD-SPECT/CT with xSPECT Bone reconstructions provided a higher accuracy compared to experienced readers. With metal artefact reduced reconstructions of CT and SPECT data (Siemens iMAR), an even higher accuracy of 95 % could be achieved, underlining the high potential of this biomarker for the diagnosis of prosthetic loosening.

Impact of different image reconstructions on PET quantification in non-small cell lung cancer: A comparison of adenocarcinoma and squamous cell carcinoma

M. A. Messerli, F. Kotasidis, I. A. Burger, D. A. Ferraro, U. J. Mühlematter, C. Weyermann, D. Kenkel, G. K. von Schulthess, P. A. Kaufmann, M. Huellner; Zurich/CH

Purpose: Positron emission tomography (PET) using 18F-fluordeoxyglucose (18F-FDG) is an established imaging modality for tumor staging in non-small cell lung cancer (NSCLC). There is growing interest in using 18F-FDG PET for therapy response assessment in NSCLC. Different reconstruction algorithms in PET may affect standardized uptake values (SUV). We sought to determine the variation of SUV in patients with NSCLC when using ordered subset expectation maximization (OSEM) and block sequential regularized expectation maximization (BSREM) in latest-generation digital PET/CT, comparing adenocarcinoma and squamous cell carcinoma.

Methods and Materials: Fifty patients (34=adenocarcinoma, 16=squamous cell carcinoma) that underwent a clinically indicated 18F-FDG-PET/CT for staging were reviewed. PET images were reconstructed with OSEM and BSREM reconstruction with noise penalty strength β-levels of 350, 450, 600, 800 and 1200. Lung tumors SUV_{max} were compared.

Results: Lung tumors SUV_{max} were significantly lower in adenocarcinomas compared to squamous cell carcinomas in all reconstructions evaluated (all $p < 0.01$). Comparing BSREM to OSEM, absolute SUV_{max} differences were highest in lower β-levels of BSREM with +3.0 ± 1.6 in adenocarcinoma and +3.8 ± 2.9 in squamous cell carcinoma, (p-values > 0.05). There was a statistically significant difference of the relative increase of SUV_{max} in adenocarcinoma (mean +34.8 %) and squamous cell carcinoma (mean +22.8 %), when using BSREM instead of OSEM ($p < 0.05$).

Conclusion: In NSCLC the relative increase of SUV when using BSREM instead of OSEM is significantly higher in adenocarcinoma as compared to squamous cell carcinoma, which implies that reconstruction settings of serial 18F-FDG-PET exams must be kept identical, even if acquired on the same scanner.

Statistical textural feature analysis in PET/CT requires exposure control for image noise invariance

G. A. Prenosil, M. Hentschel, T. Krause, B. Klaeser, A. Rominger, T. Weitzel; Bern/CH

Purpose: In PET/CT textural feature analysis must produce reproducible values independent of image count statistics. This work investigated the stability of grey level co-occurrence matrix (GLCM) derived textural features across a range of exposures. Exposure *E* was defined as phantom activity concentration times acquisition duration.

Methods and Materials: A homogeneous cylindrical phantom filled with 9.6 kBq/ml 68-Ge was imaged on a Siemens Biograph mCT with acquisition durations ranging from 3 s to 10861 s. Images with differently sized isometric voxels were reconstructed using filtered back-projection (FBP), ordered subset expectation maximization (OSEM) and the Siemens TrueX algorithm. Eleven GLCM features – taken from a 50 mm wide cube at the phantom centre – were calculated and plotted as functions of exposure *f(E)*. Feature stability was defined when $df/dE \rightarrow 0$.

Results: Feature values from FBP reconstructions with 4 mm sized voxels were the most stable, whereas values from TrueX reconstructions with 1.5 mm sized voxels varied up to three orders of magnitude. Some features shared exposure invariant islands of stability. In 4 mm FBP and OSEM acquisitions nine and ten features became stable after around ½ min, whereas 1.5 mm TrueX acquisitions took more than 30 min to achieve stability in nine features.

Conclusion: Textural features derived from GLCMs vary strongly with exposure, but some features show invariance within a limited range of exposures. Imaging with acquisition durations adjusted to expected activity concentrations will prevent the image count statistics from dominating texture values over the true object inhomogeneity. Comparable features values require acquisition protocol and PET/CT system specific acquisition durations.

Deep supervised residual U-Net for automatic characterization of lesions on 68Ga-PSMA PET/CT images

K. Shi[1], Y. Zhao[1], A. Gafita[2], G. Tetteh[2], F. Haupt[1], A. Afshar-Oromieh[1], B. Menze[2], M. Eiber[2], A. Rominger[1]; [1]Bern/CH, [2]Munich/DE

Purpose: The emerging PSMA targeted radionuclide therapy provides an effective method for the treatment of advanced metastatic prostate cancer. To optimize the therapeutic effect and maximize the theranostic benefit, there is an urgent need to identify and quantify target lesions prior to treatment. However, this is extremely challenging considering that a high number of lesions of heterogeneous size and uptake may distribute in a variety of anatomical context with different backgrounds. This study proposes a deep learning method to automatically characterize lesions.

Methods and Materials: A dataset included 71 patients with metastatic prostate cancer was collected from three medical centers. These patients underwent 68Ga-PSMA-11 PET/CT imaging. A 3D deep supervised residual U-Net was developed to detect the lesions. It works by first extracting salient features from PET and CT and then adopting the combined features to automatically detect all the lesions in a 3D manner. Compared to traditional 3D U-Net, we employed deep supervision, residual connection and instance normalization to improve the performance of the neural network.

Results: For bone lesions, the proposed method achieves precision of 97 % ± 9 %, recall of 98 % ± 7 %, and F1 score of 98 % ± 8 %. For lymph node lesions, the proposed approach obtains precision of 75 % ± 35 %, recall of 84 % ± 21 %, and F1 score of 79 % ± 22 %.

Conclusion: The preliminary test of this study confirmed the potential of deep learning methods. Increasing the amount of training data may further enhance the performance of the proposed deep learning method.

Artificial neural network for prediction of post-therapy dosimetry for 177Lu-PSMA I&T therapy

K. Shi[1], C. Dong[2], A. Gafita[2], Y. Zhao[1], G. Tetteh[2], B. Menze[2], A. Afshar-Oromieh[1], M. Eiber[2], A. Rominger[1]; [1]Bern/CH, [2]Munich/DE

Purpose: The emerging PSMA-targeted radionuclide therapy (RLT) is an effective treatment for metastatic castration-resistant prostate cancer (mCRPC). The European council mandates that treatments should be planned according to the radiation doses delivered to individual patients. However, there is no method to predict the dosimetry before RLT for treatment planning. Therefore, we aimed to prove the concept to employ artificial neural networks (ANNs) to predict the post-therapy dosimetry.

Methods and Materials: A cohort of 43 patients with mCRPC received ^{177}Lu-PSMA I&T including baseline ^{68}Ga-PSMA-11 PET/CT. After first RLT cycle, the patients underwent 3–5 planar whole-body scans for purpose of dosimetry. Organ-based SUV uptake were obtained from pretherapy PET/CT scans. Blood test values were also included. Dosimetry was calculated for kidney, liver, spleen and salivary glands using Hermes Olinda 2. A 3-layer fully connected neural network was built up in Keras. Our results were compared with population-based dosimetry from literature.

Results: The proposed ANN achieved the dosimetry prediction error of $14.0 \pm 12.4\%$ for kidney, $15.7 \pm 10.3\%$ for liver, $77.5 \pm 12.8\%$ for salivary glands and $24.3 \pm 16.1\%$ for spleen. The inclusion of blood test didn't reduce the prediction error ($p > 0.9$), $15.8 \pm 13.2\%$ for kidney, $18.2 \pm 9.4\%$ for liver, $72.2 \pm 15.8\%$ for salivary glands and $28.1 \pm 19.9\%$ for spleen. In contrast, the prediction based on literature population mean has significantly larger error ($p < 0.01$), $46.2 \pm 50.4\%$ for kidney, $99.5 \pm 238.7\%$ for liver, $705.7 \pm 377.7\%$ for salivary glands.

Conclusion: The proof of concept study shows that ANN can significantly reduce the prediction error compared to generally population-based estimation. Artificial intelligence may provide a practical solution to improve the dosimetry-guided treatment planning for RLT.

Comparison of commercial and in-house dosimetry tools for Y-90 hepatic radioembolisation

T. V. M. Lima[1], S. Gnesin[2], K. Buchauer[3], N. Schäfer[2], J. Prior[2], F. Forrer[3]; [1]Aarau/CH, [2]Lausanne/CH, [3]St. Gallen/CH

Purpose: The aim of this work was to compare absorbed dose calculations from in-house and different commercial solutions in ^{90}Y microspheres hepatic radioembolisation.

Methods and Materials: We retrospectively compared pre-treatment ^{99m}Tc-MAA SPECT/CT-based absorbed dose estimations to tumor and organs-at-risk (OAR), for the same patient, obtained using an in-house dosimetry method implemented at CHUV (image co-registration and organ segmentation obtained with PMOD software, partition model calculation performed in Matlab®) and two commercial software: Varian RapidSphere (RapidSphere Velocity, Varian, Palo Alto, USA) and Simplicit^{90}Y (Simplicit^{90}Y™, MIRADA, Oxford, UK). To minimize inter-software variability, the same set of tumor and OAR volumes delineated by intensity threshold methods on SPECT were used. Quantitative comparison was assessed in terms of absorbed dose to tumor, normal liver and lungs. The compared tools rely on the partition model formalism and the local deposition model (LDM) to derive tissue doses.

Results: The highest absorbed dose difference (–0.51%) between in-house solution and commercial solution was obtained for the tumor. For the normal liver and lungs, the variations were smaller with –0.15% and 0.00%, respectively.

Conclusion: Available commercial solutions for ^{90}Y microspheres radioembolisation dosimetry have the potential to improve clinical workflow. Our study showed that both tested commercial solutions were in very good agreement with our in-house method. Advantages of tested commercial solutions resides in the availability of advanced segmentation and registration tools coupled with convenient results presentation (3D dose distribution, multi-treatment evaluation; biological dose scaling).

Evaluation on usefulness of dose management systems in Nuclear Medicine departments across Switzerland for establishment of national dose reference levels for injected activities

T. V. M. Lima[1], K. Strobel[2], S. T. Schindera[1], E. Nitzsche[1]; [1]Aarau/CH, [2]Lucerne/CH

Purpose: The aim of this work was to determine the number of Dose management systems (DMS) in use in Swiss Nuclear Medicine (NM) departments and to evaluate its adequacy to collect data about the injected activity in patient examinations and subsequent surveys.

Methods and Materials: A survey was performed across 28 (out of the 50 registered) NM departments in Switzerland: 5 university hospitals, 17 cantonal hospitals (out of 24) and 6 corresponded to private institutions and smaller clinics (out of 21 representing 29%). The questionnaire evaluated whether DMS is available within the hospital's departments, if this covered the NM department, and which type of devices was connected to. Additionally, the departments were asked about their procedures for recording patient doses for injected activity in order to understand if injected activities were already digitalised and ready to be queried.

Results: The survey showed that although well connected to DMS the NM doses are mostly (13 out of 17 departments) collected for CT components only among the NM devices. Only 2 centres are currently collecting all dose information from both CT and injected activity parts and 2 centres partially collect all but for some of the devices. The survey also showed the heterogeneity within Swiss NM departments storage and information systems.

Conclusion: Because DMS is not implemented in most Swiss nuclear medicine departments it cannot be used for systematic collection of injected activities to establish national dose reference levels. After widespread implementation, DMS has the potential to be an important tool for dose data collection and protocol optimisation.

Report on the results from an injected activity survey across Switzerland

T. V. M. Lima; Aarau/CH

Purpose: The aim of this survey was to understand if a full national survey would provide different values for diagnostic reference levels for injected activities in Nuclear Medicine.

Methods and Materials: Centres were requested to provide at least 20 entries per chosen protocol for patient within normal weight range (65–75 kg) and 20 entries for patients outside this weight range. The protocols were chosen based on the frequency and high patient doses (F-18 FDG; Tc-99m Bone and Tc-99m Heart). Two methods were used for analyze the results, one based on ICRP definition of local DRL and the one suggested for national DRLs (NDRL). The NDRL numerical value for radiation dose quantity is derived from the 75th percentile of the distribution of median doses from the dose audit of participating facilities.

Results: Method 1 (Verification) showed little change from previous DRL for both FDG and Bone protocols, 8.5 and 2.1% respectively. In the heart protocol there is a potential huge variation (41.9%). But this is initially dictated by specific characteristics from specific cardiac device and dedicated collimator/software.

Method 2 (new ICRP DRL method) showed very good levels of reduction but is less statistical relevant due to the low number of centres surveyed (13.0, 8.1 and 44%, repectively for FDG, Bone and Heart protocols).

Conclusion: A potential dose reduction has been observed by the two methods evaluated in this study. It goes follows the expectation that DRL values would decrease with advances in technology, such as iterative reconstruction and CZT solid-state detectors.

A PET study of perfusion and metabolic changes and cortical tau pathology in Alzheimer's disease

C. Noirot, I. C. Mainta, A. Dodich, P. Andryszak, M. Scheffler, K.-O. Loevblad, G. Frisoni, V. Garibotto; Geneva/CH

Purpose: To assess the association of tau pathology (T-status, measured with Flortaucipir PET) and neurodegeneration (N-status, assessed with Florbetapir perfusion images and FDG) in patients with suspected Alzheimer's disease (AD).

Methods and Materials: In this pilot single center prospective study ongoing since November 2016, 80 subjects with cognitive complaints were evaluated. The study was approved by the institutional review board, and all participants provided signed informed consent. Eighteen participants were cognitively normal at neuropsychological evaluation, 54 presented mild cognitive impairment, and 8 major neurocognitive disorder. Five patients with biomarker-based diagnosis of non-AD neurodegenerative etiology were excluded. The N-status was estimated on 1) perfusion, namely Florbetapir images 1–6 minutes p.i., 2) metabolism by FDG at 30 minutes p.i., in a subgroup of 42 individuals, compared with a reference-database. The T-status was based on Flortaucipir distribution 75–105 minutes p.i., scored visually, considered pathological from Braak stage 3. PET images were acquired on a Biograph-64 or mCT Siemens scanner. Associations and agreements were evaluated using chi-squared, Cohen's kappa tests.

Results: A significant association was found between T and N status, as measured by Florbetapir perfusion (p < 0.001). A moderate agreement existed between neocortical tau and Florbetapir perfusion (kappa = 0.44). For the subgroup studied with Florbetapir perfusion and FDG, a substantial agreement was found between the two N measures (kappa = 0.66).

Conclusion: Our study confirms that cortical tau pathology is significantly associated with perfusional and metabolic deficits. Perfusion with Florbetapir is an adequate proxy of the N classification provided by FDG.

Characterising the metabolic pattern in synucleinopathy-associated neurodegeneration

I. L. Alberts[1], P. Wu[2], X. Han[2], H. Yu[2], I. Yakushev[3], J. Wang[2], S. Förster[4], C. Zuo[2], K. Shi[1], A. Rominger[1]; [1]Bern/CH, [2]Shanghai/CN, [3]Munich/DE, [4]Bayreuth/DE

Purpose: Synucleinopathy comprises a group of neurodegenerative disorders (Parkinson's disease PD, Lewy body dementia and multiple system atrophy), for which idiopathic REM-sleep behaviour disorder (iRBD) can be considered a prodrome. The purpose of this study was to characterise the pattern of change in cerebral metabolism observed in the progression from iRBD to PD. Hitherto, network analyses based on scalar pattern scores have had limited utility in describing the heterogeneity of regional metabolic change.

Methods and Materials: 19 polysomnography confirmed iRBD patients, 38 clinically confirmed PD patients and 19 (age and gender matched) healthy control subjects underwent FDG-PET/CT. The datasets were analysed using an automated anatomical labelling (AAL) template. Meta-regions of interest (ROI) were defined, which were then statistically analysed across the three groups. Comparison was made with clinical symptomatology by means of the UPDRS III Score.

Results: Dynamic patterns of hypo- and hyper-metabolism were observed across the three groups. Four patterns were characterised: progressive, non-progressive, reversible (observed in the iRBD group only) and late features (observed in the PD Group only). The results were in-keeping with PD-related findings in previous studies. Significantly, using the patterns characterised here, the subset of the iRBD patients at risk of PD development can be interrogated, raising the notion of a PET-based imaging biomarker.

Conclusion: This study has demonstrated that there is a heterogeneous and anisotropic pattern of cerebral metabolism over the clinical course from iRBD to PD, potentially forming the basis for future biomarker identification, for which more advanced pattern recognition algorithms and longitudinal studies are required.

When "hot is not so hot": High-resolution digital PET/CT increases 18F-FDG physiological uptake of pituitary gland

M. Meyer, J. Prior, M. Nicod Lalonde, M. Pappon, N. Schäfer, S. Gnesin; Lausanne/CH

Purpose: With improved spatial resolution of the latest SiPM digital PET/CT (dPET), normal uptake of smaller structures shows improved SUV signal recovery and might appear abnormally hot. We compared ^{18}F-FDG physiological uptake in the pituitary gland (PG) in patient imaged with dPET and with conventional PET (PET). Additionally, we performed phantom experiments to characterize signal recovery and detectability of small structures.

Methods and Materials: We retrospectively included 10 dPET and 10 PET and collected PG SUVmax, SUVmean and SUVratio (SUVr = SUVmax / cerebellum SUVmean). A modified NEMA/IEC phantom was imaged with both PET (background activity 5 kBq/mL, and 3x and 5x higher concentrations in Æ2–20-mm spherical inserts). Mean recovery coefficients (RCmean) and signal-difference-to-noise-ratio (SDNR) were computed to assess lesion detectability (needed SDNR > 3).

Results: dPET presented higher PG SUVmax and SUVr compared to PET (4.7 ± 2.05 vs 2.9 ± 0.63, p = 0.004; and 0.62 ± 0.25 vs 0.39 ± 0.10, p = 0.029, respectively), while there was no difference for SUVmean (2.7 ± 1.32 vs 2.1 ± 0.45, p = 0.39). Thus, with a SUV readout scale of 0–5g/mL, normal PG appears hot with dPET, but not with PET. Phantom evidenced higher RCmean in dPET compared to PET. For both 3x and 5x measurements, lesion detectably according to size was systematically superior with dPET.

Conclusion: dPET patients presented higher ^{18}F-FDG physiological PG uptake as compared to PET patients. These findings were supported by phantom experiments demonstrating superior signal recovery and small region detectability with dPET. Awareness of this "new, higher" normal ^{18}F-FDG uptake is important to avoid potential pitfalls in image interpretation.

Increased myocardial 99mTc-DPD uptake associated with increased LV mass allows for improved accuracy in diagnosing cardiac amyloidosis

A. Scarale[1], C. Popescu[1], R. Sara[1], L. Monaco[1], M. Spallino[1], C. Dolci[1], F. Musca[1], C. Rossetti[1], F. Caobelli[2]; [1]Milan/IT, [2]Basel/CH

Purpose: Cardiac amyloidosis (CA) is a progressive cardiomyopathy for which new therapies are now available. Non-invasive imaging like 99mTc-DPD scintigraphy can aid in the diagnostic workup. Perugini qualitative-score is a powerful tool to identify CA. However, a more quantitative approach is desirable. We aimed at validating a semiquantitative parameter able to improve the diagnostic accuracy in patients with suspected CA.

Methods and Materials: 29 Patients were retrospectively evaluated. All underwent comprehensive clinical evaluation, trans-thoracic echocardiography (TTE) and whole-body scintigraphy with ^{99m}Tc-DPD. Each scan was visually interpreted using Perugini score and semiquantitatively with cardiac uptake normalized to background activity (nCU), defined as [total counts (myocardial ROI) / total counts (background ROI)]. ROIs dimensions were identical in the same patient. TEE assessed LV volumes, function and mass. Final diagnosis was obtained by biopsy (3/29) or clinical follow-up.

Results: There was a significant correlation between Perugini score and nCU (r = 0.89, p < 0.001). nCU was unrelated to BMI (p = 0.56). CA was confirmed in 7/29 patients. ROC curves demonstrated good diagnostic performance of nCU (AUC = 0.675), optimal threshold was 1.38 (sensitivity 85.7 %, specificity 54.5 %). An optimal threshold of 317.5g/m^2 was shown for LV mass (Sensitivity 50.0 %, specificity 78.6 %). The simultaneous presence of nCU and LV mass above limits yielded improved accuracy (global chi-square 15.75, p = 0.03).

Conclusion: These preliminary data on a small cohort support at least a non-inferiority of nCU compared to the widely accepted Perugini visual score. Combining myocardial ^{99m}Tc-DPD uptake and LV mass resulted in improved diagnostic accuracy.

Quantification of myocardial blood flow using high-resolution, high-sensitivity and 211-ps SiPM 82Rb-PET/CT: Comparison of three software packages

M. Ireige, C. Kamani, G. Allenbach, M. Pappon, P. Genoud, M. Nicod Lalonde, N. Schäfer, J. Prior; Lausanne/CH

Purpose: Myocardial blood flow (MBF) quantification is a promising noninvasive tool for the evaluation of CAD, assisting in diagnosis, treatment, and risk stratification. Several analysis software packages are validated for MBF quantification. We compared results of MBF obtained using three software packages used in clinical routine.

Methods and Materials: Seventeen patients underwent dynamic ^{82}Rb-PET at rest and during adenosine stress on a latest generation SiPM PET/CT (Siemens Biograph Vision 600). Data were processed with (1) Corridor4DM , (2) FlowQuant and (3) Syngo.PET MBF. MBF and myocardial flow reserve (MFR) polar maps were computed. Comparisons used Pearson's correlation ρ (measuring precision), Bland-Altman limit-of-agreement and Lin's concordance correlation $ρ_c = ρ·C_b$ (C_b measuring systematic bias).

Results: Lin's concordance and Pearson's correlation values were fairly similar, suggesting no systematic bias between Corridor4DM and Flow-Quant with an excellent precision ρ for rest and stress MBF (ρ=0.810, $ρ_c$=0.721, C_b=0.890 and ρ=0.944, $ρ_c$=0.897, C_b=0.950, respectively) and good precision for MFR (ρ=0.929, $ρ_c$=0.896, C_b=0.965), as well as between Corridor4DM and Syngo.PET (MBF: ρ=0.791, $ρ_c$=0.458, C_b=0.579 and ρ=0.890, $ρ_c$=0.827, C_b=0.929; MFR: ρ=0.591, $ρ_c$=0.509, C_b=0.862) and Flow-Quant and Syngo.PET (MBF: ρ=0.824, $ρ_c$=0.610, C_b=0.740 and ρ=0.876, $ρ_c$=0.862, C_b=0.984; MFR: ρ=0.717, $ρ_c$=0.564, C_b=0.786). Although no mean bias was observed on Bland-Altman plots, Syngo.PET provided slightly lower values than FlowQuant and Corridor4DMat higher MBF and MFR values.

Conclusion: Concordance between software packages was excellent for MBF and MFR, despite slightly lower values by Syngo.PET at higher MBF values. Therefore, comparison of outcomes from the three software packages assessing quantification of MBF can be applied in clinical practice.

Amyloid PET imaging in cardiac amyloidosis: A pilot study using 18F-Flutemetamol positron emission tomography

S. Dietemann, R. Nkoulou, C. Noirot, V. Garibotto; Geneva/CH

Purpose: Cardiac amyloidosis is a rare disease characterized by amyloid heart deposits and is usually a part of systemic amyloidosis, in relation to systemic light chain (AL) and transthyretin (ATTR wild type or genetic) amyloidosis. Several recent studies suggest a promising role of amyloid pet imaging to image cardiac amyloidosis and several pet tracers are now available for in vivo detection of amyloid deposits. The aim of this study was to evaluate 18F-Flutemetamol in diagnosing cardiac amyloidosis.

Methods and Materials: We performed a pilot study using 18F-Flutemetamol in twelve patients, three controls subjects without cardiac amyloidosis and nine subjects with documented cardiac amyloidosis. Mean standardized uptake value (SUV) in the left ventricular myocardium and blood pool were determined and semi quantitative parameter as target to background ratio (TBR, myocardial/Blood Pool Mean SUV Ratio) between 10th and 30th minutes was calculated.

Results: Uptake of 18F-Flutemetamol in the left ventricular myocardium was present in all patients with cardiac amyloidosis except one and none in control patient. The TBR was significantly higher in amyloidosis patients than in control subjects: TBR median 1.46, IQR 1.33 – 1.74 versus 1.06, IQR 0.89 – 1.08 (p=0.016). Only one patient in our study had light chain amyloidosis and showed higher TBR than patients with transthyretin amyloidosis: TBR 3.0 versus TBR median 1.44, IQR 1.33 – 1.66.

Conclusion: Amyloid pet tracers such as 18F-Flutemetamol could be a promising tool in diagnosing and in therapy response assessment for patients with cardiac amyloidosis.

3D-Quantitated lung perfusion 99mTc-MAA SPECT/CT and assessment of SPECT-data driven respiratory gating in emphysema and lung cancer patients

A. Chirindel[1], M. Cachovan[2], A. H. Vija[3], D. Stolz[1], M. Tamm[1], D. Lardinois[1], D. Wild[1], G. Nicolas[1]; [1]Basel/CH, [2]Forcheim/DE, [3]Chicago/US

Purpose: Prior to lung resection, predicting the postoperative lung function is of paramount importance. The current practice uses planar (2D) scintigraphy. We aim to assess clinically the accuracy of 3D-quantitated lung perfusion SPECT/CT and added value of respiratory gating.

Methods and Materials: Prospective, single centre study in 106 patients. Planar and SPECT/CT lung perfusion scans were performed on a single imaging system (Intevo, Siemens). The lobar contribution to the total lung perfusion was assessed using the established 2D-projection method and the 3D-anatomical method (CT Pulmo 3D and xSPECT-Quant-Siemens). A computational anthropomorphic chest phantom was used as standard of reference (XCAT). SPECT data-driven respiratory gating was performed in 56 patients. We used Student's paired t-test for statistical analysis of matched-pair data.

Results: At the lobar level, 2D systematically underestimated the contribution of the upper lobes, and overestimated the one of the lower lobes, which in 43 patients was ≥10% of the total lung perfusion. Compared to the input data of an homogenously filled anthropomorphic phantom, 3D-method was more accurate in estimating the lobar contribution than 2D with a bias of +0.5% vs −10.4%, +0.2% vs +12.4%, +0.8 vs −6.6%, −0.1% vs −5.1% and +0.4% vs 13.3% for the left upper, left lower, right upper, middle and lower lobes, respectively. Adding respiratory gating only marginally changed the lobar contribution (mean 0.6±0.8%).

Conclusion: 3D Quantification of lung perfusion is clinically practical and is substantially more accurate than the currently used 2D-method. Further studies are warranted to assess the impact on clinical management.

First-in-human study with 18F-Azafol for folate receptor targeted PET/CT: Updated results of the PET_FOL_1 phase-I trial

A. Meisel[1], I. A. Burger[1], J. Müller[2], S. Gnesin[3], M. Siano[2], M. Früh[2], M. Choschzick[1], C. Mueller[4], S. Geistlich[4], L. Haefliger[3], S. M. Ametamey[1], R. Schibli[4], V. Treyer[1], P. A. Kaufmann[1], J. Prior[3], N. Schäfer[3]; [1]Zurich/CH, [2]St. Gallen/CH, [3]Lausanne/CH, [4]Villigen/CH

Purpose: The folate receptor (FRα) has been found to be overexpressed in various cancers. PET_FOL_1 study is assessing the safety and specificity of ^{18}F-AzaFol, a novel FRα-targeting PET radiotracer.

Methods and Materials: This multicentric trial (NCT03242993) is evaluating ^{18}F-AzaFol in patients with histologically confirmed ovarian (OC) and non-small cell lung cancer (NSCLC) regarding tracer uptake, change of overall staging, lesion detection rate, gained overall information and confidence adjusting therapy based on imaging results. Images were compared with FRα immunohistochemistry (IHC) from tumor biopsy. Dosimetry was the secondary objective.

Results: We included 12 patients and observed an IHC positivity in 38% (3/8) of NSCLC and 100% (4/4) of the OC patients. Although tumor heterogeneity was one of the main findings, all IHC-positive patients showed an ^{18}F-AzaFol uptake in the majority of the lesions. In two patients with negative IHC no uptake was observed in any of the lesions. ^{18}F-AzaFol-PET/CT enabled the detection of additional lesions in comparison to the standard-of-care imaging (FDG-PET, MR and/or CT) performed prior to study entry. In three NSCLC patients several new bone or subcutaneous metastases could be identified. Incidental findings were ^{18}F-Azafol-avid recurrent meningiomas and diffuse bone marrow uptake in two NSCLC patients. Dosimetry revealed a mean effective dose of 6.0 mSv (70-kg patient), which is comparable to ^{18}F-FDG. No drug related adverse events were reported.

Conclusion: ^{18}F-Azafol-PET/CT has been shown to be specific for identifying FRα-positive tumors. ^{18}F-AzaFol is well tolerated and holds the potential to influence overall staging of OC and NSCLC FRα-positive tumors.

18F-FDG PET/CT metabolic/volumetric parameters evaluation to predict response to neoadjuvant chemotherapy and the prognostic value in patients with Triple-Negative breast cancer (TNBC)

G. Paone, G. Treglia, M. Raditchkova, T. Ruberto, L. Ceriani, L. Giovanella; Bellinzona/CH

Purpose: The aim of this study was to assess response to NAC and prognostic value considering dynamic evolution of metabolic/volumetric parameters measured on 18F-FDG PET/CT in TNBC.

Methods and Materials: we retrospectively analyzed 42 patients with TNBC, who performed a staging PET/CT before and after neoadjuvant chemotherapy. Treatment-related changes in SUVmax, MTV and TLG were evaluated (ΔSUVmax, ΔMTV and ΔTLG) in the primary tumor. To identify the optimal cut-off value of these parameters a receiver-operating curve analysis was performed. Kaplan-Meier method was used to evaluate prognostic value. The associations between early metabolic/volumetric changes, pathological complete response (pCR), and event-free survival (EFS) were examined.

Results: Of the 42 patients, 10 (24%) achieved pCR, 14 (33%) relapsed and 10 of them died (median FU, 34 mo). No relapse was observed in patients with pCR (0.001). An optimal percent of decrease in SUVmax (cutoff value ΔSUVmax 84%, p 0.001), MTV (cutoff value ΔMTV 67%, p 0.0001) and TLG (cutoff value ΔTLG 94%, p 0.0004) had the best predictive value in terms of pCR. No significant correlation was found with SUVmax, MTV and TLG absolute value. ΔSUVmax 84% (p 0.0001), ΔMTV 67% (p 0.005) and ΔTLG 94% (p 0.0001) were significantly associated with EFS.

Conclusion: Our data suggest that only the dynamic variation of 18F-FDG PET/CT metabolic/volumetric parameters is a predictive marker for pCR and EFS following NAC in TNBC. In the future, additional chemotherapy could be applied according to percent of decrease in these parameters after standard NAC to achieve a pCR enabling breast-conserving surgery.

68Ga-exendin-4 PET/CT specifically detects insulinomas in MEN-1 patients

K. Antwi[1], G. Nicolas[1], M. Fani[1], T. Heye[1], F. Pattou[2], P. Chanson[3], J.-C. Reubi[4], A. Perren[4], B. Gloor[4], E. Christ[4], D. Wild[1]; [1]Basel/CH, [2]Lille/FR, [3]Paris/FR, [4]Bern/CH

Purpose: In patients with multiple endocrine neoplasia type-1 (MEN-1) current guidelines recommend surgical resection of pancreatic neuroendocrine tumours (PanNET) ≥2 cm and of all insulinomas defined as clinically relevant lesions. Reliable preoperative localization of clinically relevant lesions is essential for surgery planning and for sparing healthy parenchyma. We aim to evaluate the sensitivity of ^{68}Ga-exendin-4 PET/CT in the detection of clinically relevant lesions in MEN-1 patients with endogenous hyperinsulinaemic hypoglycaemia (EHH) in comparison with MRI.

Methods and Materials: Post-hoc analysis of 6 consecutive MEN-1 patients, as part of a larger prospective study of 52 patients with EHH evaluated with ^{68}Ga-exendin-4 PET/CT and MRI. Readers were unaware of other results when reading the scans. Surgery was performed based on all imaging results. Reference standard was surgery with histology and treatment outcome. True positive was considered PanNET ≥2 cm or insulinoma = clinically relevant lesions. Lesion-based analysis was carried out.

Results: Histopathology confirmed 37 neuroendocrine tumours among which 11 were insulinomas (median 11 mm; range 1–20 mm). Sensitivity (95% CI) for MRI, PET/CT and combined PET/CT+MRI was 38.5% (13.9-68.4%), 84.6% (54.6-98.1%) and 92.3% (64.0-99.8%), respectively (p-value=0.014 for the comparison of PET/CT+MRI versus MRI). MRI detected 3 insulinomas ≥20 mm in 2 patients, while PET detected 10 insulinomas in 6 patients. After surgery EHH resolved in all patients.

Conclusion: ^{68}Ga-exendin-4 PET/CT is useful in MEN-1 patients with EHH. The combination with MRI is superior to MRI alone in the detection of insulinomas among multiple PanNET and may guide the surgical strategy.

Evaluation of the CCK-2 receptor agonist 177Lu-PP-F11N for PRRT of medullary thyroid carcinoma – Results of a phase 0 „Lumed" Study

C. Rottenburger[1], G. Nicolas[1], L. McDougall[1], F. Kaul[1], E. Christ[2], M. Cachovan[3], R. Schibli[4], S. Geistlich[4], M. Behe[4], D. Wild[1]; [1]Basel/CH, [2]Bern/CH, [3]Forchheim/DE, [4]Villigen/CH

Purpose: Targeting the cholecystokinine-2 (CCK-2) receptor with radiolabelled gastrin analogues is a potential approach for radionuclide therapy of medullary thyroid carcinoma (MTC). Unfortunately, kidney and bone marrow toxicity precluded therapeutic applications of CCK-2 receptor specific radiotracers until now. The aim of this prospective first-in-man study is to test the proof of principle that the novel gastrin analogue [177Lu-DOTA-(DGlu)6-Ala-Tyr-Gly-Trp-Nleu-Asp-PheNH2] (^{177}Lu-PP-F11N) targets specifically CCK-2 receptor positive MTC and spares the kidneys and bone marrow (ClinicalTrials.gov: NCT02088645).

Methods and Materials: Six patients received two injections of 1GBq ^{177}Lu-PP-F11N, one injection with and the other without potentially kidney protective Physiogel infusion. Sequential quantitative SPECT/CT scans and blood sampling were performed for 3D tumor and organ dose estimation. Several safety parameters were measured up to 12 weeks after the second administration of ^{177}Lu-PP-F11N.

Results: Adverse reactions were mild and self-limiting (≤ grade 1, CT-CAE version 4.03). In all patients, ^{177}Lu-PP-F11N accumulation was visible in tumor tissue with a median radiation dose of 0.88 Gy/GBq (range 0.69–2.85). The highest organ uptake was seen in the stomach, resulting in a dose of 0.46 Gy/GBq (0.13–2.07). Median tumor-to-kidney dose ratios were 12.8 (6.0–52.4) without Physiogel and 12.4 (6.4–29.8) with Physiogel (not significantly different with a p-value of 0.17).

Conclusion: The administration of the novel CCK-2 receptor ligand ^{177}Lu-PP-F11N was safe in all six examined patients. Visualization of metastasized/recurrent disease in all patients provides evidence that CCK-2 receptor targeting with 177Lu-PP-F11N for PRRT is feasible in patients with MTC.

90Y- or 177Lu-DOTATOC therapy improves symptoms control and impacts on clinical management of metastatic insulinoma

M. T. Freitag[1], M. L. Braun[1], E. Christ[1], B. Goichot[2], T. O'dorisio[3], D. Bushnell[3], M. A. Walter[4], D. Wild[1], G. Nicolas[1]; [1]Basel/CH, [2]Strasbourg/FR, [3]Iowa City/US, [4]Bern/CH

Purpose: Metastatic insulinoma is an extremely rare neuroendocrine neoplasia with estimated incidence of 1-4/10'000'000. Uncontrolled hypoglycaemia is a major cause of acute morbidity and mortality in this disease. Here, we retrospectively evaluate the hitherto largest patient series on this topic assessing the value of radiolabelled somatostatin analogue (DOTATOC) for the clinical control of progressive, metastatic insulinoma.

Methods and Materials: A total of 20 Patients were enrolled between 2001–2018. Patients with metastatic insulinoma were treated with repeated cycles of Yttrium-90-DOTATOC, with consecutive cycles of Yttrium-90-DOTATOC and Lutetium-177-DOTATOC, or with Lutetium-177-DOTATOC alone. Clinical response and toxicities after DOTATOC-therapy were assessed. Standard of reference of a successful therapy was defined as reduction of medication necessary to maintain stable blood glucose level.

Results: 14 patients received Yttrium-90-DOTATOC only (1–3 cycles; range: 5.6–14.8 GBq), 2 patients received Yttrium-90-DOTATOC (1 cycle; 5.9–8.1 GBq) plus Lutetium-177-DOTATOC (2 cycles; with totally 13 and 14.8 GBq respectively) and four patients received Lutetium-177-DOTATOC only (3-4 cycles, each 5.5–7.4 GBq). 16 of 20 patients experienced grade 1/2 hematotoxicity (88%), no higher grade occurred. In 14 of 20 patients (63%), anti-hypoglycemic medication could be reduced after DOTATOC therapy. Four patients requiring permanent glucose infusion could discontinue infusion after the first cycle.

Conclusion: Yttrium-90/Lutetium-177 DOTATOC therapy is able to reduce anti-hypoglycaemic medication in a significant proportion of patients with progressive, malignant insulinoma. These results make DOTATOC a promising therapeutic option for patients with metastatic insulinoma.

Is repetitive somatostatin receptor-targeted radiopeptide therapy with 90Y- and/or 177Lu-DOTATOC effective in patients with neuroendocrine tumors? - A retrospective single-center analysis in 523 patients

M. Benz[1], R. Grkovski[2], E. Christ[1], G. Nicolas[1], D. Wild[1]; [1]Basel/CH, [2]Maribor/SI

Purpose: The aim of this study was to investigate the time to retreatment with ^{90}Y- and/or ^{177}Lu-DOTATOC somatostatin receptor-targeted radiopeptide therapy (PRRT) in patients with recurrent or progressive neuroendocrine tumors (G1, G2).

Methods and Materials: In this single center retrospective analysis, 523 patients (323 male and 200 female; age 59±11 yrs) underwent retreatment with ^{90}Y- and/or ^{177}Lu-DOTATOC between March 2000 and July 2018 for recurrent or progressive low or intermediate grade neuroendocrine tumors. 150 out of the 523 patients (29%) underwent a second ^{90}Y- and/or ^{177}Lu-DOTATOC retreatment. The time interval in months and the interquartile range were calculated between treatments.

Results: Overall, the 523 patients received a total of 2330 cycles of ^{90}Y- (n = 1230) or ^{177}Lu- (n = 1100) DOTATOC (median, 4 cycles). The median time interval was 32.5 months (IQR, 32.5) between the initial treatment and first retreatment and 29.0 months (IQR 28.2) between the first and second retreatment.

Conclusion: ^{90}Y- and/or ^{177}Lu-DOTATOC retreatments are effective and should be considered in patients with recurrent or progressive neuroendocrine tumors (G1, G2).

161Tb-based prostate cancer therapy: Investigating the "177Lu-PLUS Effect"

C. Mueller[1], V. Tschan[1], N. Gracheva[1], C. A. Umbricht[1], P. Bernhardt[2], J. R. Zeevaart[3], U. Koester[4], R. Schibli[1], V. D. M. Nicholas[1]; [1]Villigen/CH, [2]Gothenburg/SE, [3]Pretoria/ZA, [4]Grenoble/FR

Purpose: ^{161}Tb is believed to be a promising alternative to ^{177}Lu due to its emission of short-range (conversion/Auger) electrons in addition to β⁻-particles. Short-range electrons are particularly well-suited for the treatment of small lesions and single cancer cells. The aim of this study was to investigate whether ^{161}Tb outperforms ^{177}Lu in preclinical settings of prostate cancer.

Methods and Materials: The effects of ^{161}Tb-PSMA-617 and ^{177}Lu-PSMA-617, respectively, were compared in vitro using survival (MTT) and clonogenic assays. Nude mice were treated with variable activity levels of ^{161}Tb-PSMA-617 and ^{177}Lu-PSMA-617, respectively, 2 days after PSMA-positive PC-3 PIP tumor cells inoculation. The mice were monitored over 5 weeks by measuring of the tumor size and body weight every second day.

Results: In vitro, ^{161}Tb-PSMA-617 was more effective than ^{177}Lu-PSMA-617, to reduce tumor cell viability and improve survival, when applied at the same activity concentration. In vivo, endpoint criteria were reached within about 3 weeks for untreated control mice. The tumor growth was only slightly delayed when using the radioligands at low activity (2.5 MBq per mouse). At higher activity (5 MBq/mouse), ^{161}Tb-PSMA-617 was more effective at reducing tumor growth than ^{177}Lu-PSMA-617 and it eradicated most tumors entirely when applied at 10 MBq per mouse. Blood plasma parameters were in the same range for treated mice and untreated controls, indicating the absence of early side effects.

Conclusion: The "^{177}Lu-PLUS" effect was demonstrated in vitro and in vivo using ^{161}Tb-PSMA-617 in preclinical settings. These findings have paved the way towards a translation of this promising concept to clinical trials.

Automation in radiographers work: Influence and challenges for the profession

L. Marmy[1], V. N. Ho[2]; [1]Lausanne/CH, [2]Fribourg/CH

Purpose: Automation in radiology (robotics and softwares) involves an adaptation of the radiographers work methodology and the aim of this study is to analyze the influence of this phenomenon in their profession and the challenges.

Methods and Materials: Based on a qualitative approach, the study design is descriptive and exploratory. The method is semi-structured interviews and 8 radiographers from various west Switzerland institutions were interviewed. The main topics approched were automatized acts, radiographers role and human-machine association

Results: Automation offers new opportunities to radiographers in matter of fieldworks, competencies, responsibilities and educations. However, the care management implicate not enough radiographers in the institutional decision-making process when new technologies are implemented. The many challenges for the profession should be considered.

Conclusion: The automatized technologies influence deeply the occupation of technologists in opportunities, decision-making processes, work methodologies and machine controls.

Deep learning in osteoarticular imaging: The role of the radiographer

A. Al-Musibli, O. Cagdas, X. Montet, J. Schmid; Geneva/CH

Purpose: Radiologists use different systems of Computer Aided Diagnosis (CAD) that have significantly improved over time thanks to Deep Learning (DL) and Big Data. This "artificial intelligence (AI) revolution" is shaking up the world of radiology. In this context, we believe that radiographers can play an active role as experts in image acquisition and analysis. We report our ongoing collaboration in the development of an AI system aiming to detect the scaphoid bone in wrist radiographs and ultimately classify it as fractured or not.

Methods and Materials: We segmented more than 100 standard neutral postero-anterior radiographs of the wrist to train the DL-based AI system. Different training strategies were implemented to validate the automatic extraction of the scaphoid. In an evaluation database of 9000 radiographs, we isolated around 4000 standard wrist radiographs to assess the scaphoid extraction performance based on the most optimal training strategy.

Results: By selecting the correct training strategy, the mAP (mean Average Precision, ranging from 0 to 1) increased from 0.6 to 0.95 in the validation of the training stage. Visual inspection of the results on the evaluation database showed that the system efficiently detects the scaphoid, regardless of the presence or not of fractures.

Conclusion: We reported an efficient AI system to process wrist radiographs, which ultimately targets the detection of fractures in scaphoid bone. It is important that radiographers position themselves in the constantly evolving area of AI by playing an active role.

Comparing dynamic susceptibility contrast perfusion post-processing with different clinically available software among patients affected of a high-grade glioma

E. L. Delacoste, P. Wanyanga, B. Delattre, M. I. Vargas Gomez; Geneva/CH

Purpose: The main purpose of this retrospective study was to evaluate inter-software variability in patients affected of a high-grade glioma for the post-processing of dynamic susceptibility contrast (DSC) perfusion imaging in MRI.

Methods and Materials: The included patients were either anaplastic astrocytoma (WHO grade III) or glioblastoma (WHO grade IV) located in the cerebral parenchyma. The post-processing of 54 MRI DSC perfusion imaging from 46 patients using both Intellispace© (Philips) and Olea© (Olea Medical) software was performed. The hemodynamic parameter studied was the cerebral blood volume ratio corrected for the T1 leakage effect (rCBVc). The inter-operator variability within Olea and the variability between the methods proposed in Intellispace were also evaluated.

Results: Regarding inter-software reproducibility, ICC and Cohen's Kappa from therapeutic follow-up obtained were 0.74 and 0.61, close to the recommended limits of 0.75 and 0.60 respectively. Subgroups were created to complete the analysis and to evaluate the partial volume effect. Even if necrosis or vascular structures from regions of interest (ROI) were avoided, results did not improve. ROI of a minimum area of $250\,mm^2$ yielded an ICC and Cohen's Kappa above the threshold. The inter-operator reproducibility on Olea and intra-software reproducibility on Intellispace were satisfactory for a clinical valid assumption.

Conclusion: The variability between Intellispace and Olea was not ideal for a clinical context. This discrepancy can be explained by the partial volume effect and a difference in the models used. ROI with an area of at least $250\,mm^2$ improves this variability and becomes acceptable.

RSS04

Netzwerk Radiologie – Future perspective?

A. Bischof; St.Gallen/CH

Purpose: Das kantonale Netzwerk Radiologie unter der fachlichen und organisatorischen Klinikleitung der Radiologie Kantonsspital St.Gallen ist durch den Zusammenschluss der Klinik für Radiologie und Nuklearmedizin des Kantonsspitals St.Gallen, den radiologischen Abteilungen der Spitalregionen Rheintal Werdenberg Sarganserland und Fürstenland Toggenburg, des Spitals Linth und dem Ostschweizer Kinderspital St.Gallen entstanden.

An insgesamt 12 Standorten ist das Netzwerk Radiologie für die Durchführung und die Auswertung radiologischer und nuklearmedizinischer Untersuchungen zuständig. Durch Verwendung der selben Untersuchungsprotokolle und Untersuchungsstandards an allen Radiologiestandorten wird eine einheitliche hohe Bildqualität erreicht. Wie in den meisten modernen medizinischen Disziplinen, findet auch in der Radiologie eine zunehmende Spezialisierung statt. Um im gesamten Spektrum der Radiologie die höchste Qualität zu gewährleisten, ist das Netzwerk Radiologie in Fachbereiche unterteilt. So werden Untersuchungen unabhängig vom Standort, an dem diese durchgeführt wurden, von auf die jeweilige Fragestellung spezialisierten Radiologen interpretiert. Dadurch haben auch alle peripheren Standorte direkten Zugang zu spezialisierten Kaderärzten der Radiologie (Neuroradiologen, Interventionelle Radiologen, Pädiatrische Radiologen etc.).

Das Ziel ist eine einheitlich hohe Untersuchungs- und Befundqualität an allen zwölf Standorten.

· Wie ist das Netzwerk Radiologie entstanden?

· Wie erfolgt die fachbereichsbezogene Radiologieorganisation?

· Welches waren die grössten technischen, strukturellen sowie auch kulturellen Herausforderungen?

· Welche Chancen resultieren für die verschiedenen Standorte durch das Netzwerk?

· Welche Vorteile ergeben sich durch das Netzwerk Radiologie für Patienten und Zuweiser?

· Welche Teilprojekt stehen aktuell noch an?

Methods and Materials: siehe oben

Results: siehe oben

Conclusion: siehe oben

RSS05

Mapping university skills labs in radiography: Students' perspectives

K. Cronin[1], S. S. Ghotra[2], J. Fitzgerald[1], M. Gillard[2], I. Kieft[3], O. Reynolds[1], A. Sanderud[4], H. Sekkelsten[4], V. Hårsake[4]; [1]Dublin/IE, [2]Lausanne/CH, [3]Groningen/NL, [4]Oslo/NO

Purpose: Build an adequate practice and theory combination during the education is fundamental for every radiography student. The validity of a Skills Lab (SL) is crucial to allow radiography students to be ready for Clinical Placement (CP). This study will map the perspectives of radiography students concerning the SL.

Methods and Materials: This is mainly a quantitative study, just one qualitative component is present. 26 Optimax summer school students from Brazil, Canada, Ireland, Netherlands, Norway, South Africa and Switzerland completed a paper-based questionnaire. Excel was used to analyze the collected data. The questionnaire consists in 3 demographic closed questions, 6 closed questions concerning students' own SL, of which 3 were Likert Scale questions, and 1 open question regarding the way the students think the SL could be enhanced.

Results: Competent lab tutor, smaller group size and simulated patient interaction has been pointed out as relevant factors in the SL, while environmental factors (light, temperature) were less relevant. Equipment has been indicated to be of a lower standard than CP, although the students indicate that they feel well prepared for CP. Students found modern equipment not extremely important.

Conclusion: Students indicate that theoretical and practical skills labs prepare them well for their CP. Despite that, they highlight the importance of a competent lab tutor and additional time in the SL.

RSS06

Factors influencing student radiographers' assessment of chest radiograph image quality

R. Toomey[1], M. Chen[2], K. Davies[1], K. Fernandes[3], S. O. Heitmann[4], M. Selau Junior[5], M. M. Molehe[6], P. D. Pettka[4], J. A. Pires Jorge[3]; [1]Dublin/IE, [2]Groningen/NL, [3]Lausanne/CH, [4]Oslo/NO, [5]Florianópolis/BR, [6]Free State/ZA

Purpose: Differences of education between countries are likely influenced by the roles played by the radiographers in healthcare which, in turn, influence the radiography training programmes. The aim of the study is to understand how education of student radiographers influences image quality assessment.

Methods and Materials: 23 radiography students (Ireland, Netherlands, Norway and Switzerland) assessed 30 chest x-rays images and accepted or rejected them based on image quality. While completing the task students were eye-tracked to collect time data. After viewing session, participants give the reasons of rejection for each rejected image. Variable of total time, reject rate and reasons of rejection were analysed comparing them between students in early/later stages of education, with more/less clinical experience, and country of education.

Results: The results show that the in time taken to complete the view session is not influenced by the percentage of degree completed, clinical experience or country of education ($p > 0.05$). Participants with more clinical experience rejected more images than participants with less experience ($p = 0.03$). Country of education does not impact on the rejection rates ($p > 0.05$). However, Irish ($p = 0.04$) and Norwegian ($p = 0.03$) participants rejected more images due to exposure than Swiss participants. Students with less clinical experience rejected more images based on "lead markers" criterion ($p = 0.03$) while students more experienced rejected more images because of "artefacts" ($p = 0.03$).

Conclusion: The study shown that culture and clinical experience influence the image quality assessment. Clinical experience influences image rejection rates and reasons for rejection, while country of education influences rejection's reasons.

RSS07

Quel sera le métier des TRM demain ?

P. Vorlet[1], X. Realini[2]; [1]Savigny/CH, [2]Lausanne/CH

Purpose: Le Réseau de Veille Métier TRM est un outil d'anticipation de l'évolution du métier de TRM au service de la Section romande de l'ASTRM, des institutions sanitaires et de la filière TRM de la HES-SO. Le cycle de Veille Métier (VM) 2018 se centre sur les impacts de la digitalisation sur les métiers de la radiologie médicale en général et sur le TRM en particulier. Le but est de définir des scénarios d'évolution du TRM sur l'identité professionnelle, l'autonomie, les fonctions, les rôles et les compétences.

Methods and Materials: La méthodologie de la VM s'articule en 5 étapes.

1: les vecteurs de la révolution digitale dans la santé (IA, blockchain, etc.) sont inventoriés et identifiés comme des axes de veille.

2: les sources humaines (experts de la digitalisation de la santé, experts métier, etc.) et électroniques (rapports, conférences, etc.) clés sont sélectionnées et compilées.

3: des données sont recueillies auprès des sources pour définir les lignes de force de la digitalisation dans le domaine de la radiologie médicale.

4: des scénarios d'évolution du métier de TRM sont établis et analysés avec des praticiens métier et des managers métier.

5: élaboration d'une stratégie de professionnalisation des TRM qui intègre partage de l'information, redéfinition de l'identité métier, définition des besoins de formation et poursuite de la veille.

Results: Le Rapport de VM sera validé au 1er trimestre 2019. Il constituera un instrument de support à la transformation du métier et des TRM. Les points forts du Rapport seront présentés au CSR 19.

Conclusion: Résultats

RSS08

RAD-CHAT: A more efficient communication between radiologists and technologists

J. Fornaro, L. Ludes, J. Getzmann, R. P. Marcus, K. Strobel, J. E. Roos; Lucerne/CH

Purpose: Innumerable phone calls considerably interrupt the daily work routine. Adapting communication methods used in social-networks to the needs of a radiologist-technologist-communication has the potential to significantly reduce the level of disturbance by phone calls and hence to indirectly increase the staff's efficiency. The purpose of this study was to evaluate a dedicated Radiology-Chat-messaging system (RAD-CHAT) and to compare it to the daily use of a standard phone-communication (CP).

Methods and Materials: Communication time using RAD-CHAT and CP were registered for 9 h/day for a period of 10 days by 3 radiologists. Communication time was defined as the interval between incoming/outgoing inquiry and the moment of submitting a reply or hanging-up the phone, respectively. Additional inquiries for the same matter or personal attendance, interruption from work and mean processing time were also registered. Confidence rating from radiologists and technologists were assessed using a likert scale 1–6 (1 = very poor, 6 = excellent).

Results: Number of daily inquiries (RAD-CHAT: 53 ± 12/CP 64 ± 21) was similar for both technologies (p = 0.8). CP-communication showed a shorter interval of reply compared to RAD-CHAT (5 ± 2 vs 10 ± 5 min. p < 0.02). Mean time in patient assessment was not significantly different (p = 0.3). RAD-CHAT allowed a grouped reply, hence reducing the number of workflow interruptions. RAD-CHAT reduced the number of re-inquiries due to misunderstandings or incomplete conversations. Radiologists and technologists were very confident in using RAD-CHAT compared to CP (5 ± 1 and 4 ± 1.5, respectively).

Conclusion: RAD-CHAT is a well-accepted and safe communication-platform allowing a substantial reduction of workflow interruptions and hence enhancing work productivity and problem analysis.

Is MRI safe?

E. Maturana, S. Decker; Thônex/CH

Purpose: The MRI static magnetic field has substantially increased these last years and the majority of today radiology centers are equipped with the high magnetic field MRI. The professionals working in this environment are directly impact. It becomes important to consider this particular work environment and study its effects on human body.
What are the risks?
What are the recommendations in use today?
Methods and Materials: Bibliographic presentation and comparison of different medical and technical studies available till now.
Presentation of last major recommendations as ACR, ICNIRP, INRS, OMS, EU, OFSP.
Results: Different studies has been published mostly these last years trying to analyse and demonstrate the physiological effects of the magnetic on human exposure to the high magnetic fields in application with MRI.
Majority of the studies seem to consider the direct effects on the workers evolving in stray magnetic field as the transient at least on the short term.
On the other side some of the recent studies are interested in calculation of exposer on different parts of body for the workers in MRI and its long-term biological effects. It shows the large scale of impacts of the MRI magnetic field, which are still unknown. That point of view may be very important now when the new ultra-high magnetic field MRIs come in clinical trial and investigation.
Conclusion: Our aim is to see how the recommendation can modify our practice in MRI in the future as well as the recent discovery based on observation between static high magnetic field and its biological effects.

Prise en charge d'un patient porteur d'un dispositif médical implantable en IRM

C. Steiner; Vionnaz/CH

Purpose: La prise en charge d'un patient porteur d'un dispositif médical implantable (DMI) en Imagerie par Résonnance Magnétique (IRM) a souvent un caractère anxiogène pour le technicien en radiologie médical. Nous souhaitons définir une stratégie précise de vérification des DMI afin de réaliser un examen en toute sécurité pour le patient.
Methods and Materials: Analyse de la littérature permettant d'identifier les points clés et risques que comporte l'étude en IRM de ces patients porteurs de DMI.
Results: Retour d'expérience sur des situations complexes du point de vue des techniciens en radiologie et identification d'une stratégie de vérification par étape pour une prise en charge simple et sans risque.
Conclusion: L'identification des risques, la création d'une check-list et le suivi des guides de bonne pratique pour le technicien en radiologie s'avère des outils intéressants et permettent de réaliser un examen en toute sécurité chez un patient porteur d'un DMI.

Optimisation d'une séquence DTI en IRM dans le cadre du traitement du cancer de la prostate

M. I. C. Claudet[1], M. Rodari[1], L. R. Ostinelli[1], M. Martins Favre[2], C. Gaignot[1]; [1]Geneva/CH, [2]Lancy/CH

Purpose: Our main objective is to improve the DTI sequence of prostate MRI with images kindly shared by clinic La Colline. Indeed, these modifications will be possible by modifying the DTI parameters.
Methods and Materials: For this study we initially reviewed our DWI images via the Philips Intellispace post-treatment Portal to visualise the various fibres surrounding the prostate gland. Furthermore, we had, access to 6 full prostate MRI exams, which were all confirmed positive for PC. All the MRI exams were captured on a Philips 3T machine.
To ensure coherence in our study we put in place our own protocol for collecting and researching our key images guided us through the complex pelvic anatomy therefore helping us draw our several ROIs.
Results: Through our work, we introduced a method regarding, ROI positioning and the following parameters in their best settings. This method assured a relatively successful result. Indeed, the fibres in question were successfully tracked by our programme and were later merged and accentuated on T2 weighted transverses images.
Conclusion: In conclusion, it has been demonstrated that in the same way as brain DTI, this programme can, after modifying several parameters, be used on the prostate. Nevertheless, this programme still needs a strong collaboration between doctors, radiology technicians and engineers to achieve its maximum potential and to become a future reference in pre-operation management in PC positive patients.

Pacemakers and other implantable cardiac devices (ICDs) in MRI – Understanding the manufacturers' prerequisites and how to comply with each requirement to ensure patient safety

M. Bontean, B. Delattre, P. G. Challande, M. I. Vargas Gomez, J.-P. Vallee; Geneva/CH

Purpose: To present and explain the essential factors involved when scanning MRI conditional pacemakers and to understand which parameter should be limited to perform an MRI exam in maximized safe conditions.
Methods and Materials: The instructions for use (IFU) of five major manufacturers of Pacemakers, defibrillators and heart monitors were studied. A user-friendly chart, summarizing the major requirements to ensure safe MR of patients with ICDs was derived for 180 devices, using the most up to date versions of these IFU.
Results: The potential risks associated with the MRI of patients with implantable cardiac devices are described. The specific measures to take into consideration, for proper patient management concerns the region of interest, the exclusion zone, the SAR and more recently the B1+ rms, an unbiased parametric value, common to most MR vendors. Further mandatory conditions such as the prior screening for abandoned leads and other ICD defects, as well as the monitoring of the patients before, during and after MRI are explained.
Conclusion: We present the different limitations and prerequisites to follow in handling patients with ICDs in MRI on an everyday basis. As an increasing number of these patients will undergo MRI exams, it is important to fully understand these requirements, in order to perform the procedure in accordance with the manufacturers' safety guidelines and expert society recommendations.

MRI safety officers: Why do we need them?

M. Bontean, P. G. Challande, F. Riondel, B. Delattre, M. I. Vargas Gomez; Geneva/CH

Purpose: To describe the growing need for safety officers and to demonstrate the complexity of implant verification process in MRI.

Methods and Materials: Provide an insight of the goals and challenges of the MR safety officer. Explaining the growing need to comply with the requirements of each manufacturers, when it comes to the examination of patients with implantable and non-implantable devices. The management of safety education in a specialized environment, as well as the training of the staff that may enter the MR restricted zones. Furthermore, we will underline the MRI safety officers' role, which is to help expand, implement and manage safety programs, policies and procedures.

Results: Aiming to standardize safety evaluation and assessment in MRI, a new trend emerged: the quest for a proactive culture of safety in the MR environment. As a result, safety officers are being trained and hired by different MRI facilities all around the globe. This is to ensure the well-being of both patients and staff, in the MR environment. In Switzerland, the Geneva University Hospital recently adhered to the movement by appointing a technician as the new Safety Officer in MR "TRM Expert en Sécurité IRM", last April.

Conclusion: In the last five years, the industry of medical devices and conditional implants for Magnetic Resonance Imaging (MRI) accomplished extensive progress. These advances, in conjunction with the subsequent achievement of MRI as a major diagnostic modality, led to a significant change in practice, requiring a specialized staff with specific skills and expertise for implant verification.

Prostataembolisation

R. Keller, A. Strässle; St. Gallen/CH

Purpose: Die Prostataembolisation ist in der Behandlung von gutartig vergrösserten Prostata eine wirkungsvolle Methode, welche heute regelmässig zum Einsatz kommt. Welcher Patient mit einer Prostatahyperplasie für diese Behandlung in Frage kommen, wird mittels diversen Untersuchungen und interdisziplinären Abklärungen festgelegt.

Methods and Materials: Durch die erfolgreiche und umfängliche Prostataembolisation in unserer Klinik für Radiologie und Nuklearmedizin im Kantonsspital St. Gallen gehört die Prostataembolisation sowie das MR von der Prostata zu den Standarduntersuchungen.

Results: Wir möchten die MRT zur Prostata und die Prostataembolisation umfänglich für die Radiologiefachpersonen erläutern und die Untersuchungen im ganzen Prozedere eingliedern.

Unser Augenmerk liegt beim MRT und der Prostataembolisation, welche einen fixen Platz im Behandlungsprozedere einnehmen. Ausserdem soll der Behandlungserfolg und der heutige Stellenwert genau erläutert werden.

Conclusion: Die Präsentation soll für andere Radiologiefachpersonen einen tiefgründigen Einblick in die Behandlung der Prostatahyperplasie mittels der Prostataembolisation geben.

Es soll den Radiologiefachpersonen die Möglichkeit bieten, Neues zu lernen und ihr vorhandenes Wissen vertiefen zu können.

Initial experience with 7T MRI

N. Hinterholzer; Zurich/CH

Purpose: In 2017 Siemens obtained CE approval for the 7 Tesla MRT Magnetom Terra. It is the first ultrahighfield device admitted for clinical and also research purposes. There are only a few comparable devices all over the world. In the swiss center for musculoskeletal imaging (SCMI) Balgrist Campus, Zurich a Magnetom Terra was ramped in October 2018. Various publications report significant advantages such as twofold higher signal-to-noise ratio at 7T than at 3T.

The question is: **The stronger the better?**

Methods and Materials: This work shall give a wider understanding of the possibilities and chances created through this new imaging device, show possible limitations and report first experiences through the eye of a radiographer.

Application spectrum, safety and side effects, as also structural, technical and physical differences will be covered. Furthermore pros and cons of such a system in comparison with a 3T system will be discussed.

Results: 7T imaging can keep up with lower field strengths.

Conclusion: 7T imaging is a very interesting topic but not many radiographers have the possibility to work with ultrahighfield devices – so this is a great opportunity to learn something about it.

Patient installation for brain CT scan: Using a CT head holder guarantee of a good positioning?

V. Berclaz, J.-B. Ledoux, C. Bruguier, C. Chevallier, C. Dromain; Lausanne/CH

Purpose: The quality of a brain CT scan goes through an optimal patient positioning. The use of accessories provided by CT constructors as head holders should permit the radiographer to install safely and adequately the patient for these types of exams. Other accessories can be used, as a foam head cushion, put directly on the table. Our study aims to demonstrate that the accessory used is a guarantee of a good positioning and thus an exam of good quality.

Methods and Materials: This retrospective study analyses brain CT scan during 3 months on the three different CT in our institution. Centering is evaluated using DoseWatch quality evaluation and straightness is visualized using SSDE view scout, as well as the use of a foam cushion or the CT head holder. 200 cases were randomly chosen, split between the emergency CT (100 cases, 24/7 activity) and both diagnostic service CT (50 cases each, open days hours).

Results: The results show that centering is overall good, but still with outliers demonstrating a misuse of the accessory chosen. The choice is also depending on the situation, 1% using CT head holder in the Emergency CT vs 25% for the conventional CT.

Conclusion: This result demonstrates good practice of the radiographers for centering but outliers drive us to propose a sensitization and adequate use of the different accessory for brain CT with workshop or presentation to the radiographers.

Use in routine practice of „dual-energy" in an emergency tomodensitometric imaging context

G. Sinz, *I. A. Garcia*; Geneva/CH

Purpose: Démontrer l'importance de la Dual Energy (DE) dans différents protocoles cérébraux, thoraciques et abdominaux lors de l'utilisation du CT du Service des urgences des Hôpitaux Universitaires de Genève (HUG).

Methods and Materials: Sur la base d'études menées par les radiologues cadres des HUG, plusieurs cas ont été étudiés. L'ensemble des acquisitions des images a été réalisé à l'aide d'un CT SOMATOM Force bi-tube et traité avec le logiciel *syngo.via®* de SIEMENS.

Results: La littérature scientifique et les diverses recherches menées au sein de notre institution confirment l'utilité de l'implantation de protocoles utilisant la DE pour préciser ou exclure certaines pathologies. Ainsi, nous réalisons une imagerie en DE pour les indications suivantes : contrôles de thrombectomie mécanique à 24h ; les recherches d'embolies pulmonaires (cartes de perfusion); les caractérisations entre tumeur et lithiase vésiculaire; les saignements actifs abdominaux.

Conclusion: L'utilisation en routine de la DE est une plus-value significative pour le diagnostic de plusieurs pathologies. Le traitement informatique associé en post-acquisition permet une meilleure caractérisation de certaines lésions et dans certains cas de s'affranchir d'acquisition native.

Communication et technique au service de la radiologie gériatrique; approche par CT

E. Maturana, *D. Delarbre*; Thônex/CH

Purpose: La gériatrie s'impose ces dernières années de plus en plus comme une discipline singulière. L'augmentation de durée de vie confronte la radiologie à une inévitable adaptation aux nouvelles pathologies, mais aussi une prise en charge des ainées. Cela dicte au TRM une approche de la problématique aussi bien du point de vue du soignant que de celui de l'expert en technique radiologique.

Methods and Materials: Notre thématique est organisée autour de l'activité au CT-scan dans le domaine exclusivement gériatrique avec un recul de 4 ans. Nos résultats portent sur les deux dernières années avec des mises en place des process qualitatives et techniques visant à optimiser la réalisation des examens CT et in fine du diagnostic.

Results: Notre réflexion porte sur une analyse de la problématique psychologique tout comme somatique des patients gériatriques d'une moyenne d'âge de 84 ans. La mise en place des protocoles techniques au CT adaptés aux patients non collaborant et une stratégie d'évaluation avec un algorithme. Le résultat porte sur l'analyse statistique de 493 examens thoraco-abdominaux réalisés durant le premier semestre 2018.

Conclusion: Il s'avère, au vu de nos résultats, évident qu'il est non seulement possible, mais aussi indispensable d'adapter notre pratique radiologique à l'environnement gériatrique tout en gardant en ligne de mire la qualité grâce à une approche rigoureuse tant du côté de la prise en soin que du respect de paramètres techniques lors de la réalisation des examens.

Interdisziplinärer Workflow bei Stroke-Patienten/-innen anhand der radiologischen Penumbra-Evaluation

J. Flury, *D. Koller*; St. Gallen/CH

Purpose: In der Schweiz ereignen sich jedes Jahr rund 16.000 Strokes, von welchen jede/-r dritte Patient/-in das Spital zu spät erreicht um wirksam behandelt zu werden. Mit interdisziplinären Kooperationsnetzen wie das Ostschweizer Schlaganfallnetzwerk, wird eine bestmögliche und moderne Behandlung von Schlaganfallpatienten/-innen in der gesamten Region ermöglicht, was sich positiv auf das Outcome für die Patienten/-innen auswirkt.

Methods and Materials: Die computertomografische Bildgebung beinhaltet bei einem akuten Stroke ein natives CT, eine CT- Angiografie der intra- und extrakraniellen Gefässen, sowie eine CT-Perfusion mit anschliessender Penumbra-Evaluation. Seit dem Vorliegen von neuen Studienergebnissen lösen sich auch im Stroke Center des Kantonsspitals St. Gallen immer mehr die strikten Zeitfenster zwischen Symptom- und Therapiebeginn für die endovaskuläre Intervention auf. Der individuelle Nutzen einer endovaskulären Therapie für den Patienten/-in wird dabei massgebend anhand der Penumbra-Evaluation quantifiziert.

Results: Durch die Ergebnisse von serverbasierten Bildbearbeitungsplattformen in Kombination mit der Klinik des Patienten/-in wurde das mögliche Zeitfenster für eine endovaskuläre Behandlung in der interventionellen Neuroradiologie bei grossen, proximalen Verschlüssen der intrakraniellen Gefässen von 6 auf 16 (24) Stunden erweitert. Vorgestellt wird die Durchführung und Konfiguration der Penumbra Evaluation anhand der Syngo.Via Plattform von Siemens Healthineers.

Conclusion: Die dipl. Radiologiefachpersonen tragen im Bereich der Therapieentscheidung von Stroke-Patienten/-innen mit ischämischen Hirninfarkten mit der Durchführung der CT-Untersuchung massgebend zur Entscheidungsgrundlage bei.

Spezifität von Herz MR und Herz CT

M. Müller, V. Heine; St. Gallen/CH

Purpose: Unser Vortrag handelt sich um zwei unterschiedliche Herz-Untersuchungen – Herz MRT und Herz CT. Wir stellen den Untersuchungsablauf der beiden Methoden vor, wie wir sie am Kantonsspital St. Gallen durchführen. Technische Hintergründe werden dazu erläutert und zum Schluss wird aufgezeigt, welche Untersuchungsmethode für welche Indikation am besten geeignet ist.

Methods and Materials: PowerPoint mit Fallbeispielen, Screenshot von den Workstation

Results: Auf was muss bei einer Untersuchung vom Herzen beim CT oder beim MRT geachtet werden? Bei welcher Indikation wird welche Untersuchungsmethode bevorzugt.

Conclusion: Es muss individuell von Patient zu Patient entschieden werden, welche Untersuchungsmethode/Untersuchungstechnik zu spezifischen Fragestellungen angewand wird.

RSS21

Definition of quality control criteria for breast implants mammography imaging

I. Gremion, C. Reis, N. Richli Meystre; Lausanne/CH

Purpose: To identify the most suitable criteria to assess mammography imaging of breast implants (MIBI) from radiologists and radiographers perspective and to apply those criteria to assess MIBI acquired in clinical practice.

Methods and Materials: Delphi method in 2 rounds was applied to identify the level of agreement between experts, asking to participants to rank each image criteria encountered in the literature for craniocaudal, mediolateral-oblique, lateral, as well as the presence or absence of Eklund manœuvre.

249 mammography with breast implants (MIBI) were assessed based on 24 criteria already established for standard mammography related to positioning, compression, artifacts and exposure parameters. The location of the implant and the positioning technique were also included to assess their impact on image quality. A threshold of 75% of achievement was expected for a criterion to be considered as applicable.

Results: In both Delphi rounds there was weak agreement among the experts (Kendall W0.253-0.382). Radiologists gave more importance to criteria related to «artifacts» and «technical parameters» while radiographers valued «positioning» and «prosthesis visualisation».

Assessment of the MIBI sample, showed that 14 out of 24 criteria reached the threshold. A significant statistical correlation (p=000.1) was observed between «breast tissue missing» and the location of implant and/or positioning technique.

Conclusion: Mammography experts do not consider image quality criteria for MIBI the same way. Quality criteria applied for standard mammography seem to be inadequate for MIBI. Dedicated quality criteria for MIBI need to be developed using aligned radiographers and radiologists perspectives.

RSS22

Introducing the extremity cone beam computed tomography

G. Weber, R. Scaglia; Geneva/CH

Purpose: Cette présentation propose d'expliquer le principe de fonctionnement du Cone Beam dédié aux extrémités, ses avantages, ses inconvénients ainsi que son apport dans le domaine de la radiologie.

Methods and Materials:
· Bases physiques
· Utilisation technique de la machine
· Spécificités de la charge
· Indications cliniques et avantages
· Inconvénients et limite d'utilisation
· Comparatif CBCT-CT
· Perspectives de développement d'examen

Results: Bien que le Cone Beam ait été créé il y a maintenant plus de vingt ans, son utilisation s'était jusque-là restreinte à la sphère ORL. Principalement utilisé pour l'imagerie dentaire et maxillo-faciale, le CBCT développe ses atouts et fait son entrée en orthopédie.

Depuis 2017, le service de radiologie de l'hôpital Universitaire de Genève dispose de ce nouvel appareil ; un CBCT Carestream dédié aux extrémités. Étant le premier hôpital de Suisse Romande équipé, les HUG sont devenus un Centre de référence quant à l'utilisation de cette nouvelle modalité, permettant désormais d'inclure la charge, afin d'optimiser le diagnostic de certaines pathologies.

Conclusion: Nous proposons à nos collègues TRM de découvrir une présentation sur une méthode d'imagerie en plein essor, moins irradiante que le scanner et dont la moyenne d'examen est en nette augmentation. De plus, des études telles qu'un comparatif arthrographie CBCT-CT, l'apport de l'imagerie en charge, les outils de correction d'artefact ou encore le développement d'un examen CBCT injecté, sont susceptibles de découler de l'introduction de cette modalité. Nous souhaitons transmettre les connaissances théoriques et pratiques, d'une méthode d'imagerie qui tend à devenir incontournable dans le monde de la radiologie.

RSS23

Optimization of CT and PET patient's doses with the latest SiPM PET/CT

M. Pappon, C. Pozza, M. Meyer, J. Prior, S. Gnesin; Lausanne/CH

Purpose: Since its clinical introduction in the 2000s, PET technology has advanced significantly. Recently, new detector technology has become available, such as Silicon Photo Multipliers (SiPM), providing better time-of-flight resolution. This new detector technology allied with extended field-of-view and smaller crystal size allow reduced administrated activity with increased image quality.

The principal aim of this work was to evaluate the dose reduction for patients of a recently installed SiPM PET/CT in our department, and to find the optimal balance between injected dose and CT irradiation.

Methods and Materials: We first performed phantom experiments, with a modulation of administrated activity and time acquisition. Based on these first results, we started list-mode clinical acquisition with lower administrated activity, and the raw data were rebinned to simulate scans acquired with reduced acquisition times.

Simultaneously, we performed the same optimization for the CT acquisition. We created 3 modulated protocols corresponding to our 3 different clinical uses: attenuation correction only, attenuation correction with CT interpretation and full radiological acquisition. We also performed phantom experiments to ensure to keep the lower necessary dose.

Results: We compared our results to our previous generation PET/CT. In the fact, we were able to reduce the injected activity of ^{18}F-FDG from 3.5 MBq/kg to 2 MBq/kg (4.6 mSv to 2.6 mSv for a 70 kg patient or −43%). CT doses were also significantly reduced (DLP from vs 608±194 to 420±155 or −31%, n=208 patients, p<0.001).

Conclusion: We conclude that we could optimize CT and PET patient doses with the latest generation of SiPM PET/CT.

RSS24

Imagerie multimodale préclinique pour une nouvelle approche théranostique en oncologie.

R. Salomir[1], C. Pepin[2], O. Lorton[1], M. Gulizia[1], J.-N. Hyacinthe[1]; [1]Geneva/CH, [2]Avignon/FR

Purpose: Ce travail s'inscrit dans le cadre du projet de recherche européen Sonotherag. Il a pour objectif le développement d'une nanotechnologie théranostique. L'objectif de ce travail est d'analyser la capacité de concentration de nanoparticule de perfluorocarbone (PFOB) dans une tumeur avec l'application ciblée d'ultrasons émis à haute intensité et focalisés (HIFU). Nous avons évalué l'efficacité de cette application et la qualité d'imagerie employée pour la guider et contrôler la concentration.

Methods and Materials: Nous avons comparé un groupe contrôle et un groupe traitement. Nous avons injecté 300 µlitres iv de PFOB aux deux groupes greffés d'une tumeur. Le traitement HIFU a été délivré après injection et guidé avec des séquences IRM proton pour le positionnement et la calibration. Une séquence de thermométrie confirme l'échauffement local induit. La concentration est analysée à l'aide de séquence IRM 19 fluor pour confirmer la présence de fluor. Le rehaussement de la concentration est quantifié entre le jour du traitement et à 24 h en imagerie de fluorescence. Cela permettant d'évaluer l'effet du traitement.

Results: D'après nos résultats préliminaires, l'application HIFU permet d'augmenter la concentration des nanoparticules d'une certaine taille dans la tumeur. La thermométrie manque de sensibilité mais est suffisante pour ce traitement. L'IRM fluor est suffisante qualitativement pour prouver la présence de fluor dans la tumeur. L'imagerie de fluorescence est optimale pour quantifier la concentration.

Conclusion: L'application d'insonications pulsées permet le rehaussement de la concentration des nanoparticules injectées à partir d'un seuil à définir. Les moyens de contrôle du traitement et de suivi sont suffisants pour cette étude.

RSS25

Brain CO_2 MRI study in the diagnosis of Moyamoya disease

S. Adamastor, F. Lazeyras, J.-N. Hyacinthe, M. I. Vargas Gomez; Geneva/CH

Purpose: The purpose is to optimize the BOLD test protocol: gas delivery, the gas delivery paradigm, the analysis of BOLD signal change dynamic.

Methods and Materials: Retrospective data refer to 15 patients with Moyamoya disease. The first patient is admitted between February 2011 and July 2018. The average age is 47±14.9, min 17 max 67. 60% are women and 40% are men. They inhaled a BOLD CO_2 through nasal cannula with the paradigm: OFF (60 s) ON (120 s) OFF (120 s) ON (120s) OFF (120 s). TE = 30 and TR = 3000 on MRI 3T, head 20 coils. The data is analyzed with a FSL optimized fit with the four variables. These variables are compared to the prospective data acquired on 14 volunteers. The average age is 30 years±11.8, min 21 max 61. 64% are women and 35% are men. They performed two exams with an operating mask and a nasal cannula.

Results: The visual analysis of the retrospective data graphs has been adjusted correctly with the BOLD time signal. In 9 out of 13 cases, underhoot was observed before CO_2 inhalation. In 7/13 have signal images at the end of inhalation. The analysis of the compared data between retrospectives and prospectives data are not done yet: my Master Thesis will be done on January 2019.

Conclusion: The difference in signal between the mask and the cannula is not confirmed, but in comfort, most volunteers preferred to wear the mask. The delivered gas was less unpleasant.

RSS26

Establishment of reference values for density measurement in Post-Mortem Computed Tomography (PMCT) and Multiphase PMCT-Angiography (MPMCTA)

I. Lanitis-Handschin[1], P. Vaucher[1], D. P. Genet[2], C. Egger[1], S. Grabherr[2]; [1]Geneva/CH, [2]Lausanne/CH

Purpose: Dans la pratique clinique en Radiologie, les diagnostics se basent partiellement sur la mesure des densités (Unités Hounsfield (UH)).

Les liquides, les organes ainsi que certaines pathologies sont indexés. Les UH peuvent être utilisées dans le diagnostic de certaines maladies (tumeur etc.) et differents liquides (sang etc.). En postmortem (pm), non seulement la disposition du sang et du gaz est différente, mais aussi la distribution du produit de contraste après injection peut influencer les UH. Les UH applicables en antemortem (am) ne peuvent donc pas s'appliquer en pm.

Le but de cette étude est de trouver et référencier les UH pour les examens pm.

Methods and Materials: Il s'agit d'une étude rétrospective avec 45 cas (cause du décès d'origine cardiaque, délai pm < 4 jours). Chaque cas a été vu par 3 observateurs indépendants, un radiologue, un médecin légiste, un TRM. Les UH ont été mesurées dans des régions prédéfinies avec des ROI (Region of Interest) de taille prédéfinie, proportionnelle à l'organe (cerveau, foie, thyroïde, rate, pancréas) investigué.

Results: Les résultats démontrent qu'il est possible d'établir des UH de référence pour des cas pm. Si la méthode est facilement reproductible (ICC > 0,678 < 0,949), plusieurs interrogations se sont posées, concernant notamment la justification scientifique de la méthode ou la position des ROI dans les organes et leur taille.

Conclusion: Bien que les résultats soient intéressants, nous n'avons pas encore assez de recul par rapport à l'impact réel de ceux-ci. Pour pouvoir en dire plus il faudra investiguer plus de cas.

PO01

Is age a factor in the evaluation of liver fibrosis by T1 relaxometry as a biomarker

H.-C. Breit; Basel/CH

Purpose: To evaluate the effect of aging on T1 relaxation times of the liver in a healthy population and to determine T1 relaxation time thresholds for identifying fibrotic parenchymal changes.
Methods and Materials: 36 healthy patients (32–87 yrs) without known liver disease and 17 patients (41–86 yrs) with clinical or biopsy proven diagnosis of liver fibrosis or cirrhosis were included. Patients with liver metastases or status post chemotherapy were excluded.
A retrospective ROI based examination of routine liver MRIs with a three-point Dixon based T1 Mapping at 1.5 T was performed. A second-year resident performed the evaluation by placing ROIs with a minimum area of 1000 mm^3 in the right and the left liver lobe.
Statistic evaluation was performed with Kolmogorov–Smirnov and Shapiro-Wilk-test for normal distribution, t-test for the hypothesis test and Pearson coefficient for correlation.
Results: There was a significant difference of liver T1 values (p < 0.05) between healthy subjects (mean 592 ms, SD 82 ms, range 404–889 ms) and patients with known fibrosis or cirrhosis (mean 685 ms, SD 76 ms, range 584–909 ms). There was no linear correlation between patient's age and the measured liver T1 values (r = 0.139).
Conclusion: T1 Mapping allows to non-invasively identify hepatic fibrosis or cirrhosis and separate those findings from healthy subjects. Since there is no correlation between age and T1 relaxation time changes it seems promising to establish age independent thresholds for disease detection.

PO02

Liver vein to cava attenuation (LVCA) improves prediction of clinically significant fibrosis when combined with liver volumetry and caudate-right lobe ratio (crl-r) on portal venous CT scans

C. Marx, V. C. Obmann, J. Hrycyk, L. Ebner, A. Berzigotti, J. T. Heverhagen, A. Christe, A. Huber; Bern/CH

Purpose: This study hypothesized that the liver vein to cava attenuation (LVCA) on portal venous abdominal CT scans is a helpful add-on to liver volumetry and the caudate-right lobe ratio (crl-r) to detect clinically significant liver fibrosis.
Methods and Materials: Fifty consecutive patients with portal venous phase abdominal CT scans and gradient-echo based MR elastography within 3 months without portal vein thrombosis or prior liver surgery were included. One patient was excluded because of insufficient MR elastography quality. Thirty-six patients had a liver stiffness ≤3.5 kPa, while twelve patients had a stiffness >3.5 kPa, consistent with clinically significant liver fibrosis (corresponding to a fibrosis stage ≥f2). Liver segmental volume ratio (LSVR), defined as Couinaud segments I–III to segments IV to VIII, as well as LVCA (1–3: liver vein attenuation higher, equal and lower than vena cava, 4: liver veins not contrasted) were calculated. LSVR-A was defined as LSVR * LVCA, while LIMA-FS (liver imaging morphology and attenuation based fibrosis score) was defined as crl-r * LVCA.
Results: In accordance with earlier publications, LSVR correlated well with MR elastography measurements (r = 0.63, p < 0.001). However, LSVR-A showed an even better correlation (r = 0.71, p < 0.001). Caudate-right lobe ratio was not very useful (r = 0.18, p = 0.214), while LIMA-FS was just slightly inferior than volumetry (r = 0.52, p < 0.001).
Conclusion: LVCA is a helpful add-on to volumetry on portal venous abdominal CT scans. LIMA-FS, a combination of LVCA and crl-r, allows a just slightly inferior prediction of clinically significant liver fibrosis than volumetry without time-consuming image post-processing.

PO03

Intra-abdominal fat necrosis in patients with acute pancreatitis: A MDCT based study

M. Pucci[1], A. C. O. Rocha[1], C. Mottet[2], A. Hedjoudje[3], S. Malekzadehlashkariani[1], J.-L. Constantin[1], C. Constantin[1], M. E. Kamel[1]; [1]Sion/CH, [2]La Chaux-de-Fonds/CH, [3]Cergy/FR

Purpose: To describe the incidence and the typical radiological pattern of intra-abdominal fat necrosis (IAFN) along the disease course of patients with acute pancreatitis subjected to MDCT.
Methods and Materials: All CT scans of patients with acute pancreatitis (Balthazar B-E) between September 2015 and July 2018 were analyzed. Patients who demonstrated nodular or reticulonodular implants of high attenuation within the areas of intra-abdominal fat distribution were selected. A simple score was assigned (grade I for unilateral flank involvement, grade II for bilateral involvement and grade III for diffuse abdominal involvement). No patient had history of malignancy. Regression analysis was chosen to find out any potential correlation between CT-detected IAFN and lipase level, leukocytosis, abdominal pain, vomiting and fever.
Results: Two hundred seven patients with acute pancreatitis were identified. Of those, 24 (12 %), mean age 61y ± 14, presented with typical radiological pattern of IAFN (grade I, n = 14, grade II, n = 4, and grade III, n = 6). IAFN appeared within 3 weeks after establishing the diagnosis of acute pancreatitis (mean 8.3 day, ± 6). Regression analysis revealed that lipase level was the only parameter that correlated with the grades of IAFN (*p* = 0.0110). The vast majority of lesions decreased in size or eventually completely resolved on subsequent CT, confirming their benign origin.
Conclusion: Acute pancreatitis induced IAFN is observed in up to 12 % of patients along their disease course. This self-regressing process must be clearly identified and reported to avoid mistaking it for other abdominal pathologies like peritoneal carcinomatosis.

PO04

Radiation exposure of the female breast during abdominal CT

N. Sasse, H. von Tengg-Kobligk, J. T. Heverhagen, P. Vock; Bern/CH

Purpose: The breast gland is one of the most radio-sensitive tissues, listed with a weighting factor of 12 % in the ICRP 103 recommendations. We aimed at estimating the average portion of breast glandular tissue exposed during standard abdominal CT examinations.
Methods and Materials: Abdominal CT examinations performed in 2017 at one designated CT scanner were retrospectively collected. The patient population encompassed 64 female patients (ages 10–<60 years). The percentage of exposed breast tissue (average of both sides), identified as non-fatty structures on PACS images, was estimated semi-quantitatively. Data of individuals with a non-synchronous chest CT exam were used to validate this method.
Results: An average of 21 % of breast glandular tissue volume was included in abdominal CT scans (median 8 %, range 0–92 %). Validation of the estimate using concurrent chest CT scans showed a mean overestimation of 4 % of the glandular volume (median 0 %, range 0–21 %) by our method.
Conclusion: This study showed a wide range of portions of glandular breast tissue unintentionally exposed by abdominal CT scans. Although these are usually small they may occasionally reach most of the gland. While the position of the breast is hardly ever considered in protocol planning, exposure cannot be neglected in view of the stochastic risk of cancerogenesis. Thus, one has to be aware of an average exposure of roughly 20 % of the breast tissue during standard abdominal CT examinations and, maybe, to address this problem by questioning traditional protocols.

PO05

The feasibility of apparent diffusion coefficient measurement as non-invasive biomarker for aggressiveness of prostate cancer: Correlation with Gleason Score

M. H. Wahba, S. Ahmed Emadaldin, Y. Alamir; Cairo/EG

Purpose: Our aim was to find the correlation between apparent diffusion coefficient (ADC) measurement and Gleason score (GS) in patients with prostate cancer.

Methods and Materials: Forty consecutive patients of prostate cancer were prospectively enrolled in this study. All patients underwent MRI examination of the prostate including DWI at b values of 0, 300, and 600 sec/mm². MRI examinations were performed before TRUS or at least 3 weeks after. ADC measurements of prostate cancer were obtained and correlated with the GS.

Results: There was a significant negative correlation between ADC values of prostate cancer and Gleason score (p value < 0.001). The mean ADC value of GS 4+3 (0.781× 10–3 mm²/s) was significantly lower than ADC value of GS 3+4 (0.812× 10–3 mm²/s). Receiver operating characteristic (ROC) curve analysis was performed to assess the accuracy of ADC measurement in prediction of tumor aggressiveness. An ADC value < 0.7725 indicated high grade tumor with GS > 7, whereas an ADC value > 0.8620 indicated low grade tumor with GS < 7. Both values reported sensitivity and specificity of 100 %.

Conclusion: ADC measurement can be used for assessment of the aggressiveness of prostate cancer and discriminating low and high grade tumors.

PO06

Correlation of magnetic resonance imaging and radical prostatectomy pathology in prostate cancer

M. Martins Favre, S. Rohner, I. Szalay-Quinodoz, S. Regusci, A. Caviezel, S. Tran, G.-A. de Boccard, C.-H. Rochat; Geneva/CH

Purpose: To determine the performance of the MRI to detect and localize prostate cancer using a correlation with gold-standard histopathology of radical prostatectomy specimens.

Methods and Materials: We compare 100 patients who underwent 3T MRI prostate before biopsy to the histopathology radical prostatectomy specimens. The radiologist and the pathologist used the same sectorisation Dickinson schema with 27 prostate sectors. Each focus cancer localization was compared with the localization of the previous MRI. The PIRADS classification was used and correlate with the final Gleason classification. Consistency of tumor localization (not only the index lesion), tumor volume and capsular integrity were also compared

Results: We obtained a good concordance between MRI images and the whole prostatectomy specimen with a VPP estimated at 97 % and a sensitivity at 82 %. The VPN was also very good (96 %)

Conclusion: The excellent correlation between MRI images and the gold standard prostatectomy specimens confirms the high sensitivity of MRI in detect significant cancer however the expertise of the radiologist and the pathologist is crucial and the multidisciplinary tumorboard can help to keep the quality.

PO07

An MRI-guided HIFU-triggered wax-coated capsule for supertargeted drug release

O. Wuerthinger[1], S. Matoori[1], M. Roveri[1], A. Romagna[1], P. Tiefenboeck[1], O. Kolokythas[2], J. M. M. Froehlich[1]; [1]Zurich/CH, [2]Winterthur/CH

Purpose: To develop a thermoresponsive drug delivery system for personalized non-invasive therapy, which consists of a gadolinium-based contrast agent (GBCA) to visualize, a MRI-guided high-intensity focused ultrasound (HIFU) trigger to externally control and MRI to monitor the drug release in the gastrointestinal tract.

Methods and Materials: Different mixture ratios of lanolin/cetyl alcohol were tested to obtain a suitable melting point. Capsules were filled with lyophillized GBCA, coated with the most optimal wax layer of lanolin/cetyl alcohol 1:1 and placed in a HIFU gel phantom. The melting of the wax-coating was tested by applying a MRI-guided 200 W HIFU pulse. The release of the encapsulated contrast agent was monitored using T1- and T2-weighted MRI before and after the HIFU beam.

Results: Capsules were coated with a 1:1-mixture of lanolin/cetyl alcohol (melting point 43°C). The T2-hypointensity of the wax coated capsule enabled to localize the drug delivery system. The T1-hyperintense signal was lacking before application of the HIFU pulse. After application of this pulse the T1-hyperintense signal was observed in proximity to the capsule, indicating that the HIFU pulse was able to selectively melt the coating and cause hydration and outflux of the GBCA content from the capsule.

Conclusion: We developed a novel thermoresponsive wax-coated capsule for temporally and spatially supertargeted drug release in the gastrointestinal tract. We present a proof-of-concept of using MRI-guided HIFU for triggering and T1-/T2-MRI sequences for visualizing the release of the capsule content. As a result, this externally controllable and monitored drug delivery system promises to enable targeted no-invasive therapy of gastrointestinal diseases.

PO08

Typical mpMRI findings of prostate cancer and pitfalls

S. Malekzadehlashkariani[1], B. Andrieux[2], J. A. Vidal[3], L. Abraszek[3], H. C. Thoeny[4]; [1]Sion/CH, [2]Villars-sur-Glâne/CH, [3]Fribourg/CH, [4]Bern/CH

Learning objectives: To describe the typical multiparametric MRI (mpMRI) findings of prostate cancers and to illustrate the potential pitfalls that can challenge the interpretation of prostate mpMRI leading to inaccurate overdiagnosis or underdiagnosis of prostate cancers.

Background: Although, the diagnosis of prostate cancer was traditionally made based on elevated PSA level, suspicious digital rectal examination and consequent TRUS biopsy, currently mpMRI is the imaging modality of choice for cancer detection, local extension and post-treatment residual/recurrence thanks to the anatomical and functional sequences. However, mpMRI accuracy is sometimes limited by certain pitfalls which can mimic prostate cancer.

Imaging findings or procedure details: MpMRI of the prostate comprises anatomical (T2WI) and functional (DWI, DCE) sequences. T2WI and DWI are considered the dominant sequences for transitional and peripheral zones tumors, respectively. Typically, the transitional zone tumors are defined as a poorly-defined round, oval or lenticular hypointense lesions, whereas the peripheral zone tumors appear as ill-defined hypointense lesions on T2WI, impeded diffusion and focal enhancement. Several benign conditions such as BPH and prostatitis, as well as morphological variants including hypertrophic anterior fibromuscular stroma, periprostatic venous plexus and post-biopsy hemorrhage are known potential pitfalls mimicking tumors. However, meticulous image analysis and knowledge of normal variants allow the differentiation of benign and malignant lesions in the vast majority. Furthermore, mpMRI can guide targeted-biopsy to explore the suspicious lesions.

Conclusion: MpMRI plays a pivotal role in the diagnosis of prostate cancers. Radiologists should be familiar with typical mpMRI findings of prostate cancer and know the typical mimickers of cancer in order to avoid misdiagnosis.

Texture analysis of the pancreas prior to Whipple surgery: Prediction of fistula formation

M. Mannil, P. E. Herrera, J. von Spiczak, P. Kambakamba, P.-A. Clavien, H. Alkadhi; Zurich/CH

Purpose: To evaluate the prognostic value of texture analysis (TA) on pre-operative, non-contrast enhanced CT images of the pancreas regarding fistula formation after Whipple procedure.

Methods and Materials: In this IRB-approved study, we included 109 patients with pre-operative (21.9 ± 23.8 d) non-contrast enhanced CT undergoing the Whipple procedure. TA of the pancreas was performed using free-hand regions-of-interest on axial images. A total of 304 features were computed. Dimension reduction was performed using intraclass correlation coefficients (ICC ≤ 0.6) and a correlation matrix (Pearson correlation coefficient r > 0.8). Five common machine-learning classifiers (artificial neural network Multilayer Perceptron, decision tree J48, NaïveBayes, R c Forest (RandomForest), and Sequential Minimal Optimization) were applied to assess histopathologically-proven fistula formation, discriminating between clinically relevant (1) postoperative pancreatic fistulas (POPF) B or C fistuals from (2) absent fistulas or mere biochemical learks (POPF A).

Results: There were 38 patients (34.9 %) with POPF B or C fistulas and 71 patients (65.1 %) with POPF A or absent fistulas. Dimension reduction led to 10 TA features carrying prognostic information. The RandomForest machine learning classifier showed overall best performance with a sensitivity of 76 %, specificity of 64 %, precision of 0.75 and an area-under-the receiver operating characteristics curve of 0.78.

Conclusion: This study is the first to identify TA features on non-contrast enhanced CT that predict fistula formation after Whipple surgery.

NI-RADS pitfalls and errors form the daily practice

M. Y. Moshebah, P. Hagmann, P. Simon, J. Prior, R. A. Meuli, V. Dunet; Lausanne/CH

Learning objectives:
· To describe the basics of the Neck Imaging Reporting and Data System (NI-RADS) classification.
· To learn common pitfalls that lead to wrong classification and management plan of patients with head and neck cancers (HNC).
· To learn some tips and tricks to optimize NI-RADS classification.

Background: NI-RADS was developed for imaging evaluation in patients with treated HNC. It aims to provide numerical levels of suspicion for residual/recurrent tumor, generate data-mineable reports and standardize management recommendations. Nevertheless, accurate knowledge of common pitfalls is mandatory to optimize patient's management.

Imaging findings or procedure details: NI-RADS classification is based on the combination of morphological (CT, MRI) and molecular (F-18-FDG-PET) imaging. In this poster, along with the description of the four NI-RADS categories, we present the most frequently made pitfalls. Errors in NI-RADS classification can be divided into those related to technical aspects (metal or motion artefacts, PET resolution, scan timing, single imaging method), normal (physiological F-18-FDG uptake) or tumor (low baseline F-18-FDG uptake, necrosis) conditions and those related to treatment induced changes (inflammatory scar, necrosis, trophic ulcer, infection). Common errors resulting in patients' over- or understaging according to the NI-RADS scale may also be divided into those avoidable « at first sight » and those needing more experience. Tips and tricks will hence be illustrated to learn how to minimize the risk of NI-RADS misclassification.

Conclusion: Accurate knowledge of typical post-treatment imaging patterns as well as of common pitfalls is mandatory to expend the use of NI-RADS, thus allowing standardization of patients' imaging report and care.

Percutaneous and peroperative cryoablation of extra-abdominal desmoid tumors: A single center experience and review of the literature

S. Saltiel[1], P. Goetti[1], F. Becce[1], A. Denys[1], P. E. Bize[2]; [1]Lausanne/CH, [2]Genolier/CH

Purpose: Although extra-abdominal desmoid (EAD) tumors are not malignant, they remain challenging to treat because of their high local recurrence rate.

Methods and Materials: We enrolled all EAD tumors treated with cryoablation and follow-up with MRI, between November 2012 and July 2017. Fourteen procedures were performed on 9 patients (1 male/8 female, mean age 30.2 years, ± 16.7 (SD)). Contrast-enhanced MRI was performed before treatment and after 3, 6 and 12 months follow-up, and then depended case by case. The tumor volume was measured and any residual enhancement of the tumor was considered as viable tumor. Effect on pain was evaluated before and after cryoablation.

Results: A mean volume reduction of viable tumor of 76.6 % for six patients at 6 months, and 93.5 % at 12 months follow-up for five patients. Six patients had residual viable tumor tissue at one year, with 4 deemed incompletely treated. Two had a complete response with no enhancement of tumor and a significant size reduction of the total tumor. Disease progressed in four cases. Mean follow-up was 23,2 months. Eleven out of 14 procedures were performed percutaneously. We observed 2 complications: 1 iatrogenic lesion of the common peroneal nerve, and 1 colo-cutaneous fistula. Pain decrease was significant for three patients.

Conclusion: Percutaneous or peroperative cryoablation, appears to be safe and well tolerated. We found a quite similar percentage of recurrences compared to other treatments option, ranging from 22 to 35 %. To lower the risk of iatrogenic lesion, perioperative cryoablation might be an alternative to protect nearby neurovascular structures.

A novel CT perfusion protocol for planning prostate artery embolization – Proof of concept study

A. Kobe, G. D. Puippe, H. Alkadhi, T. Pfammatter; Zurich/CH

Purpose: To evaluate the visibility of the prostatic artery (PA) prior to prostate artery embolization (PAE) in benign prostatic hyperplasia (BPH) using a novel CT perfusion protocol.

Methods and Materials: 22 patients (mean age 67.1 ± 6.6 years) were included prior to PAE. Dynamic CT perfusion of the pelvis (scan range: 22.4 cm, cycle time: 1.5 s, scan time: 44s, 25 scan cycles, 70 kVp, 100 mAs) was performed after the administration of sublingual nitroglycerin using 70 ml iodinated contrast media at 6 ml/s and a 10 s scan delay. Temporal MIP images were reconstructed. Signal-to-noise ratio (SNR) and contrast-to-noise ratio (CNR) of the right internal iliac artery were calculated. Visibility of the prostate artery was scored using a classification system from 1 to 4 (score 1 = not seen, to score 4 = intraprostatic PA branches seen). Digital subtraction angiography was used as the gold standard for PA anatomy.

Results: The average $CTDI_{vol}$, DLP and effective dose of the CT perfusion protocol was 35.7 ± 6.8 mGy, 737.4 ± 146.3 mGy·cm and 10.6 ± 3.2 mSv, respectively. SNR and CNR were 77.1 ± 30.5 and 65.5 ± 27.8, respectively. Type I anatomy (according to de Assis et al) was found in 36.4 %, type II in 22.7 %, type III in 6.8 %, type IV in 29.6 %, and type V in 4.6 % of the PA. The mean visibility score was 3.6 ± 0.6. All scans were diagnostic with only one PA being only proximally identifiable due to unilateral hip prosthesis.

Conclusion: We introduced a novel CT perfusion protocol of the pelvis enabling the visualization of the PA for treatment planning at a reasonable radiation dose.

PO13

**Infected extrahepatic splanchnic venous stent (–grafts):
Clinical presentation, imaging and treatment**

L. Widmer, G. D. Puippe, T. Pfammatter; Zurich/CH

Learning objectives: To know the indications of percutaneous revascularization of the portal vein or its tributaries.
To categorize the causes of stent infections according to the delay between stent placement and symptoms.
To recognize imaging features orienting towards infectious complication after splanchnic stent placement.
To understand the treatment options of infected splanchnic venous stent.
Background: Percutaneous revascularization of the portal vein and its tributaries is a minimal invasive procedure to decompress prehepatic portal hypertension and treat its potentially fatal complications. Infections of stents and stent-grafts placed in the splanchnic veins are uncommon. 3 cases collected at a single liver transplantation center over ten years are presented.
Imaging findings or procedure details: Fever of unknown origin or sepsis was the leading symptom. The delay between the primary intervention and the infection ranged from 1 to 31 months. Blood cultures were positive in 2 out of 3 cases for a mixed bacterial flora. CT showed stent-thrombosis in 2 patients and peri-stent fat stranding in all. FDG-PET was positive in all 3 patients. Antibiotic regimen was successful in two patients and failed in one. At operative removal of the infected meso-caval stent-graft, erosion into the duodenum was recognized.
Conclusion: Splanchnic venous stent infection is an exceedingly rare but serious complication requiring a complex medico-surgical management. Early recognition of related imaging features may improve chances of recovery.

Intra-Voxel Incoherent Motion MRI in OSA patients

S. Thiel[1], T. Gaisl[1], F. Lettau[1], A. Boss[1], S. Winklhofer[1], J. R. Stradling[2], M. Kohler[1], C. Rossi[1]; [1]Zurich/CH, [2]Oxford/UK

Purpose: Obstructive sleep apnoea (OSA) is a highly prevalent sleep-related breathing disorder associated with impaired peripheral vascular function and an increased risk of stroke. Evidence suggests that abnormalities of the cerebral microcirculation may be present in these patients. The coexistence of both, hypertension and OSA might suggest a further deterioration of capillary morphology and function. We evaluated whether the presence of hypertension may affect the cerebral capillary architecture and function assessed by Intravoxel Incoherent Motion (IVIM) MRI in OSA patients.

Methods and Materials: 41 patients (88 % male, mean age 57 ± 10 years) with moderate-to-severe OSA were divided in two groups (normotensive vs hypertensive). All hypertensive OSA patients were adherent with their antihypertensive medication. Cerebral microvascular structure and function was assessed using IVIM-MRI in grey (GM) and white matter (WM), respectively, at 3 Tesla. Group comparisons were performed with the Wilcoxon-Mann-Whitney-Test.

Results: Diffusion and perfusion-related indexes in middle-aged OSA normotensive patients were quantified in both tissue types (D $[10^{-3}\,mm^2/s]$: GM $= 0.83 \pm 0.03$; WM $= 0.72 \pm 0.03$; D* $[10^{-3}\,mm^2/s]$: GM $= 7.7 \pm 0.9$; WM $= 7.4 \pm 1.0$; f: GM $= 0.09 \pm 0.01$, WM $= 0.06 \pm 0.01$). In the examined tissues types, hypertension did not result in changes on the estimated IVIM indexes.

Conclusion: IVIM indexes, as a measure of cerebral microvascular structure and function, showed no difference between hypertensive and normotensive patients with moderate-to severe OSA. Treatment adherence with antihypertensive drug regime and, in turn, controlled hypertension is not a condition affecting microvascular structure and perfusion assessed by IVIM-MRI.

In vitro DE CT visualization of nasal drug deposition using an iodine-based nasal spray – A feasibility study

T. Sartoretti, M. Mannil, J. M. M. Froehlich, S. Biendl, H. Alkadhi, M. Zadory; Zurich/CH

Purpose: To visualize and characterize qualitatively the nasal deposition of drugs applied with a nose spray containing iodinated contrast agents using dual energy CT.

Methods and Materials: A nasal cast of synthetic epoxy resine made by stereolithography based on computed tomography (CT) data was used as a nasal replica model. CT data were acquired from a 33-year-old woman without known nasal disease. A single-dose nasal spray device containing an aqueous iodinated contrast media solution with a concentration of 92.5 mgI/ml was applied into the nasal cast 5 times. With each puff 0.1ml of the solution was applied into one nostril with the same angle and depth of penetration in a standardized manner. The optimal iodine concentration had been defined with preliminary scans ensuring minimal artefacts and sufficient efficacy. Dual energy CT scans ($0.75\,mm^3$ isotropic voxels) were acquired at 90 and 150 kVp covering the entire nasal cast and was initiated between 60–120 sec after the administration. Following iodine mapping, 3D rendering was performed to generate a 3D distribution image of the distribution.

Results: Hyperdense iodinated deposited droplets within the cast were clearly identifiable after nasal application. 3D rendering allowed a qualitative assessment of the deposition patterns within the nasal cavity and pharynx allowing their allocation to the different nasal compartments. Droplets were evenly distributed within the nasal cavity with some droplets even reaching into the olfactory regions.

Conclusion: Dual energy CT may be used to qualitatively assess and visualize nasal deposition of drugs administered via nasal applicators with high spatial and temporal resolution.

Quantification of cerebral veins in patients with acute migraine with aura: A fully automated quantification algorithm

P. S. Breiding, F. Kellner-Weldon, L. Grunder, A. Scutelnic, U. Fischer, J. Gralla, M. El-Koussy, N. Denier; Bern/CH

Purpose: Susceptibility weighted imaging (SWI) is a very sensitive technique that depicts increased deoxyhemoglobin in veins (IDV) in patients with acute migraine with aura (MwA). Interpretation of visual venous asymmetry (VVA) between brain hemispheres by radiologists is gold standard. Our goal was to develop an automated algorithm for segmentation and quantification of cerebral veins.

Methods and Materials: Expert readers visually evaluated SWI of patients with acute MwA for VVA. Subsequently a fully automated algorithm based on 3D normalization and 2D imaging processing using SPM and MATLAB software was used to quantify cerebral veins and to calculate volumetric differences between hemispheres.

Results: 50 patients with MwA, were examined with SWI. Average time between aura onset and SWI was $4\,h\,44\,min \pm 6\,min$. VVA was present in 40 % of patients, (left sided VVA 75 %). In 27 of 30 patients (90 %), the fully automated calculation agreed with the side of visually depicted IDV. Patients with VVA had significantly larger vein volume on the hemisphere with IDV compared to patients without ($4.89 \pm 1.95\,ml$ vs $3.28 \pm 1.4ml$; p < 0.05). Mean difference in venous volume between hemispheres in patients with VVA was $1.74 \pm 1.96\,ml$ compared to $0.53 \pm 0.52\,ml$ for patients without (p < 0.05). Average time between aura onset and SWI correlated negatively with IDV volume (r = – 0.414; p < 0.05).

Conclusion: A fully automated algorithm can identify and quantify cerebral venous distribution. Absolute quantification may be useful in measuring degree of IDV.

Leptomeningeal enhancement on post-contrast FLAIR in Multiple Sclerosis – Observations of enhancement kinetics

R. Engisch[1], D. Titelbaum[2]; [1]Lucerne/CH, [2]Brockton/US

Learning objectives:

· To understand the two-compartment model for vascular-extravascular space exchange of contrast agent in dynamic contrast enhancement (DCE) in MRI.

· To understand the possible clinical applications of DCE for leptomeningeal enhancement (LME) in Multiple Sclerosis (MS).

Background: Three types of enhancement curves illustrating exchange between plasma and extravascular space were described by Tofts and Kermode in 1999 (1), and have been useful in characterizing various pathologies.

Recently described LME in MS is thought to be due to vascular leakage of contrast secondary to adjacent meningeal inflammation. General consensus is that 10 minutes post-injection is the optimal time for 3D-FLAIR acquisition, but optimal timing has not been studied (Absinta 2015; Zivadinov 2017).

Imaging findings or procedure details: Methods: Two patients known to have LME were evaluated by 4 successive enhanced 3D-FLAIR sequences obtained between 2–45 minutes post injection. ROIs were averaged in 2 orthogonal planes, normalized by dividing by thalamic ROI and then plotted vs time. One follow up study was performed 9 months later.

Findings: Kinetic properties of 7 foci of LME in 2 MS patients could be grouped into the 3 types of Tofts enhancement curves. Initial slope of intensity and mean time-to-peak enhancement were derived from the curves. Kinetic properties were stable over time.

Conclusion: LMEs are heterogenous in terms of their kinetic properties, without a single optimal image acquisition time. Best estimate for optimal timing is between 10–25 min post-injection. Certain kinetic parameters of vascular permeability can be extracted and may provide further insight into LME characterization in the future.

PO18

HPV-positive and HPV-negative oropharyngeal cancer: Differences in imaging features and implications of the new AJCC cancer staging system on diagnosis and staging

R. Correia, V. Lenoir, C. de Vito, M. Becker; Geneva/CH

Learning objectives: To highlight the modifications of the 8th edition of the AJCC staging system in oropharyngeal cancer (OPC) and to discuss the role of CT, MRI and PET-CT. To review the cross-sectional imaging features and textural parameters of HPV-positive in comparison to HPV-negative OPC.

Background: The epidemiology of OPC has changed in recent years due to the increasing incidence of HPV-positive cancers. This tumor with specific demographics, risk factors and distinct clinical presentation has certain imaging features that can help clinching the diagnosis. The improved response to treatment in HPV-positive compared to similar stage HPV-negative OPC has led to a separate staging system in the new 8th AJCC edition.

Imaging findings or procedure details: We first review the modifications of the new AJCC staging system regarding OPC after which we summarize the characteristic CT, MRI and PET-CT features. Based on a series of patients seen in our institution, we highlight the key imaging features of HPV-positive versus HPV-negative OPCs: small size, more homogeneous enhancement, well-defined borders, exophytic growth and less pronounced invasion of adjacent muscles. We discuss differences regarding ADC and SUV metrics including textural features. We illustrate the characteristic imaging aspect of metastatic nodes in HPV-positive OPC, such as cystic metastases. The implications of the AJCC classification on the nodal status, including extracapsular extension, are highlighted.

Conclusion: HPV-positive OPC is a distinct tumor entity, with characteristic imaging and textural features and an own staging system. We summarize the relevant facts radiologists should be aware of when imaging OPC.

PO19

Oversizing strategy of the WEB for intracranial aneurysms

A. Guenego, A.-C. Januel, F. Bonneville, C. Cognard; Toulouse/FR

Purpose: To compare: the influence of the oversizing technique (proposed WEB diameter was oversized 1 mm compared with the mean aneurysm diameter) on complete and adequate occlusion, recanalization rate, peri and post procedural complication rate.

Methods and Materials: Single-center, retrospective analysis of prospectively acquired data. We identified consecutive patients between March 2012 and March 2017. All patients presented a wide neck aneurysm. WEB was judged the best option possible at the time.

Results: 45 cases were performed at our institution over 45 patients. The oversizing technique led to a real oversizing of the WEB (WDAD was −0.3 before and 0.8 after). The occlusion rate at 3/6 months after Oversizing was significantly higher (48 % CO vs 12 % CO p = 0.023). At last follow-up, rate of WEB compaction, recanalization, adequate final occlusion, complications rate were not significantly different.

Conclusion: Oversizing tends to decrease: the rate of recanalisation and compaction.

PO20

Dynamic anatomic relationship of coronary arteries to the valves part 1: Tricuspid annulus and RCA

R. M. M. Hinzpeter, M. Eberhard, A. Pozzoli, R. Manka, F. Tanner, M. Taramasso, F. Maisano, H. Alkadhi; Zurich/CH

Purpose: To gain insights into the physiology and pathophysiology of the dynamic anatomic relationship between the tricuspid annulus (TA) and right coronary artery (RCA) using CT image data.

Methods and Materials: Eighteen patients (mean age 68 ± 15 years) without valvular heart disease (*controls*) and eighteen patients (mean age 61 ± 12 years) with severe functional tricuspid regurgitation (FTR ≥ 3 +) undergoing a dedicated contrast-enhanced cardiac CT protocol optimized for the right heart were included. Using a prototype visualization, segmentation and image analysis software, the geometry of the TA and distances to the RCA were measured throughout the cardiac cycle by two independent, blinded readers.

Results: Interreader agreement for all measurements in all phases was high (ICC: 0.84 – 1.0). There were significant differences between patients with FTR and controls regarding the size of the TA and length of the RCA (p < 0.001,all). Distances between the TA and RCA were significantly shorter in controls compared to patients along the entire course of the RCA and in all cardiac phases (p = 0.002 – 0.005). Shortest distances between the TA and RCA were 5.1 mm in controls (distal/diastole) and 6.5 mm in patients (distal/systole). In both groups, distances between the TA and RCA were significantly smaller distally than proximally (p = 0.005 – 0.01). Only in patients with FTR, there was a consistent short segment of the mid to distal RCA, adjacent to the antero-posterior commissure, showing an increase in distance to the TA.

Conclusion: Our study demonstrates the dynamic physiology and pathophysiology of movements between the TA and RCA showing considerable differences in movement patterns and distances between controls and patients with severe FTR.

PO21

Quantitative comparison of 2D and 3D LGE imaging in patients with myocarditis

M. Polacin, I. Kapos, M. Gastl, F. Morsbach, A. Gotschy, H. Alkadhi, R. Manka; Zurich/CH

Purpose: Late gadolinium enhancement (LGE) imaging helps diagnosing myocarditis and the patient's outcome depends on the presence of myocardial fibrosis. We compared a 3D single-breathhold (3D LGE) MR sequence with an established 2D multi-breathhold sequence (2D LGE) and evaluated image quality and the amount of myocardial fibrosis.

Methods and Materials: 2D LGE and 3D LGE (same spatial resolution 1.2 x 1.2 mm²; slice-thickness 8 mm; field of view, 350 x 350 mm²) were acquired in 30 patients with myocarditis (12 female, mean age 37.5 ± 16 years) at 1.5 T (Achieva, Philips, Best, Netherlands). Image quality was evaluated by two blinded readers using a 5-point Likert scale. Myocardial and fibrotic mass and total fibrotic tissue percentage were quantified for both sequences.

Results: There was no significant difference in image quality between 3D und 2D acquisitions (1.4 vs 1.5, p = 0.3) with good interreader agreement (weighted κ = 0.7 vs 0.6). There were no significant differences between 3D and 2D acquisitions for myocardial mass (110.6 g ± 33 vs 111.1 g ± 32, p = 0.2), fibrous tissue mass (7.5 g ± 5 vs 7.8 g ± 6, p = 0.1) and total fibrous percentage (6.3 ± 3 vs 6.4 ± 3, p = 0.1). Acquisition time was significantly shorter for 3D (26 ± 4 s) as compared to the 2D LGE sequence (350 ± 57 s, p < 0.001).

Conclusion: In myocarditis patients 3D LGE imaging shows equal diagnostic quality compared to standard 2D LGE imaging but with a significantly reduced acquisition time.

PO22

Prognostic value of texture analysis in cardiac magnetic resonance imaging in patients with Takotsubo Syndrome: A machine learning based approach

M. Mannil, K. Kato, R. Manka, J. von Spiczak, F. Ruschitzka, J. L. Ghadri-Templin, C. Templin, H. Alkadhi; Zurich/CH

Purpose: To evaluate the prognostic value of texture analysis (TA) based on CMR images in patients with TTS using machine learning.

Methods and Materials: In this multicenter trial (InterTAK Registry), we investigated CMR imaging data of 58 patients with TTS. CMR imaging was performed in the acute and subacute phase (median 4 days) of TTS. TA of the left ventricle was performed using free-hand regions-of-interest in short axis T1-weighted contrast-enhanced (T1Gd) and T2-weighted (T2w) images. A total of 608 TA features adding the parameters age, gender, and body mass index (BMI) were included. Dimension reduction was performed removing TA features with reduced intraclass correlation coefficients (ICC ≤ 0.6) and those being redundant (correlation matrix with Pearson correlation coefficient r > 0.8). Five common machine-learning classifiers (artificial neural network Multilayer Perceptron, decision tree J48, NaïveBayes, RandomForest, and Sequential Minimal Optimization) were applied to assess 5-year outcome including major adverse cardiac and cerebrovascular events (MACCE). A 10-fold cross-validation was used.

Results: Dimension reduction yielded 10 TA features carrying prognostic information which all were based on T2w images. The NaïveBayes machine learning classifier showed overall best performance with a sensitivity of 82.9 % (CI 80 – 86.2), specificity of 83.7 % (75.7 – 92), precision of 0.88 (0.83 – 0.92) and an area-under-the receiver operating characteristics curve of 0.88 (0.83 – 0.92).

Conclusion: This study is the first to identify unique T2w-derived TA features that predict long-term outcome in patients with TTS. These features might serve as imaging prognostic biomarkers in patients with TTS.

PO23

Different CT features of abdominal aortic aneurysm in emergency setting

A. Sobieh, D. Radcliffe, H. Lo; Worcester/US

Learning objectives: Present a series of cases of complicated and uncomplicated abdominal aortic aneurysm. Describe CT findings required to diagnose different types of abdominal aortic aneurysm.

Background: Abdominal aortic aneurysms represents the 10th most common cause of death in the western world. It is focal dilation > 3 cm. It could be due to atherosclerosis, mycotic, inflammatory. Among its main complications: rupture, infection, pseudoaneurysm formation, aortocaval fistula and aortoenteric fistula, distal thromboembolism.

Imaging findings or procedure details: Abdominal aortic aneurysms could be saccular, fusiform dilation of the abdominal aorta > 3 cm. In this educational exhibit, we review the CT findings of noncomplicated and complicated abdominal aortic aneurysm.

Imaging features of complication: Periaortic stranding. Periaortic hematoma. Contrast extravasation. focal discontinuity of intimal calcification.

Conclusion: Early detection and timely diagnosis of complications of abdominal aortic aneurysm is a crucial factor in timely treatment offering a better prognosis and surgical outcome. MDCT plays an important role given its high sensitivity and specificity.

PO24

Extracorporeal Membrane Oxygenation (ECMO) and contrast-enhanced CT: What needs the radiologist to know?

S. Saltiel, Y. Maeder, D. C. Rotzinger, R. A. Meuli, S. Schmidt; Lausanne/CH

Learning objectives: The aims of our educational poster are:
· Briefly review history and principles of the two systems of Extracorporeal Membrane Oxygenation (ECMO)
· Describe the effects of altered hemodynamics seen on contrast-enhanced CT images in ECMO patients and point out typical pitfalls

Background: ECMO means a cardiopulmonary bypass implemented in patients with severe cardiac and/or pulmonary failure to provide oxygenation and hemodynamic support. ECMO was developed by Theodor Kolobow in 1963 and first successfully used in 1972.

Today, ECMO is an established tool for circulatory (V-A) and respiratory (V-V) support. Thus, we need to distinguish two systems, the veno-arterial or veno-venous ECMO.

The growing frequency of the use of ECMO results in an increasing need for imaging in ECMO patients. However, the altered hemodynamics introduced by this device cause patterns of mixing of the contrast material with unenhanced blood recognized on CT images. Therefore, we need special considerations regarding intravenous contrast injection and acquisition timing.

Imaging findings or procedure details: After reviewing angio-CT images of ECMO patients, we have worked out specific technical considerations. We will familiarize radiologists with both types of ECMO and draw attention to certain imaging pitfalls, such as apparent aortic dissection.

Conclusion: Contrast-enhanced CT of patients with ECMO flow requires knowledge of both ECMO systems to optimize contrast injection and timing of the data acquisition. Reduction of the ECMO flow, selection of the injection site and increasing volume or flow rate are special considerations. Veno-venous ECMO does not influence the flow rate of contrast-injection.

PO25

Comparison of mechanical thrombectomy in single vs biplane angiosuites

A. Guenego[1], P. J. Mosimann[2], R. Fahed[3], J. Gralla[4], R. Blanc[3], M. Piotin[3], C. Cognard[1]; [1]Toulouse/FR, [2]Essen/DE, [3]Paris/FR, [4]Bern/CH

Purpose: To assess differences in radiation, contrast exposures, procedure duration and outcomes between cerebrovascular mechanical thrombectomy (MT) procedures performed in single-plane (SP) or biplane (BP) angiosuites.

Methods and Materials: Consecutive patients treated by MT from four centers between January 2014 and May 2017 were included. Patients and MT characteristics (including type of the angiosuite [SP/BP], recanalisation score, modified Rankin Scale at 3 months, complications, scopy duration, procedure duration, Dose-Area Product (DAP), Kerma and Contrast load) were assessed. Multivariate analysis were performed (with Bonferroni correction) to compare angiosuites regarding MT efficacy and safety, patient radiation and contrast exposure, fluoroscopy duration.

Results: Within four centers, 906 patients underwent a MT (576 on a biplane angiosuite, 330 on a single-plane). After multivariate analysis, BP angiosuites significantly decreased contrast load (100 vs 200 mL, 50 % lower, relative effect 0.75 (CI: 0.67 – 0.84), p < 0.0001) and fluoroscopy duration (22 vs 27 min, 19 % lower, relative effect 0.83 (CI: 0.74 – 0.94), p = 0.0001) compared with SP angiosuites. There was no difference regarding procedure duration, radiation doses, rate of successful recanalisation, outcome or procedural complications. Interestingly, performing a pre-intervention diagnostic cerebral angiogram before MT significantly increased procedure duration (46 vs 40 min, 15 % increase, p = 0.05), DAP (161 vs 122 Gy·cm², 33 % increase, p < 0.0001), and contrast load (180 vs 80 mL, 125 % increase, p < 0.0001).

Conclusion: Our study shows that BP angiosuites significantly decreased iodine contrast exposition. Furthermore, decision to realise a pre-intervention diagnostic cerebral angiogram before a MT should be clinically motivated to avoid any useless increase in radiation, contrast load and procedure duration.

Stable machine learning algorithm for evaluation of pulmonary hypertension on conventional x-rays

V. D. Phi van, T. Frauenfelder; Zurich/CH

Purpose: Evaluation of pulmonary hypertension is essential for monitoring intensive patient. The grading of pulmonary hypertension shows low inter-reader agreement between different radiologist. The purpose of our study is to establish a stable machine learning algorithm, which can detect the stage of pulmonary hypertension reproducibly.

Methods and Materials: 800 images thoracic conventional x-ray images were graded by a senior radiologist (>20 years experience) into three stages: none, low to intermediate hypertension, pulmonary edema. A first convolutional neural network were trained to segment the lung parenchyma and mediastinal shape. The dataset were reduced to the lung segmentation. A part of the new dataset (train set) were fed into a second convolutional neural network with the labelling. Prediction were performed on a test data set.

Results: Lung segmentation were successfully performed and controlled by junior radiologist. Overall correct prediction of the pulmonary hypertension stage lies at 78.5%. The best prediction rate were archived in images with no pulmonary hypertension (81.2%), followed by the group of low to intermediate pulmonary hypertension (78.2%) and the group with lung edema (71.2%).

Conclusion: We could establish a 2-step algorithm with two different convolutional network, which could stably detect and stage pulmonary hypertension on conventional x-rays in intensive patient.

Is AP plus LAT topogram better than a single AP?

D. Thor, G. Poludniowski, T. B. Brismar; Stockholm/SE

Purpose: To compare the outcome in image noise and radiation dose in the subsequent CT scan following a single anterior-posterior (AP) vs AP plus Lateral (AP+LAT) topograms.

Methods and Materials: After approval by the local ethics committee, 300 prospective patients referred for a routine thorax examination were randomly assigned a single AP or AP+LAT topogram. Measurements of noise and patient size (water equivalent diameter) was performed in the thorax- and liver, and the corresponding effective tube current (effmAs) at these positions were collected. The analysis of performance was done by fitting curves of effmAs and noise against patient sizes and comparing the normalized root mean squared error (nRMSE) of the fits. A smaller nRMSE indicates more consistent inter-patient image noise and effmAs for a given size. The reference effmAs in both protocols was set to correct for known differences in average mAs.

Results: There was a statistically significant difference in nRMSE for both noise and effmAs in the thorax region but not in in the liver (nRMSE for effmAs ±95%-CI was for AP vs AP+LAT: 7.0%±0.67% vs 4.1%±0.40% in the thorax and 3.1%±0.43% vs 2.5%±0.37% in the liver). A post-hoc analysis indicated that a subgroup of females (about 20%) with laterally protruding breast tissue was over-exposed in the thorax region when using the single AP topogram.

Conclusion: The study suggests that using AP+LAT topogram yields more consistent noise and radiation dose than a single AP.

Pitfalls in diagnosis of infiltrative lung disease

C. Du Pasquier, R. Lazor, R. Hajri, A. F. M. Ponti, S. Gidoin, N. Villard, D. C. Rotzinger, C. Beigelman; Lausanne/CH

Learning objectives: To put into perspective potential pitfalls related to the acquisition, post-processing, and interpretation of chest CT for the diagnosis of infiltrative lung disease (ILD).

Background: The diagnosis of ILD may be challenging, especially in non-typical presentations, and knowing the most common technical and interpretative mistakes is crucial to delivering an accurate report.

Imaging findings or procedure details: Different factors have to be considered when performing and reading a chest CT examination for ILD, as each of them may represent a source of pitfalls. First, abnormalities that may be related to technical issues such as patient positioning, the lack of deep inspiration or too low dose with high noise index must be recognized and fixed. Second, reconstruction parameters have to be set carefully, including the optimal choice of kernels (balance between spatial resolution and noise), or iterative reconstructions algorithms used, which may alter image texture. Moreover, interpretation mistakes related to false-positive findings, the lack of accurate description of predominant features related to the complexity of findings or errors due to the satisfaction of reading must be avoided. Finally, clinical context, co-existing conditions, and previous examinations must be integrated to establish the most appropriate differential diagnosis.

Conclusion: First, the correct analysis of ILD requires knowledge of various technical factors that may affect the recognition and diagnosis of interstitial abnormalities. Second, a systematic approach is required for an optimal interpretation, and pathology mimickers have to be identified in order to avoid wrong reporting.

Chronic pulmonary aspergilllosis: Several patterns for different patients

C. Du Pasquier, A. F. M. Ponti, R. Hajri, S. Gidoin, F. Lamoth, J.-A. Collinot, C. Beigelman; Lausanne/CH

Learning objectives: To review the various aspects of chronic pulmonary aspergillosis (CPA) as their differentials that may be associated.

Background: A few among approximately 300 species of Aspergillus are known to be pathogen for humans, the most common being *Aspergillus fumigatus*. Several forms of CPA exist, commonly complicating pre-existing cavitary lung disease in immunocompetent or moderately immunocompromised hosts. The diagnosis of CPA requires a combination of characteristics, including compatible images on chest CT, direct evidence of Aspergillus infection or an immunological response to Aspergillus spp. and exclusion of alternative diagnoses, all present for at least 3 months.

Imaging findings or procedure details: Single aspergilloma is a single fungus ball within a unique pulmonary cavity. Chronic cavitary pulmonary aspergillosis (CCPA), the most common form, consists of uni- or bilateral alveolar consolidations, cavities with thick walls, with/without aspergilloma, and associated with pleural thickening and dense extra pleural fat. Lesions may progress to chronic fibrosing pulmonary aspergillosis if untreated. Aspergillus nodule is a focal nodular lesion that can mimic a tumoral lesion. All these patterns are seen in immunocompetent hosts with prior or current cavitary lung disease. Subacute invasive pulmonary aspergillosis has the same imaging findings as CCPA but develops faster (<3 months) and usually affects moderately immunocompromised hosts. Evolutive profiles as well as differential diagnosis and associated forms will be detailed.

Conclusion: CPA has different patterns that have to be recognized in order to avoid the common delay in the diagnosis. Differential diagnosis as well as associated forms must be kept in mind.

PO30

The HRCT features of idiopathic interstitial pneumonias

*S. Malekzadehlashkariani[1], D. Hennion[2], H. C. Thoeny[3]; [1]Sion/CH,
[2]Fribourg/CH, [3]Bern/CH*

Learning objectives: To outline the characteristic HRCT patterns of idiopathic interstitial pneumonias (IIP) and to define a practical approach to differentiate the unique patterns.

Background: IIP are a heterogeneous group of diffuse interstitial lung diseases compounding various degrees of inflammation and fibrosis. Patients usually present with non-specific symptoms such as cough, fever and dyspnea. IIP include idiopathic pulmonary fibrosis (IPF), non-specific interstitial pneumonia (NSIP), cryptogenic organizing pneumonia (COOP), desquamative interstitial pneumonia (DIP), lymphoid interstitial pneumonia (LIP) and acute interstitial pneumonia (AIP).

Imaging findings or procedure details: IPF, the idiopathic subtype of usual interstitial pneumonia, is characterized by honey-combing, irregular reticulation and traction bronchiectasis with predominantly basal and peripheral distribution. NSIP classically presents as a dominant ground glass opacity with a mild degree of reticulation and honey-combing peripherally located, while typically sparing the immediate subpleural space. COOP is recognized by peripheral and peribronchovascular consolidation with a lower lobe predominance. DIP commonly demonstrates with centrilobular nodules of ground glass opacity mostly found in lower lobes and is commonly associated with cigarette smoking. LIP, which is usually associated with connective tissue disorder or immunosuppression, classically shows ground glass opacities with pulmonary cysts. AIP demonstrates ground glass opacity and consolidation primary demonstrating peripheral distribution and becoming diffuse while the disease progresses. Although these patterns are characteristic, it is not uncommon that they appear with atypical images.

Conclusion: HRCT is frequently performed in the diagnosis the IIP, highlighting the role of radiologists to characterize IIP patterns. However, the HRCT patterns should be interpreted with pathological and clinical information to describe a more complete diagnosis.

PO31

How and when to apply Reduced dose and Ultra-reduced dose CT in chest imaging

*S. Gidoin, C. Du Pasquier, D. C. Rotzinger, N. Villard, M. Bernasconi,
C. Beigelman; Lausanne/CH*

Learning objectives: To reiterate the ALARA principle and the basic rules regulating spatial resolution, contrast and noise. To identify situations benefiting from reduced dose (RD)/ultra-reduced dose (URD) CT and those where dose reduction should be avoided. To provide a dose reduction scheme for follow-ups.

Background: Knowledge and application of RD (1–3mSv)/URD CT (<1mSv) is required due to the frequency of chest CT examinations. Despite the availability of several tools such as dose modulation, choosing of the optimal dose for a given scenario is not an easy task in routine practice.

Imaging findings or procedure details: We will first discuss dose reduction tools available today. We will then review circumstances in which RD or URD CT should be privileged, and the appropriate CTDI determined. We will propose a dose reduction scheme for diseases requiring numerous follow-ups according to the signs reviewed at CT. We will also highlight situations where dose reduction techniques may mislead the radiologist either by mimicking or concealing a pathological condition.

Conclusion: The role of both radiologists and clinicians is reinforced through understanding and appropriate use of CT dose reduction. Here, we introduce a new personalized approach to adapt the dose for chest CT according to (a) any previous examination, (b) the specific question asked by the referring physician, and (c) patient size and the equipment used. We emphasize how URD-CT, delivering comparable dose than a posteroanterior and lateral chest X-Ray, could change practice.

PO32

How to deal with multiple lung nodules: A systematic approach

*A. F. M. Ponti[1], C. Du Pasquier[2], R. Hajri[2], F. Zanchi[2], G. P.-O. Marie[2],
S. D. Qanadli[2], H. C. Thoeny[1], C. Beigelman[2]; [1]Fribourg/CH, [2]Lausanne/CH*

Learning objectives: The objectives of this educational poster are to review the principle of analysis and management of multiple lung nodules (MLN) and to elaborate a systematic diagnostic approach.

Background: The discovery of MLN requires, as for single nodule, a careful analysis to attempt further characterization. In particular, lesion distribution and integration of clinical data are necessary to determine their etiologies and ensure the correct management. This can be particularly complex due to the numerous causes to consider, that vary according to the number of the nodules as well as the clinical context. Furthermore, they are commonly combined in a single patient.

Imaging findings or procedure details: Lung nodules are characterized by CT mainly on their density, morphology and when indicated, temporal evolution. In all cases, MLN must be correctly detected and independently analysed. The clinical presentation is of utmost importance, particularly the distinction between apyretic and pyretic patients. We propose to classify multiple lung nodules firstly according to the clinical context and secondly according to their morphology, texture and temporal evolution when available. Differential diagnosis between each group will be reviewed and illustrated. Rare cases related to drug toxicity or orphan diseases must be kept in mind.

Conclusion: This educational poster is aiming helping radiologists to deal with MLN based on an appropriate technical approach and analysis, this being fully integrated in the clinical context. This will ensure the optimal overall management for the patients.

Develop the second set of diagnostic reference levels and achievable dose from 13 adult CT protocols and a paediatric head CT protocol in Korea

S.-W. Yun; Seongnam/KR

Purpose: To develop the second set of diagnostic reference levels (DRLs) and achievable dose (AD) from 13 adult CT protocols and a paediatric head CT protocol in Korea.

Methods and Materials: A survey of 13,625 CT examinations of 13 adult CT protocols, and paediatric non-contrast brain CT protocols, grouped according to age, were collected using 369 CT systems. Of these adult CT protocols, DRLs of intracranial CT angiography, low dose chest CT, CT aortography, and coronary artery calcium score CT were surveyed for the first time. Data were collected using two methods: web page data collection and direct data collection from CT equipment using the radiation dose information collection system by DICOM radiation dose structured report (RDSR) and header information. The 25th and 75th percentiles for CT dose index volume ($CTDI_{vol}$) and dose-length product (DLP) were calculated from this data.

Results: Most of the CT protocols from this survey had similar DRLs relative to data from other countries. Chest and abdomen-pelvic CT in this survey had lower DRLs than the DRLs found in the first Korean national survey and in surveys from other countries. Paediatric non-contrast brain CT protocols in each age group, except the age between 11 and 15 years showed lower DRLs than that of other countries.

Conclusion: This was the second Korean national survey of CT DRLs and the DRLs presented here are similar to, or lower in some protocols than the CT DRLs presented in the first Korean national survey and DRLs from other countries

Integration challenges of vocal recognition in a standardized structured reporting system

P. Benedict[1], H. Brat[2], C. Thouly[2], D. Lallemand[2], B. Rizk[3], D. Fournier[2]; [1]Morges/CH, [2]Sion/CH, [3]Villars-sur-Glâne/CH

Purpose: To present adaptations needed to succeed in vocal recognition (VR) integration in a pre-existing multicenter standardized structured reporting (SSR) architecture without impairing productivity and report quality.

Methods and Materials: Continuous audit process started in August 2017 to progressively adapt VR software, the work of secretaries and radiologists according to the existing SSRs.

Results: Improved productivity, software stability, RIS integration and less transcription errors to fit radiologists, secretaries and referring doctor's needs are presented: Generating a VR template architecture adapted to existing SSR templates Setting up an interpretation console layout to fit 25 radiologists Improving accuracy of our 100 SSRs template subsections and contents Creation of a live multicenter forum/chat for problem solving and productivity improvement Providing monthly meetings to support secretaries in their conversion from typewriting to reviewing Information of repeated errors to a single radiologist-secretary quality managing team Bi-weekly radiologists discussion to standardize transcriptions of specific terms Tips and tricks sharing shortcuts and unsolved problems workarounds Iterative VR software improvements to minimize transcription errors and RIS-integration related bugs

Conclusion: Multivariant changes in routine work are necessary in order to successfully achieve VR integration in a SSR system.

Keys to maintain productivity and report quality are continuous audit process, teamwork, human accompaniment, education, partnership with stakeholders and commitment.

Gadolinium retention: Incorporation of gadolinium in calcium-deficient hydroxyapatite

B. Le Gars Santoni[1], R. Egli[2], J. T. Heverhagen[2], C. Stähli[1], M. Bohner[1]; [1]Bettlach/CH, [2]Bern/CH

Purpose: Assess the interaction of gadolinium (Gd) with calcium-deficient hydroxyapatite (CDHA) in order to understand the role of bone in the retention of Gd in brain after contrast enhanced MRI.

Methods and Materials: Gd-containing CDHA powders were produced by precipitation of diammonium phosphate ($(NH_4)_2HPO_4$, calcium nitrate $Ca(NO_3)_2$ and gadolinium nitrate $Gd(NO_3)_2$ solutions. The reagents were used in quantities to obtain a [Ca+Gd]/[P] molar ratio of 1.50. The synthesis was filtered, cleaned twice with 250 ml of ultrapure H_2O and dried. The Gd content was determined using inductively coupled plasma mass spectrometry (ICP-MS).

Results: The precipitated CDHA powder contained 1.48 wt% Gd, corresponding to 35% of the Gd initially present in the solution. Only trace amounts of Gd (<1 ppm of the Gd in the powder) were released into the water used for cleaning.

Conclusion: Initial data reveals that Gd is permanently incorporated into CDHA during crystallization. This affinity of CDHA for Gd indicates that Gd *in vivo* may be absorbed into the mineral phase of bone tissue from where it is released into circulation in due course, thus supporting the hypothesis that bone may be the long-term storage compartment of Gd. Further work examining this hypothesis, in particular on the crystal structure of Gd-substituted calcium phosphates, is ongoing and will be presented at the meeting.

Radiologists and nuclear medicine physicians are looking forward to a cross-curricular training

S. Y. Kim, M. H. Maurer; Bern/CH

Purpose: To obtain an overview of the attitudes toward interdisciplinary further education of residents and consultants in radiology and nuclear medicine and preferences regarding a future joint training curriculum in Switzerland.

Methods and Materials: A 34-item questionnaire was sent electronically (SurveyMonkey online survey tool) to 1,244 radiologists and nuclear physicians (residents and consultants) in XXX. The items asked about the motivation for further education in each other's specialty and preferences regarding a joint further education curriculum in radiology and nuclear medicine.

Results: Overall, 370 questionnaires were analyzed (370/1,244, 30%). There were 280 (76%) board-certified physicians in either radiology (238/370, 64%) or nuclear medicine (42/370, 12%) and 65 (18%) residents (radiology: 54/370, 15%; nuclear medicine: 11/370, 3%). More than half of all residents (34/65, 52%) stated their conviction that a wide range of expertise in both disciplines could be fully guaranteed through adequate cross-curricular training. For responders already at a consultant level in radiology or nuclear medicine, the willingness to undergo further training in each other's specialty significantly increased with a shorter training period. The preferred option for a possible future joint training curriculum was a combination of a 5-year radiology training program with 2 years of further training in nuclear medicine.

Conclusion: Both residents and board-certified physicians in Switzerland are highly interested in a cross-curricular training curriculum in radiology and nuclear medicine.

"Iodine allergy" is a fake diagnosis

P. Lombardo, K. Nairz, I. Böhm; Bern/CH

Learning objectives:
· To learn that an "iodine allergy" does not exist.
· To realize that the term "iodine allergy" covers different diagnoses (e.g. CM-allergy, allergy against iodinated disinfectants).
· Future omission of the term "iodine allergy".

Background: Although several papers point to the fact that the term «iodine allergy» is incorrect and puzzling, it is still in clinical use.
Recently, a clinical retrospective study showed that this inexact diagnosis is associated with an increased rate of adverse events as compared to more specific diagnoses like „contrast medium allergy" or the exact diagnosis, which clearly states the name of the culprit contrast medium.
Since the term «iodine allergy» is associated with a spectrum of different allergies, radiologists should ascertain its exact cause. In retrospect, this may be time consuming and would be avoidable by a proper documentation.

Imaging findings or procedure details: We present a medical comic featuring this topic in order to teach the radiological community.

Conclusion: In order to exterminate the inexact designation "Iodine allergy" we term it „fake diagnosis" and in order to reinforce the message additionally use comics as stylistic device to strengthen the case.

Cardiac implantable electronic devices in MRI – A global analysis to define best practice and workflow improvements.

B. Delattre, M. Bontean, H. Burri, D. Carballo, P. G. Challande, M. I. Vargas Gomez, J.-P. Vallee; Geneva/CH

Learning objectives: To give an overview of the recent studies and recommendations regarding the management of patients with a cardiac implantable electronic device (CIED) undergoing MRI.

Background: The instructions for use (IFU) of five major manufacturers of pacemakers, defibrillators and implantable loop recorders were studied and the most significant aspects of the extensive safety measures pertaining to MRI are presented. Recent studies as well as guidelines regarding the examination of patients with CIEDs undergoing MRI are also reviewed.

Imaging findings or procedure details: For decades, CIEDs were banned from MRI because of safety concerns.
Since the introduction of MR-conditional devices, safe MR examination can be performed, providing that the requirements specified in the IFU are met. Studies and guidelines also cover MR examinations in non-MR conditional CIEDs. In this work, the potential risks associated with MR procedures in managing patients with CIEDs are described. Common mistakes and practical guidelines are presented based on our clinical experience.

Conclusion: Recommendations regarding MRI in patients with CIEDs and their manufacturer's prerequisites to ensure safe examinations are rapidly evolving. It is essential to be aware of the latest concepts and adapt in-house policies accordingly to implement best practices and maintain a safe MR environment.

Gadolinium Deposition Disease – just imagination or more?

J. M. M. Froehlich[1], S. Ignjatovic[2], O. Wuerthinger[1], R. A. Kubik-Huch[2]; [1]Zurich/CH, [2]Baden/CH

Learning objectives: To shed more light on the Gadolinium Deposition Disease (GDD) described in the context of contrast-enhanced MRI.

Background: Single patients with normal renal clearance report suffering toxic symptoms resembling GDD of varying severity. Diagnosis is based on a temporal link with gadolinium administration (1 month), often with persistent clinical symptoms such as intense burning skin, boring pain in the bones or joints, mental confusion, muscle fasciculations, skin pins, a sharp feeling of needles, head pain or various skin alterations (Richard Semelka, 2016). Single published cases have reported prolonged renal gadolinium clearance (>30 d). The clinical significance of GDD and causal relationship with gadolinium has not been established. Often, in these cases no other alternate preexistent disease or known process is present to account for the etiology.

Imaging findings or procedure details: The vary sparse case reports are mostly not well documented and thus difficult to assess. Gadolinium retention in patients with normal renal function is not comparable with NSF. Apart from the gadolinium associated NSF fibrotic changes there aren't any clear toxic effects that could be linked. Accordingly, the question arises whether low Gd tissue levels in certain circumstances might still trigger GDD. In view of the limited data, we recommend a thorough anamnesis about all influencing factors, including a precise calendar description about the pain evolvement, and if possible urine Gd tests.

Conclusion: The parallels between the early studies of gadolinium intoxication with NSF and GDD, advocate for keeping attentive both from the side of the clinicians and radiologists.

Analysis of radiological incidents in a radiology department for improving patient and staff radiation safety

M. Casiraghi, L. Bellesi, M. A. Piliero, F. Pupillo, D. Gaudino, S. Presilla; Bellinzona/CH

Purpose: The work aims to improve the radiation protection of patients and workers in radiology by implementing a radiation safety program for record and analysis of radiological incidents.

Methods and Materials: An incident reporting system was implemented in a multisite radiology department.

An awareness campaign promoting the safety culture was made. A multidisciplinary group comprising Radiologists, Medical Physicists, RTTs, and Quality Managers was created. Meetings are regularly organized for analyzing the reported incidents with event revision, root cause analysis and identification of corrective actions. The communication of the analysis results to the staff is done as a part of the program of continuous education in radiation protection.

In this work, a statistical analysis of the incidents was performed and a recurrent event was selected for a Failure Mode and Effects Analysis.

Results: 35 incidents were reported in 10 months, 25 adverse events and 10 near misses. The events were reported by Doctors, RTTs, and Physicists. The 52 %, 39 % and 9 % of the incidents were caused by human error in the exam execution, technical errors, and errors in the prescription process, respectively.

The process of the exam prescription and justification was selected for the FMEA. The analysis lead to a revision of the internal procedures and workflow.

Conclusion: The analysis of radiation incidents is fundamental for upgrading radiology procedures in order to minimize the risk of both patient and worker unintended exposure.

Communication of analysis results is important to raise the awareness of staff members on actions leading to incidents and promote the introduction of corrective actions.

Evaluation of occupational radiation exposure of the eye lens in fluoroscopy-guided surgical procedures

J. Ekeberg, K. Karava, N. Saltybaeva, K. Zeimpekis, S. Tanadini-Lang, M. Guckenberger, A. Stüssi; Zurich/CH

Purpose: The yearly limit for the occupational equivalent dose to the eye lens was recently reduced from 150 mSv to 20 mSv, averaged over a period of five years, with no year exceeding 50 mSv. Therefore, additional protection of the eyes for some medical professionals is required. This study aims to define the group of professionals for whom lead goggles should be mandatory.

Methods and Materials: The evaluation has been done for the working groups (surgeon, surgical assistant, anesthesiologist and attendant for surgical positioning) performing fluoroscopy-guided procedures (FGPs) in different operation theaters. The measurements were performed for the most common and dose-intensive FGPs by means of digitally assigned dosimeter badges (I2, Raysafe, Sweden) enabling real-time dose monitoring. This assessment was complemented by measurements performed by thermo-luminescent material dosimeters attached to the frame of the lead goggles enabling a conservative estimate of the monthly eye lens doses during a 3-month time span.

Results: The study has shown that dose values strongly depend on the type of FGP and the use of external protective devices. For example, the eye lens dose for the primary surgeon was equal to 3 µSv and 83 µSv for two cases of catheter ablation and heart catheterization FGPs, respectively.

Conclusion: The study defines the group of medical professionals for whom lead goggles are needed for ensuring compliance with the dose limits.

Implementation of a new software and server infrastructure for more efficiency in patient registration and safety

A. Lutoschkin[1], A. Peters[1], R. Grosswiler[1], R. Siegrist[2], R. A. Kubik-Huch[1], T. Niemann[1]; [1]Baden/CH, [2]Givisiez/CH

Purpose: In order to automize the workflow of patient identification in computed tomography we designed a nationwide unique software and server infrastructure.

Methods and Materials: Prior to an examination, patients are registered manually on the control panel. Despite prudent adherence to standard operating procedures, patient misidentification may still occur, mainly due to human failure. To automize the patient registration process and hence increase both efficiency and patient safety, we designed a new IT-supported solution based on bracelet and dedicated server infrastructure.

The specific case number on the patients' bracelet needs to be transferred in a DICOM-tag, which can be read by the modality. Since a DICOM-tag for the specific case number is not available by default, an intermediary proxy solution converts the patient case number in a corresponding DICOM-tag to the modality.

Results: In close collaboration with our industrial partner Avintis we implemented a novel software and server infrastructure. This infrastructure requires scanning the patient's bracelet to unblock image registration for the technician. Through communication among the proxy servers and with the RIS, the generated CT images are automatically assigned to the correct patient.

In addition to this workflow automatization, our solution eliminates potential patient mix-ups and contributes to further increase of imaging efficiency.

Conclusion: Our IT-supported automatization of patient identification may substantially enhance procedure efficiency and patient safety.

Relative Encoding-Associated Signal-Intensity (rEASI) scaling values as a measure for quantitative MRI sequence comparisons

N. Hinterholzer, C. von Deuster, S. Sommer, D. Nanz; Zurich/CH

Purpose: To suggest a measure for quantitative comparisons of signal strength across platforms, anatomies, contrast weightings, or echo-formation types for a given spatial encoding.

Methods and Materials: In a single-center prospective phantom study the product of nominal voxel volume and square root of the total signal-sampling time was hypothesized to allow quantitative comparisons of MR imaging protocols. It represents a measure of the Encoding-Associated Signal-Intensity (_EASI_) scaling of a sequence – irrespective of sequence type (e. g., spin- or gradient echo), magnetization relaxation times, details of the phase-encode ordering, receive coil, or magnetic-field strength.

We suggest using relative, dimensionless _rEASI_ values for actual comparisons:

$rEASI = EASI / EASI_{ref}$, with $EASI_{ref} = 0.1 \, mm^3 * sec^{½}$.

A formula was obtained for the calculation of _rEASI_ values for all sequences from parameters that can be set on the graphical user interface of a particular scanner (3T Siemens Prisma, Software syngo MR E11). Calculated _rEASI_ values were compared with experimentally measured (phantom) SNR values and with manufacturer provided „relative SNR" values.

rEASI values for various clinical imaging protocols at different field strengths were obtaiend and compared.

Results: Calculated _rEASI_ values correlated well with experimental SNR values and were identical with scaled relative SNR values within experimental error – with some prominent exceptions (systematic deviations from apparent experimental SNR, non-systematic deviations (asymmetric echo, …) compared to relative SNR values) that will be discussed in the talk.

Conclusion: The _rEASI_ values could provide a valuable tool for quanitative sequence comparisons, in particular if they were provided by the manufacturers.

Visualization of intramuscular botulinum toxin propagation without contrast media using a new B-Flow sequence

S. J. Sanabria, L. Ruby, K. Martini, T. Frauenfelder, D. A. Ettlin, L. M. Gallo, M. Rominger; Zurich/CH

Purpose: To visualize intramuscular distribution processes in order to optimize injection procedures (number of injections, amount/injection), which are currently based on empiric evidence. Conventional contrast-enhanced ultrasound (CEUS) affects the viscosity of botulinum toxin and its distribution process. Therefore, ultrasound sequences not requiring contrast media are necessary.

Methods and Materials: This prospective study was approved by the institutional review board. 5 units botulinum toxin type A dissolved in 0.1 ml normal saline (0.9 % NaCl) were injected at three defined locations of an ex-vivo porcine masseter muscle 12 hours after explantation. B-mode cine-loop images were obtained using a 9-MHz probe (GE Logiq E9). A novel image registration method based on 2D-digital image correlation (2D-DIC) was used to compensate for tissue deformation during injection, allowing high sensitive detection of B-mode changes due to botulinum toxin propagation.

Results: 2D-DIC allowed visualization of the injected fluid without a contrast medium. Botulinum toxin propagated along the fiber structure of the muscle without propagating into the fascia. The propagation appeared to be anisotropic with a threefold larger axial compared to lateral expansion. Tissue displacements due to injection were more pronounced in the axial than lateral direction with a compressive strain both above and below the needle.

Conclusion: Due to greater axial compared to lateral propagation, multiple injections of smaller amounts instead of a single injection using a larger amount of botulinum toxin are recommended. Resembling a b-flow, the presented 2D-DIC method is a promising method not only for botulinum toxin, but also a wide range of other applications, where CEUS is not feasible.

Establishing DRL for CT examinations: The role of a dose management system

M. Sans Merce, J.-C. Mourin, R. Rodriguez, X. Montet; Geneva/CH

Purpose: Dose Reference Level (DRL) for CT examinations were setup by means of a dose management system (Radimetrics, Bayer HealthCare) for all 6 CT scanners in the Division of Radiology of the University Hospital of Geneva.

Methods and Materials: Patient radiation doses are registered into the dose monitoring system allowing the follow up of the doses delivered to each patient as well as the protocols used for each clinical task. Radimetrics has allowed us to retrieve around 540 individual protocol with their associated dose values for all 6 CT scanners. Within the context of the EUROSAFE accreditation and following the European Project on Clinical Diagnostic Reference Levels (EUCLID), these protocols grouped into 220 standardized protocols have been linked to a clinical indication.

Results: The comparison of the individual protocols with the National established DRL allows us to detect protocol with higher than expected dose, and to work on optimization.

Conclusion: Working with a dose management system allowed us to point out at those individual protocols that are needed to be optimized in order to ensure that patient doses are as low as reasonably achievable for the clinical purpose of the examination.

Online platform for fast and accurate assessment of radiation dose received by conceptus in clinical CT

N. Saltybaeva[1], A. Platon[2], P.-A. Poletti[2], H. Alkadhi[1]; [1]Zurich/CH, [2]Geneva/CH

Purpose: Computed tomography (CT) is sometimes required during pregnancy. In this case the radiation dose received by conceptus should be evaluated. Existing methods are either limited in their accuracy or require complicated calculations. The aim of this study is to develop a tool for conceptus radiation dose assessment, which can be used in clinical routine.

Methods and Materials: The tool is based on the doses derived from Monte Carlo (MC) simulations performed for generic CT system on virtual phantoms, representing patients at various gestational stages. For validation, the values provided by the tool were compared against doses calculated by detailed MC simulations, using real data from 30 pregnant patients, underwent abdominal CT examinations on two different systems (Siemens, GE). Detailed MC simulations took individual patient geometry and scan parameters into account. After the validation the online tool with intuitive user interface was created.

Results: The validation of the tool has shown that the average error of the dose values calculated by the online tool was 23 %, with the overestimation of about 41 % in case of obese patients and in patient with additional hardware (fixation devices). The tool requires input of only few parameters such as CTDIvol, tube voltage and the scan length. The radiation dose recieved by conceptus is calculated in real time.

Conclusion: The online platform provides fast and reliable evaluation of the radiation dose, received by conceptus from CT examination of any kind. This tool can be used for performing risk-benefit analysis and training purposes.

BOLD-response to hyperoxic challenges in intracranial malignancies: Dependency on the gas administration protocol

S. Stieb, O. Riesterer, A. Boss, T. Weiss, M. Guckenberger, P. S. Özbay, D. Nanz, C. Rossi; Zurich/CH

Purpose: Literature reports contradicting results on the response of brain tumors to vascular stimuli measured in T2*-weighted MRI. Here we analyzed the potential dependency of the MRI-response to (hypercapnic) hyperoxia on the order of the gas administration.

Methods and Materials: T2* values were quantified at 3 Tesla in eight consenting patients at rest and during inhalation of hyperoxic/hypercapnic gas mixtures. Patients were randomly divided into two groups undergoing different gas administration protocols (group A: medical air-pure oxygen–carbogen; group B: medical air–carbogen-pure oxygen). Mann-Whitney U test and Wilcoxon signed rank test have been used to test differences in T2* regarding respiratory challenge or different groups, respectively.

Results: T2* values for grey and white matter were 50.3±2.6 ms and 46.1±2.0 ms, respectively, and slightly increased during challenge. In tumor areas, T2* at rest were: necrosis = 74.1 ± 10.1 ms; edema = 60.3 ± 17.6 ms; contrast-enhancing lesions = 48.6 ± 20.7 ms; solid T2-hyperintense lesions = 45.0 ± 3.0 ms. Contrast-enhancing lesions strongly responded to oxygen (+ 20.7 %) regardless on the gas protocol (p = 0.482). However, the response to carbogen significantly depended on the order of gas administration (group A: + 18.6 %; group B: − 6.4 %, p = 0.042). In edemas, a different trend between groups was found when breathing oxygen (group A: − 9.9 %; group B: + 19.5 %, p = 0.057).

Conclusion: Preliminary results suggest that the gas administration protocol is an important factor in the interpretation of the T2*-response in areas of abnormal vascular growth.

Fast pseudo-diffusive fluid motion contaminations in DTI

S. Stieb, M. Klarhoefer, T. Finkenstaedt, M. Wurnig, A. S. Becker, C. Rossi; Zurich/CH

Purpose: To quantify the fast pseudo-diffusion contamination by blood perfusion or cerebrospinal fluid on the measurement of the diffusion tensor metrics in healthy brain tissue.

Methods and Materials: Diffusion-weighted imaging (15 b-values, 20 diffusion-encoding directions) was performed on five healthy volunteers at 3 Tesla. Diffusion tensor elements were computed using a conventional two b-value approach (2b), by fitting the signal to a monoexponential curve (mono), and by correcting for fast pseudo-diffusion compartments using the biexponential intravoxel incoherent motion model (IVIM) (bi). Fractional Anisotropy (FA) and Mean Diffusivity (MD) were quantified in white matter areas, gray matter areas, and the ventricles.

Results: A significant dependence of the MD from the evaluation method was found in all selected regions. A larger dependence was found in the nucleus caudatus (bi: median $0.86 \cdot 10^{-3}$ mm^2/s, Δ2b: -11.2%, Δmono: -14.4%; p = 0.007), in the anterior horn (bi: median $2.04 \cdot 10^{-3}$ mm^2/s, Δ2b: -9.4%, Δmono: -11.5%, p = 0.007) and in the posterior horn of the lateral ventricles (bi: median $2.47 \cdot 10^{-3}$ mm^2/s, Δ2b: -5.5%, Δmono: -11.7%; p = 0.007). In the FA, the deviation depended on the evaluated region with significant differences mainly in the nucleus caudatus (bi: median 0.15, Δ2b: $+39.3\%$, Δmono: $+14.7\%$; p = 0.022) and putamen (bi: median 0.19, Δ2b: $+3.1\%$, Δmono: $+17.3\%$; p = 0.015).

Conclusion: Fast pseudo-diffusive regimes locally affect diffusion tensor imaging metrics in the brain. The IVIM-based method proposed in this study can correct signal contaminations through liquor or perfusion.

Factors influencing iodinated contrast enhancement in computed tomography

J. A. Vidal[1], H. C. Thoeny[2], J. M. M. Froehlich[3]; [1]Fribourg/CH, [2]Bern/CH, [3]Zurich/CH

Learning objectives:
· To understand how physico-chemical characteristics of iodine-based contrast media (ICM) influence the CT enhancement parameters.
· To elucidate how patient related factors potentially influence the ICM dynamics
· To shed some light on the interrelationship of these parameters in view of clinical experience.

Background: The continuing advances in CT technology have led to challenges on how to administer ideally intravenous iodinated contrast media in relation to scanning time. Various physico-chemical characteristics of ICM will be discussed in relationship to patient physiology, ICM pharmacokinetics and dynamics potentially influencing the enhancement patterns and thus CT scanning parameters. Based on previous published models (Bae KT, Radiology 2010) basic influencing factors will be validated clinically.

Imaging findings or procedure details: CT attenuation depends on a multitude of factors such as the injected iodine amount per second, injection duration and velocity, patients' cardiac output and/or body-mass index, kVp, saline flushing schemes, and finally yet importantly the location of interest (vascular/parenchymal). Differentiation on how these factors may influence the temporal profile or the magnitude of CT enhancement is required. The ultimate goal is to achieve the optimal diagnostic contrast level within the target organ using the minimum amount of iodine, although further protocols still need to be elaborated. Herefore various injection algorithms based on BMI and cardiac function will be discussed.

Conclusion: Individualized ICM administration schemes tailored to the CT scanning protocol allow improvement of patient care.

Extravasation of contrast media: Update of essentials to manage the patient

J. Hrycyk, J. T. Heverhagen, I. Böhm; Bern/CH

Learning objectives: The radiologist is able to manage patients with contrast medium (CM) extravasation, knows the risk factors, and takes care for its prevention.

Background: Although rarely (~0.2 to 1.2%), extravasation regularly occurs in clinical radiological settings. Since radiologists are not always familiar with its treatment, and extravasation is a potential harmful adverse event (tissue necrosis, compartment syndrome), herein we present its management that depends on the as-soon-as-possible recognition, the adequate treatment, and possibly its prophylaxis in the future.

Imaging findings or procedure details: Extravasation is possible in every patient. The most important risk factor is a history of extravasation. Prophylaxis includes use of plastic needles in the antecubital vein with pre-warmed iodinated contrast medium.

The management comprises of its diagnosis including stopping both the scan, and the CM-infusion, followed by a close clinical observation for 2–4 h to recognize immediately disease progression (i.e. pain, swelling, sensory alteration, blistering and/or ulceration of the skin), as well as a conservative treatment (e.g. hot or cold packs, elevation of the limb) for mild extravasations and surgical consultations for severe ones.

Conclusion: Most cases are mild self-limiting events, and only very rarely, severe extravasation occurs that needs surgical treatment.

PO51

Comparison of Cone beam-CT with plain film x-ray in the acute trauma of the wrist and the distal forearm

D. Bilecen[1], S. Vitez[2], J. Ederer[2], B. K. Kovács[3], R. Hügli[2]; [1]Laufen/CH, [2]Bruderholz/CH, [3]Basel/CH

Purpose: To study the value of cone beam-CT (CBCT) compared to plain film x-ray after acute trauma of the hand and to determine the sensitivity and specificity of both imaging modalities.

Methods and Materials: 52 Patients (36 men, 20 women, mean age, 56,3 years) were retrospectively selected from the digital database (PACS) between 2016 until 2017. All patients had an acute trauma of the hand and distal forearm. CBCT and plain film x-ray was performed. The interval between both studies was no longer than two weeks.

Sensitivity and specificity were calculated for each of the three board certified readers. Inter-observer reliability was assessed by calculation of the kappa correlation.

Results: Two radius fractures, nine fractures of carpal bones and three fractures of metacarpal bones and phalanx bones were missed in plain film x-ray. Plain film x-ray showed a moderate inter-observer reliability ($\kappa = 0.572$) whereas inter-observer reliability of CBCT was good ($\kappa = 0.603$). Mean sensitivity of plain radiography was 0.83, mean specificity was 0.79. Mean sensitivity of CBCT was 0.99, mean specificity 0.90.

Conclusion: Conclusion: CBCT is superior to plain x-ray in detecting radius and hand fractures in an emergency setting and may pose an alternative first line imaging tool.

PO52

Usability of automated ultrasound in musculoskeletal imaging of the hand and wrist

F. A. Huber, L. Ruby, M. Marcon, M. Rominger, R. Guggenberger; Zurich/CH

Purpose: To investigate the diagnostic value of automated ultrasound (AUS) in musculoskeletal imaging of the wrist/hand.

Methods and Materials: We built an experimental Plexiglas container, which featured a front side made from ultrasound (US) permissive film. The container was filled up with water, a regular transducer for breast AUS (GE Invenia, 10 MHz) was applied to the US permissive side to examine the field of view underwater. Two radiologists with 6 years of musculoskeletal US experience and no experience, respectively, examined both hands of each other. Additionally, the same region was scanned analogously by both observers with handheld ultrasound (HHUS; GE Logiq E9, linear transducer, 15 MHz). Image loops and recording times were documented. Both examiners rated all images by four qualitative parameters (assessability of tendons/joints/cortical bones, homogeneity of image quality) on a four-point Likert scale (0–3, „non-diagnostic'-'perfect'). Statistical analysis included Cohen's Kappa for interreader agreement and student t-testing for differences between AUS and HHUS.

Results: Examination time of both readers showed no significant differences between AUS and HHUS (132 vs 129 seconds, p = 0.93). Interreader agreement was considered moderate (0.4–0.6). Average homogeneity of image quality in AUS and HHUS was 2.25 vs 1.38 (p < .05), mean assessability of structures was 1.75 vs 1.63/1.38 vs 1.38/1.88 vs 1.69 for tendons/joints/cortical bone, respectively.

Conclusion: AUS imaging of the hands delivers significantly better overall image quality and joint assessability at comparable examination times to HHUS, even with untrained examiners.

PO53

Automatic MRI-based 3D models of hip cartilage using a 3D U-net-like fully convolutional network for improved morphologic and biochemical analysis

F. Schmaranzer, R. Helfenstein, T. Lerch, G. Zeng, K. Siebenrock, M. Tannast, G. Zheng; Bern/CH

Purpose: The time-consuming and user dependent post-processing of biochemical cartilage MRI has prevented their wide-spread use. A time efficient, fully-automated analysis of biochemical 3D Images could provide more straightforward and comprehensive information on cartilage thickness, surface area and volume.

Methods and Materials: IRB-approved study on 25 symptomatic hips undergoing a contrast-enhanced MRI at 3T including a 3D dGEMRIC sequence (0.8 mm^3). Development of a fully-automated deep learning based approach for 3D segmentation of hip cartilage models was based on two steps: (1) 3D training data of hip cartilage was provided by one reader ('manual 3D analysis'); (2) a deep neural network for fully automated cartilage segmentation ('automated 3D analysis) and a software for 3D analysis was developed. dGEMRIC index, cartilage thickness, surface area and volume were measured in the four joint quadrants and compared. Mean average surface distance and mean Dice coefficient were calculated.

Results: Regional patterns were comparable for manual/automated 3D methods. Highest dGEMRIC indices were found postero-superiorly ($602.1 \pm 158.4 \text{ ms}$, $601.8 \pm 158.4 \text{ ms}$). Thickest cartilage was found antero-inferiorly ($5.3 \pm 0.8 \text{ mm}$, $4.3 \pm 0.6 \text{ mm}$). Smallest surface area was found antero-inferiorly ($134 \pm 60 \text{ mm}^2$, $155 \pm 60 \text{ mm}^2$). Largest volume was found antero-superiorly ($2343 \pm 492 \text{ mm}^3$, $2294 \pm 467 \text{ mm}^3$). Mean average surface distance was $0.26 \pm 0.13 \text{ mm}$ and mean Dice coefficient was $85.7 \pm 2.7 \%$.

Conclusion: This validation paves way to large-scale use of this method for fully-automatic 3D cartilage segmentation for an improved morphological and biochemical analysis of hip cartilage.

PO54

Traction MR arthrography of the hip for characterisation of femoral head necrosis and resulting femoral cartilage damage in patients eligible for joint preserving surgery

F. Schmaranzer, T. Lerch, J. L. Cullmann, J. T. Heverhagen, K. Siebenrock, M. Tannast; Bern/CH

Purpose: To assess (1) location of necrosis, (2) location and pattern of femoral cartilage damage, (3) diagnostic accuracy to detect femoral cartilage lesions using direct, traction MR arthrography (MRA).

Methods and Materials: IRB-approved retrospective study. The institutional database (2016–2018, 360 hips) was reviewed for patients with AVN and complete radiographs and direct, traction MRA of the hip at 3T. Thirty patients were included (mean age 31 ± 9 years, 60 % female; ARCO stages (I = 30 %, II = 57 %, III = 13 %). Fourteen (47 %) hips underwent joint preserving surgery (10 open, 4 arthroscopic). Traction technique included weight-adapted traction (15–23 kg), a supporting plate to avoid pelvic tilt. Imaging protocol included coronal, axial, sagittal and radial 2D PD-w TSE sequences without fat saturation obtained under traction. Location of necrosis and lesions was described circumferentially and allocated to 4 joint quadrants. We assessed (1) location of necrosis, (2) location and pattern of femoral cartilage damage (normal/delamination/thinning/defect) on traction MRA; (3) diagnostic accuracy of traction MRA to detect femoral cartilage lesions in the 14 patients (14 x 4 = 56 quadrants) undergoing surgery.

Results: (1) Necrosis was located most frequently in the antero-superior quadrant (93 % of hips). (2) Most frequently femoral cartilage delamination was found in the antero-superior quadrant (87 % of hips). (3) Sensitivity was 93 % (25/27), specificity was 100 % (29/29) of traction MRA to detect femoral cartilage lesions.

Conclusion: AVN predominantly affects the antero-superior quadrant and leads to corresponding femoral cartilage delamination which can be detected accurately using traction MRA.

Beyond the popcorn matrix – A diagnostic approach to cartilaginous tumors for the general radiologist

J. K. Walenczak, M. Hamard, A. Neroladaki, L. C. Farracho, D. E. Saiji, C. D. Becker, S. Boudabbous; Geneva/CH

Learning objectives: To review the radiological appearances of benign cartilaginous tumors and typical signs of malignant transformation on imaging. To learn how to correlate imaging with the clinical findings. To determine the role of the radiologist in the multidisciplinary diagnosis process of indeterminate or suspicious lesions.

Background: Cartilaginous lesions may be discovered incidentally or following nonspecific MSK complaints. Although some are easily diagnosed on the basis of clinical and radiographic criteria, others will necessitate an in-depth review consisting of several imaging modalities. Furthermore, certain localizations and multiplicity should raise our index of suspicion and require an appropriate assessment. Biopsies should be used sparingly and in knowledge of the risk of undergrading and tumor seeding. The final diagnosis will influence the management, which may consist of a simple clinical follow-up or a complex surgical procedure that will be the result of a discussion conducted by a multidisciplinary team.

Imaging findings or procedure details: Cartilaginous cap measurement on MRI dictates the management of osteochondromas. Radiologic semiology of enchondromas is of paramount importance given absence of clear histopathological signs of low grade malignant transformation. Rarer cartilaginous tumors are misunderstood as malignant entities and discussed to complete the overview. Finally, an algorithm based on imaging feature of cartilaginous tumors is provided to help the diagnosis, the management and the follow up.

Conclusion: Sufficient theoretical background in cartilaginous tumors imaging is necessary to avoid inappropriate biopsies and frequent follow-up studies of benign lesions.

Soft tissue vascular malformations: Classic and unusual appearances

A. L. Falkowski[1], V. Kalia[2], J. A. Jacobson[2], A. Hirschmann[1], O. Magerkurth[3]; [1]Basel/CH, [2]Ann Arbor/US, [3]Baden/CH

Learning objectives: Patients with vascular malformations can present with classic, but also with unusual imaging features and clinical symptoms. The classification of vascular anomalies has traditionally emphasized clinical and imaging features. Additionally, differential diagnoses can be developed through specific findings allowing for optimal evaluation.

Background: Vascular malformations consist of different entities with low- and high-flow lesions, which can be uni- or multifocal. Although children are mostly affected, lifelong symptoms are possible. The International Society for the Study of Vascular Anomalies redefined vascular malformations into (a) simple or (b) combined vascular malformations, (c) those of major named vessels, and (d) those associated with other anomalies.

Imaging findings or procedure details: Typical imaging features of vascular malformations in the soft tissues, e.g. phleboliths or fatty infiltration of muscle due to vascular steal phenomenon will be presented. Vascular malformations that will be discussed include venous and lymphatic malformations, arteriovenous lesions (malformation and fistula). Different imaging modalities, as well as therapeutic options will be emphasized. Additionally, unusual imaging and clinical appearance of vascular malformations in the soft tissues and their differential diagnoses, e.g. periosteal thickening, without phleboliths or para-periosteal contrast enhancement will be shown.

Conclusion: Vascular anomalies range from simple to complex, isolated to syndromic. Radiologist knowledge of the different entities, as well as their pitfalls, and interdisciplinary approach to each case can foster appropriate diagnostic and therapeutic recommendations.

Soft tissue vascular tumors: Pearls and pitfalls

A. L. Falkowski[1], V. Kalia[2], J. A. Jacobson[2], A. Hirschmann[1], O. Magerkurth[3]; [1]Basel/CH, [2]Ann Arbor/US, [3]Baden/CH

Learning objectives: Patients with vascular tumors can present with characteristic imaging findings, but in some cases atypical imaging features and clinical symptoms can cause a diagnostic dilemma. Knowledge of both typical and atypical appearances, as well as their pitfalls will allow a correct diagnosis.

Background: Vascular tumors consist of different entities ranging from benign, locally aggressive, to malignant. They can arise de novo at any age. Although benign lesions are most common in children, 2 % of vascular tumors are malignant and their correct diagnosis is crucial. The 2014 revised classification of vascular lesions from the International Society for the Study of Vascular Anomalies will be used as a guideline for this exhibit.

Imaging findings or procedure details: Important imaging features of vascular tumors in the soft tissues will be emphasized in this educational exhibit, such as cutaneous location mimicking an inflammation in cases of angiosarcoma. Other tumors to be discussed include congenital hemangioma and Kaposi sarcoma. Multiple imaging modalities including MR imaging and ultrasound will be reviewed. Additionally, pitfalls of hyperemic soft tissue masses other than vascular tumors, such as pseudoaneurysm or hyperemic masses, will be shown emphasizing key features to enable differentiation.

Conclusion: Vascular tumors range from benign, locally aggressive or borderline, to malignant. Radiologist knowledge of the different entities, as well as their pitfalls, and interdisciplinary approach to the cases can foster appropriate diagnostic and therapeutic recommendations.

Identification of sarcopenia in ultrasound using a generic deep learning analysis software: A pilot study

L. Ruby, S. J. Sanabria, C. Blüthgen, K. Martini, G. Freystätter, T. Frauenfelder, M. Rominger; Zurich/CH

Purpose: To investigate the potential of a deep learning software (DLS) to identify sarcopenia based on B-mode ultrasound images.

Methods and Materials: B-mode ultrasound images of both legs for 11 healthy, young (28 ± 3.9 years (mean $\pm$ std)) and 10 elderly (82 ± 7 years) women were retrospectively reviewed. Approval by the institutional review board and informed consent by all participants were obtained. A DLS (ViDi Suite v.2.0) was used with computations performed on a GeForce GTX1080 graphics card. The DLS was trained with a variable number of images and the remaining images were used for performance validation. A human reader (first-year radiology resident) evaluated the validation set with anonymized, randomized images. Diagnostic accuracy, area under the curve (AUC) and performance differences (DeLong method) were assessed.

Results: 42 images were available. Training times were 2 minutes for both DLS and human reader. Evaluation times for the test data set were 4.13 minutes for the human reader and 0.00012 minutes for DLS. With 8 training images (19 % of dataset), we found an AUC = 1.0 (sensitivity = 100 %, specificity = 100 %) for DLS and AUC = 0.886 for the human reader, which were significantly different from each other (p = 0.0129). With 21 training images (50 % of dataset), AUC values were 1.0 for DLS and 0.955 (sensitivity = 100 %, specificity = 90.9 %) for the human reader with no significant difference (p = 0.1473).

Conclusion: DLS provides texture analysis of ultrasound B-mode images with automatic unsupervised learning of texture features. DLS showed a higher diagnostic performance with few training data and a faster evaluation than the human reader.

PO59

Arthro-Cone Beam Computed Tomography for the detection of osteoarthritis

S. Boudabbous, L. C. Farracho, M. Hamarad, A. Neroladaki, M. Sans Merce, X. Montet; Geneva/CH

Purpose: XR remain the gold standard for establishing an imaging-based diagnosis of osteoarthritis. However, the criteria of Kellgren and Lawrence classification (KLC) are delayed and lack of sensitivity and specificity. CBCT is an emerging modality in extremity's imaging allowing low dose radiation with diagnostic quality images.
Evaluation of the image quality and irradiation in Arthro-Cone Beam Computed Tomography (Arthro-CBCT) compared to X-rays (XR) in the diagnosis of osteoarthritis.

Methods and Materials: 32 arthro-CBCT requested for osteoarthritis assessment, preceded by XR were performed. All Arthro-CBCT were reconstructed with Modeled Based Iterative Reconstruction and were analysed by 2 independent-blinded MSK radiologists for the overall quality (3-point Likert scale). Contrast, bone density and minimal joint space width (JSW) were evaluated. The stage of Kellgren and Lawrence was compared between Arthro-CBCT and XR as well as sclerosis and erosions using 3-point Likert scale. P value was calculated using the Wilcoxon test. Finally, radiation dose was estimated and compared between the two modalities.

Results: The image quality was excellent in all cases of arthro-CBCT with excellent inter-observer concordance (kappa = 1). The mean of density was 1966,328,812 and 330 respectively for the contrast, the trabecular bone, the subchondral cortex and for the cartilage. An under classification of osteoarthritis was noticed with XR regarding the JSW ($p = 0.02$), the detection of osteophytes (< 0.0001) and the KLC ($p < 0.0001$). The dose for arthro-CBCT and XR were estimated at 4.9 and 0.05 mSv

Conclusion: Arthro-CBCT may be a new way to assess osteoarthritis due to its high image quality and low radiation dose.

„b-box": A hardware standalone for workflow improvement in digital mammography screening using deep learning

A. Ciritsis, C. Rossi, A. Boss; Zurich/CH

Purpose: Cancer detectability in mammography depends on image quality and individual gland tissue breast density. Each mammographic examination is currently rated by the radiologist in terms of breast density and of image quality; this is a costly, time-consuming and reader-dependent practice.

Methods and Materials: The „b-box" is a hardware standalone which offers software solutions based on deep learning algorithms, and overtakes disliked tasks, like breast density classification and quality assessment of the acquired mammographic images. It introduces a standardization of procedures, and additionally monitors quality performances of the mammographic unit over time.

Results: The „b-box" was installed as testing and research device at our institute and successfully rated more than 800 different mammographic images. The reception of the radiological technicians using the „b-box" in their daily routine was positive throughout. With the implementation of the „b-box" in the clinical workflow a reduced waiting time for the individual patient was measured. Furthermore the b"-box" offers the possibility to trace and improve the quality of the acquired mammographic images.

Conclusion: By using the lean workflow of the „b-box" the radiological institute can perform up to 2 additional mammography examinations per day and drastically reduce waiting time for patients and number of recall examinations.

FEMDep: An e-learning platform designed to improve the quality of mammographic breast cancer screening programs.

D. Lepori, J.-Y. Meuwly, C. Ducros; Lausanne/CH

Purpose: FEMDep *(Formation et Enseignement en Mammographie de Dépistage)* is an e-learning platform designed to improve the diagnostic capability, quality and performance of radiologists involved, or requiring training, in mammographic breast cancer screening programs.

Methods and Materials: The medical team of the Vaud breast cancer screening program, with the support of an academic radiologist, created an e-learning platform to assist radiologists in acquiring and strengthening skills in mammography interpretation (initial training and continued learning).

The platform is based on the FEMDep training software, available online via a website, developed specifically for training sessions in the field of screening mammography. FEMDep offers the possibility of creating lists of training cases and of synchronizing playlists and image opening. The software includes automatic performance analysis with the calculation of a results table (PDF files generated) after reading exercises.

Results: Currently the FEMDep database contains around 2'500 anonymous mammograms: 260 cases of documented breast cancer, 190 cases of benign abnormalities and 2'000 cases of normal mammograms. FEMDep is now available in four academic radiology-training centers (FMH training in radiology) and two breast cancer screening centers (ongoing training of radiologists involved in a screening program). Thirty radiologists have already completed reading in total over 30,000 mammograms.

Conclusion: FEMDep is a useful and user-friendly e-learning platform for training radiologists. It will help to improve the quality of the mammographic breast cancer screening programs.

First clinical application of spiral breast CT: Patient-specific radiation dose assessment

N. Saltybaeva, S. S. Shim, A. Boss, H. Alkadhi; Zurich/CH

Purpose: Dedicated breast CT (BCT) has demonstrated superior image quality compared to digital Mammography (DM) and breast tomosynthesis (BT), however the radiation dose from BCT was also higher than the one from DM and BT, especially when referring to screening settings.

The novel BCT scanner equipped with photon-counting detector allows for more efficient dose utilization. The aim of the study is to assess the radiation dose from the first clinical in-vivo application of the spiral-BCT.

Methods and Materials: This study included 30 patients underwent breast CT examination on the spiral- BCT system equipped with CdTe photon-counting detector (Nu-view, Erlangen, Germany). A fixed tube voltage of 60 kV and tube current of 25 mA were used based on preliminary studies. The individual patient DICOM data together with patient-specific scan parameters were used as an input for Monte Carlo simulations performed by ImpactMC tool. The accuracy of this tool was validated against the measurements performed on the same BCT system using ionization chamber in 16-cm CTDI phantom. For each patient the average glandular dose (AGD) was calculated based on the individual 3D dose distribution acquired by MC simulations.

Results: The MC simulation has shown high accuracy comparing to the direct dose measurements, with the mean difference of 4.4 %. The average glandular dose ranged from 4.6 to 6.1 mGy, depending in the breast size. The mean ADG was found to be 5.2 mGy.

Conclusion: BCT system with photon-counting detector allows performing breast examinations with full 3D imaging capabilities using the dose comparable to that for two-view DM.

Factors affecting the accuracy of preoperative tumor size assessment on magnetic resonance imaging of T1 (≤2cm) invasive breast carcinoma

E. Y. Yoo, S. Y. Nam, M. J. Hong, H.-Y. Choi; Incheon/KR

Purpose: To evaluate MRI-pathology concordance of tumor size in patients with T1 (≤ 2 cm) invasive breast carcinoma.

Methods and Materials: Data from 200 histologically confirmed T1 invasive breast carcinomas were analyzed retrospectively. Preoperative breast MRI was reviewed for size, lesion type (mass versus non-mass enhancement), morphology, and dynamic contrast-enhanced (DCE) tumor kinetics. MRI Tumor size (greatest diameter) was compared to size measurement of tumor at pathology. Concordance was defined as a diameter difference of ≤0.5 cm. Clinical features and histological factors for MRI-pathology discordance were investigated.

Results: The mean size on MRI was 1.48 ± 0.49 cm. The overall correlation between pathology and MRI measurements was strong (Spearman's rho = 0.740, $p < 0.001$). MRI-pathology concordance was found in 179/200 (89.5 %) cases; the size was overestimated in 15 (7.5 %) tumors and underestimated in 6 (3 %). On univariate analysis, MRI-pathology discordance was associated with human epidermal growth factor receptor type 2 (HER2) positivity ($p = 0.027$) and DCE kinetics ($p = 0.028$). On multivariate analysis, HER2 positivity was significantly influenced MRI-pathology discordance ($p < 0.05$).

Conclusion: HER2 positivity was strongly associated with MRI-pathology discordance in T1 invasive breast carcinomas. Awareness of this factor might improve surgical planning.

Imaging of breast implant: Tomosynthesis, ultrasonography and MRI

L. Crivelli, M. A. Rojas Soldado, B. Popal, E. V. Tenisch, J.-Y. Meuwly; Lausanne/CH

Learning objectives: Review of normal appearance of breast implants in the different imaging modalities. Understand the specificities of breast implant imaging with the multiple techniques. Review the appearance of the complications of implants with different imaging modalities (post surgical, capsulitis, rupture, lymphoma).

Background: Breast implants are frequently seen in general practice, due to an esthetic and reconstructive use in women. It is important for the radiologist to know how to image adequately and recognize the normal appearance and the signs of implant complications.

Imaging findings or procedure details: Normal appearance: prosthesis component, morphology and position.

Eklund technique in tomosynthesis and MRI breast implant protocols: routine sequences with silicone specific sequence

Complications:

· Post-surgical: hematoma, infection

· Breast implant rupture, collapse and herniation
  – Intracapsular: US (stepladder sign), MRI (tear drop, keyhole and linguine sign)
  – Extracapsular US (snowstorm appearance), MRI (free silicone and silico-nomas)

· Capsulitis: capsular contracture, calcifications

· Rarely breast implant-associated anaplastic large cell ymphoma

Conclusion: Profound knowledge of normal and pathological appearance of breast implants is mandatory to adequately recognize complications of this surgical procedure.

Breast lesion in pregnant and lactating women: What the radiologist needs to know

R. Troxler[1], B. Pauchard[2], H. C. Thoeny[3], Q. D. Vo[4]; [1]Fribourg/CH, [2]Lausanne/CH, [3]Bern/CH, [4]Romont/CH

Learning objectives: To know: the modalities of breast imaging adapted during pregnancy and lactation as well as their contraindication; the main breast pathologies related to pregnancy and lactation; the management of breast pathologies according to BIRADS; the treatment of pregnancy-associated breast cancer.

Background: The discovery of a breast lump during pregnancy must be immediately investigated. Although 80% of them are benign, the malignant ones trend to be more aggressive with often delayed diagnosis and consequent management. Ultrasound is the modality of choice to reassure or to confirm the presence of a suspicious lesion that needs further investigation (mammography, biopsy). Furthermore, management is performed according to BIRADS. Finally, the treatment (surgery, chemotherapy, radiotherapy) must be adapted to the stage of pregnancy.

Imaging findings or procedure details: This poster aims to familiarize the radiologist with the diagnosis and the management of a breast lump during pregnancy and lactation by presenting a series of typical findings.

Conclusion: The discovery of a breast lump during pregnancy must be immediately investigated by ultrasound as a first step.

Preoperative localization of non-palpable breast lesions with Iodine-125 Seeds

S. Bucher, E. Klinger, N. Schmidt, R. M. Eichenberger, C. Kurzeder, W. Weber, S. Dellas; Basel/CH

Learning objectives: The accurate localization of non-palpable breast lesions intraoperatively for best therapeutic outcome remains challenging. At the same time, removing the smallest amount of surrounding healthy glandular tissue possible for optimal cosmetics constitutes a competing objective.

As a preoperative localization technique Iodine-125 radioactive seeds (RSL) can be used as an alternative to wire-guided localization.

Background: Preoperative localization with I-125 seeds was performed in 68 patients between January and October 2018 (67 Mamma, 14 Axilla). No neoadjuvant chemotherapy patients were included. Mammography and ultrasound were used for placement. The seeds were tracked and documented throughout the entire process. That includes the numbers of seeds placed, seeds removed during surgery including the radiography of the specimen and seeds removed by a pathologist. A gamma detection probe was used for intraoperative localization and for histopathological analysis.

Imaging findings or procedure details: All 81 seeds were successfully removed after a mean retention time of 6.8 days (1–70 days). Mean radioactivity at time of localization was 9.07 MBq (4.13–10.9 MBq) and at time of removal 8.5 MBq (4.13–10.78 MBq). During the whole procedure RSL provided many advantages over wire localization, such as offering flexible scheduling as an outpatient intervention. The techniques for placement are faster, easier and more accurate without limiting the surgical incision and dissection route.

Due to radioactivity, safety rules for the safe and secure handling were established.

Conclusion: RSL is a safe and accurate procedure. It provides many advantages over wire localization with improving patient satisfaction. Additional safety features need to be established.

PO67

18F-FDG PET/CT in relapsing polychondritis: A case report

S. Dietemann; Geneva/CH

Learning objectives: 18F-FDG PET/CT in relapsing polychondritis: a case report to demonstrate the powerful value of 18F-FDG PET/CT for the diagnosis and also in the follow-up and the therapy response.

Background: Relapsing Polychondritis (RP) is a rare disease characterized by destructive inflammation of the cartilaginous structures and other connective tissues in many oragans. Here we describe a case of RP initially presenting with sudden onset painful cough followed by dyspnea at rest and wheezing. The patient was referred to our hospital for further examinations including computed tomography pulmonary angiography (CTPA) for suspected pulmonary embolism. The CTPA revealed laryngeal, tracheal and bronchial wall thickening with airway narrowing suggestive of RP, but differential diagnoses with sarcoidosis or vasculitis remained open.

Imaging findings or procedure details: The patient underwent a 18F-FDG PET/CT wich showed high FDG uptake in the larynx, trachea and major bronchi, in correlation with wall thickening and the absence of arguments for other localisation, sarcoidosis or vasculitis.

Conclusion: In conclusion, 18F-FDG PET/CT is a useful tool to assess the disease activity and its extension, and several publications suggest that it is equally a powerful tool in the follow up and therapy response of RP.

PO68

Influence of novel image PET reconstruction techniques on the response assessment in Hodgkin lymphoma patients – Preliminary results

P. Radojewski, A. Baur, J. Enders, C. Furth, I. Schatka, H. Amthauer, J. Rogasch; Berlin/DE

Purpose: Bayesian penalized likelihood reconstruction algorithms for PET (e.g. Q.Clear, GE Healthcare) increase the lesion detectability. We aimed to assess the influence of image reconstruction techniques on response assessment with FDG-PET in Hodgkin lymphoma (HL) patients.

Methods and Materials: Retrospective analysis of 11 patients (male, 5; age, 42 [32–80]) with HL and FDG-PET/CT for response assessment following chemotherapy. PET-data were reconstructed using Q.Clear, PSF+TOF and OSEM+TOF and read by 3 blinded readers using Deauville score (DS) to assess lesions. Changes in DS between 3 and 4 were rated as clinically relevant. SUVmean of lesions and reference sites (liver, mediastinal blood pool [MBPS]) and respective signal-to-background ratios (SBR) were calculated.

Results: In the 11 FDG-PET/CT scans a total of 25 HL lesions were identified and rated. In the standard OSEM+TOF reconstruction 11 lesions were rated DS 3. DS was significantly higher with Q.Clear than with PSF+TOF and OSEM+TOF (Wilcoxon, p<0.05) but comparable between PSF+TOF and OSEM+TOF (p=0.78). The score increased from 3 to 4 for at least one reader in 1/11 lesions from OSEM+TOF to PSF+TOF, in 4/11 lesions from OSEM+TOF to Q.Clear and 3/11 lesions from PSF+TOF to Q.Clear. Downgrading from 4 to 3 was not observed. SUVmean of residuals was significantly higher in Q.Clear (median, 2.0) than in PSF+TOF (1.7) or OSEM+TOF (1.6; p<0.05) while PSF+TOF and OSEM+TOF were similar (p=0.16). SBR values were higher in Q.Clear than in PSF+TOF and OSEM+TOF.

Conclusion: The Q.Clear reconstruction technique may result in a shift towards more positive reads.

PO69

Subacute and long-term hepatotoxicity risk after 90Y- OR 177LU-DOTATOC therapy – Is hepatic tumour burden on 68Ga-DOTATOC PET/CT predictive of liver dysfunction?

A. Chirindel, Y. Anongpornjossakul, D. Wild, G. Nicolas; Basel/CH

Purpose: Peptide-receptor radionuclide-therapy (PRRT) is an effective therapy for metastatic neuroendocrine tumour (NET) but dose-limiting toxicities may occur. Hepatic tumour burden may represent a risk factor for developing subacute hepatic dysfunction (SHD) or long term liver toxicity (LHT) after PRRT.

Methods and Materials: Consecutive NET-patients undergoing 68Ga-DOTATOC-PET/CT before 90Y-/177Lu-DOTATOC were evaluated. Normalized changes from baseline were calculated for each liver function parameter. Any change within the worse quartile was considered a significant deterioration. SHD was defined as deterioration of ≥3 liver parameters, within 3 months after one cycle of PRRT. LHT was evaluated at >12 months after therapy completion according to CTCAE-v5.0. Semiautomated liver and liver tumour segmentation was performed on 68Ga-DOTATOC-PET/CT(MIM®). Several PET-derived metrics were collected: standardised uptake value (SUV), tumour volume (TV) and percent of liver involvement (%TLV). Comparative analyses were applied.

Results: Among the 58 patients enrolled, 13 demonstrated SHD. LHT (any grade) developed in 6 patients of whom 4 had no SHD. Prior to PRRT, 15 patients had liver surgery and 5 liver-directed therapies. The mean TV was 292 ± 65ml. There was no difference between patients with and without SDH according to the following PET-derived metrics SUV_{tumor} (p=0.7), $SUV_{whole-liver}$ (p=0.8), TV (p=0.9) and %TLV (p=0.4), however %TLV was significantly different for LHT (8 vs 22%, p<0.04). The relative risks of surgery and liver-directed therapy for SHD were 0.6 (95% CI 0.1–2.2) and 1.9 (95% CI 0.6–6.2), respectively. No correlation between LHT and number of PRRT cycles or choice of radionuclide.

Conclusion: High liver tumor-burden is not associated with increased risk for SHD after PRRT. However, it may be significant for LHT.

PO70

68Ga-PSMA-11 for prostate cancer imaging: Quality control requirement and analytical method validation

K. Casagrande, J. Delage, J. Costes, O. Fabre, J. Caputo, J. de Figueiredo, N. Schäfer, J. Prior, F. Sadeghipour; Lausanne/CH

Purpose: As 68Ga-PSMA-11 is a non-registered radiopharmaceutical without Pharmacopeia monograph, a Quality Dossier have to be submitted to Swissmedic. Among the needed quality controls (QC), some must be realized before radiopharmaceutical release: appearance, radioactive concentration, pH, sterilizing filter integrity, amount of PSMA-11 precursor (HPLC), identification of 68Ga-PSMA-11 (HPLC) and determination of radiochemical purity (TLC and HPLC). Radionucleidic purity, ethanol content (GC), microbiological analyses are realized on validation batches or after radiopharmaceutical release.

Methods and Materials: The HPLC method uses a C18, 3 µm 3x150 mm column with a constant flow rate of 0.6 mL/min of a gradient mixed from mobile phase A (TFA/water 1:999 V/V) and mobile phase B (TFA/acetonitrile 1:999 V/V), gradient program: 0–30s: 5%B; 30s–10min: 5–40%B; 10–11min: 40–5%B; 11–16min: 5%B. The TLC is developed upon 10 cm in methanol/ammonium-acetate 1M 1:1 on an ITLC-SG plate. The GC method uses a HP-1 column, 30 m, 0.32 mm 0.25 µm with a helium flow rate of 3.0 mL/min and FID detection at 300°C. Other QC tests are realized according to the Pharmacopeia.

Results: HPLC, as a non-pharmacopeia-described method, was validated, according to ICH guidelines Q2R1, through accuracy (error: −3.01 to 1.47%), linearity (r^2=0.9993), quantitation limit (0.07 MBq/mL), specificity (Rs>1.6) and high-resolution tests. Three batches were produced to validate the QC protocol, they all matched the required specifications. For example, radiochemical purity specification is ≥95% and we obtained not less than 98.03% (HPLC) and 98.62% (TLC).

Conclusion: Our work will provide easier access to 68Ga-PSMA-11 for nuclear medicine patients at our center.

First experience of durable cytoreduction in chronic lymphoid leukemia with 177Lu-DOTATATE

M. Meyer, J. Prior, M. Da Mota, M. Nicod Lalonde, N. Schäfer; Lausanne/CH

Purpose: We reported on the case of a 75-year old female with B cell chronic lymphoid leukemia (CLL), and well-differentiated metastatic neuroendocrine tumor of terminal ileum.

Methods and Materials: The patient did not receive any treatment for the CLL because she was in Binet stage A.

The neuroendocrine tumor was diagnosed in 2015 and was treated by surgery. The patient relapsed in 2016 with metastatic liver lesions, and was treated with Lanreotide sc. In 2018, she further progressed and a treatment with ^{177}Lu-Dotatate was decided.

Results: The pre-treatment images showed multiple metastatic liver lesions with high uptake of ^{68}Ga-DOTATATE, and no uptake of ^{18}F-FDG. The blood count showed increased number of total leukocytes (57.3 G/L) and lymphocytes (50.5 G/L), due to the leukemia, and normal levels of hemoglobin and platelets.

The patient received a reduced dose of ^{177}Lu-DOTATATE (3800 MBq), as to avoid possible hematologic toxicity of the treatment. The patient did not have any complications and was discharged after 3 days.

One month after the therapy, the blood test showed normalization of total leukocytes (6.3 G/L (N: 3.8–10.7 G/L)) and lymphocytes (2.9 G/L (N: 1.5–4.8 G/L)), and still normal levels of hemoglobin and platelets. This leukocytes and lymphocyte normalization lasted for at least three months, before the next treatment cycle (leucocytes 7.6 G/L, lymphocytes 4.24 G/L).

Conclusion: To our knowledge, this is the first case of durable cytoreduction in CLL after initial PRRT treatment with ^{177}Lu-DOTATATE. The patient presented no short-term adverse events to the PRRT treatment.

PSMA-ligand PET enables a more accurate therapy response evaluation of bone metastases in prostate cancer compared to computed tomography – A case report

V. Fech, T. Krause, A. Rominger, A. Afshar-Oromieh; Bern/CH

Purpose: We present a case, which demonstrates the challenges in imaging of prostate cancer (PC) with conventional modalities. Following different therapies of PC, CT or MRI may show increasing volume of bone metastases despite effective systemic therapies, demonstrated by falling PSA. On the other hand, ^{68}Ga-PSMA-11 PET/CT provides additional metabolic information which enables a better evaluation of treatment response.

Methods and Materials: One of our patients (74 y/o, radical prostatectomy 2007, Gleason Score 8) was referred for a ^{68}Ga-PSMA-11 PET/CT in October 2017 due to a PSA elevation to 16.2 ng/ml despite androgen deprivation therapy with bicalutamide. The scan showed multiple bone lesions (n > 20) with moderate PSMA expression. Afterwards, bicalutamide was stopped and treatment with docetaxel and denosumab was initiated. Thereafter, PSA decreased to 0.9 ng/ml until May 2018 when a second ^{68}Ga-PSMA-11 PET/CT was conducted.

Results: In the second ^{68}Ga-PSMA-11 PET/CT mentioned above, a volume progress was visible in the CT-component of the PET/CT for all bone lesions. In contrast, the PET-component showed a remarkable reduction of tracer uptake in all lesions. This result correlated with the PSA decline.

Conclusion: In summary, the volume progress shown by the CT must not be classified as tumor progress but rather as remodeling processes following effective therapy. This case demonstrates that PSMA-ligand PET can be a more reliable tool for therapeutic response evaluation of bone metastasis of PC compared to CT. Future studies including more patients are needed to confirm our observation, which could possibly change the management of patients.

Comparison of statistical tests and their power applied to tumour volume growth in mice

L. Pedrelli, D. Viertl, J. Prior; Lausanne/CH

Learning objectives: To understand and discuss statistical tests and their implications in tumour growth study in mice. Power and effect size group will be calculated as well to discuss the minimal sample size needed in the experiment.

Background: In typical experiments to test antitumour efficacy of a drug, mice are randomly distributed into treatment and control groups and tumour volumes are recorded in time. The volume of tumours at one or more discrete time points are compared by using statistical tests. Five methods are currently used for this kind of analysis: the ANOVA test on tumour volumes on final day of measurements, the ANOVA test on doubling time of tumour volumes, the factorial repeated ANOVA test on the entire set of observations, multivariate methods, and the log-rank test on Kaplan-Meier curves.

Imaging findings or procedure details: Based on a literature review the five most common statistical tests used to compare tumour growth were applied on a dataset to compare their powers and discuss which one is the most relevant. The Monte-Carlo approach was implemented to estimate powers by applying the tests on simulated data and counting the fraction of significant p-values. Power calculations for the different tests were done to estimate the smallest sample size. These calculations permitted to establish the minimal number of animals needed in the experiment to determine if treatments were effective, without wasting resources.

Conclusion: To calculate a relevant sample size it is important to estimate accurately the size effect before starting each experiment by producing a pilot study or by researching in the literature.

Renal blood flow (RBF) measurements with Rb-82 PET/CT: First results

G. Allenbach, M. Meyer, N. Testart, M. Nicod Lalonde, J. Prior; Lausanne/CH

Purpose: Rb-82 dynamic perfusion PET is used to quantify myocardial blood flow. With the extended field of view in newest PET scanners it becomes possible to measure renal Rb-82 uptake opening the door to renal blood flow quantification. Aim: To verify the feasibility of renal blood flow (RBF) quantification with Rb-82 and to evaluate effect of adenosine infusion on measured RBF.

Methods and Materials: We selected 5 consecutive patients referred for suspicion of myocardial ischemia, with normal myocardial perfusion imaging (no ischemia) and normal myocardial flow reserve (>2). Myocardial 6-min adenosine stress and rest PET acquisitions were obtained after injection of 300–700 MBq of Rb-82. On the 6-minutes dynamic PET series 3 spherical VOI were placed on the upper pole of each kidney. A VOI on the aorta was used for vascular input function. Using the PMOD software, a 1-compartment model was used to compute K1 without further corrections applied.

Results: Mean RBF at rest was 1.47 ± 0.35 ml/min/g (range 1.18–2.05) for the left kidney and 1.43 ± 0.43 ml/min/g (1.11–2.12) for the right kidney. Mean RBF at stress was 1.38 ± 0.27 ml/min/g (0.90–1.62) for the left kidney and 1.44 ± 0.33 ml/min/g (0.91–1.81) for the right kidney. Individual changes where observed with an increase of >18 % of RBF in 2 patients, and a decrease of >17 % in 2 patients. In the last patient, only minor 3 % changes were observed.

Conclusion: Assessment of RBF during cardiac perfusion scan is possible. The effect of adenosine stress on RBF remained low.

Myocardial mapping of relaxation times

S. P. Hüttenmoser; Bern/CH

Learning objectives: After viewing this poster, radiographers will understand the principles of T1, T2 and T2* mapping and understand the relevance and advantages of these imaging approaches.

Background: While T2* mapping has been routinely performed for the diagnosis of myocardial iron deposition disorders, T1 and T2 mapping are more recent developments. In conventional MRI images, repetition- and echo times influence the image contrast. Different tissues present with different signal intensities (SI) on the resulting image. Accurate diagnosis can be made by comparing enhanced tissue to reference myocardium. In global myocardial disease, there is however no healthy reference tissue and a diagnosis can be difficult.

Imaging findings or procedure details: T1, T2 and T2* sequences acquire multiple images after defined echo or inversion times after an excitation pulse. These images will be lined up with motion correction and different SI will form a relaxation curve for each image pixel. At 37% of the initial SI for T2 and T2* mapping sequences will define the respective time constant, while recovery of T1 to 63% of the initial SI will generate the T1 constant. A secondary quantitative image will be generated with these relaxation constants. This will be highlighted with selected images in this poster.

Conclusion: The measured relaxation times can be compared to reference values. Therefore, even globally affected myocardium can be categorized into healthy or diseased tissue and even the nature of the underlying pathology can be inferred (e.g. edema, fibrosis). Radiographers will more frequently encounter mapping techniques in the future and should thus know their principles.

La douleur induite en radiologie interventionnelle: Valeur réelle et perspectives

C. Knuchel; Geneva/CH

Purpose: Le guidage des gestes par imagerie a permis le développement de son rôle interventionnel.

Ces procédures ont un caractère invasif qui dépend de divers paramètres : le terrain (douleur préexistante, anxiété), la position de la procédure, le type de geste et le matériel utilisé. Ainsi, la douleur induite est inhérente à ces interventions incluant celles réalisées à but thérapeutique (exemple : infiltration). L'évaluation de cette douleur est devenue une nécessité d'une part, pour optimiser la prise en charge et le confort des patients et d'autre part, pour recenser les besoins en termes d'assistance anesthésique adaptée.

Évaluation de la douleur induite selon le type d'intervention dans le Service de radiologie par la mise en place d'un indicateur standardisé et l'analyse des données recueillies.

Methods and Materials: Recueil prospectif des données de la douleur induite par toutes les procédures interventionnelles selon l'échelle visuelle analogique (EVA) entre 1er novembre 2017 et 30 novembre 2018.

Results: 8606 patients sont inclus consécutivement dans cette étude observationnelle. 28.33% des patients ont eu une douleur 4 (considérée comme significative selon les recommandations de l'institution) et 2% des patients ont eu une douleur 9 à 10. La douleur n'était pas recensée dans 12% des cas.

Conclusion: Ce travail d'évaluation d'un critère de qualité de soins dans le Service de radiologie a permis de montrer des valeurs élevées de douleur induite dans certains types de geste avec une disparité en cas d'assistance ou non anesthésique. La douleur induite est sous-estimée et une prise en charge ciblée est entamée pour une meilleure gestion.